Polymer Based Electrospun Nanofibers as Diagnostic Probes for the Detection of Toxic Metal Ions in Water

A thesis submitted to Rhodes University in fulfillment of the requirements for the degree of

Doctor of Philosophy (Science)

by

Dezzline Adhiambo Ondigo

Supervised by

Prof. Nelson Torto

February 2013

Dedication

This thesis is dedicated to my incredible family for their endless support, understanding and unconditional love despite the long absence.

Acknowledgements

Above all, am grateful to the almighty father to whom I owe everything. *"I can do everything through him who gives me strength." (Philippians 4:13 NIV)*

Abstract

The thesis presents the development of polymer based electrospun nanofibers as diagnostic probes for the selective detection of toxic metal ions in water. Through modification of the chemical characteristics of nanofibers by pre- and post-electrospinning treatments, three different diagnostic probes were successfully developed. These were the fluorescent pyridylazo-2-naphthol-poly(acrylic acid) nanofiber probe, the colorimetric probe based on glutathione-stabilized silver/copper alloy nanoparticles and the colorimetric probe based on 2-(2'-Pyridyl)-imidazole functionalized nanofibers. The probes were characterized by Fourier transform infrared spectroscopy (FTIR), Energy dispersive x-ray spectroscopy (EDX), Scanning Electron Microscopy (SEM) and Transmission Electron Microscopy (TEM). The fluorescent nanofiber probe was developed towards the determination of Ni^{2+}. Covalently functionalized pyridylazo-2-naphthol-poly(acrylic acid) polymeric nanofibers were employed. The solid state Ni^{2+} probe exhibited a good correlation between the fluorescence intensity and nickel concentration up to 1.0 mg/mL based on the Stern-Volmer mechanism. The detection limit of the nanofiber probe was found to be 0.07 ng/mL. The versatility of the fluorescent probe was demonstrated by affording a simple, rapid and selective detection of Ni^{2+} in the presence of other competing metal ions by direct analysis without employing any sample handling steps. For the second part of the study, a simple strategy based on the *in-situ* synthesis of the glutathione stabilized silver/copper alloy nanoparticles (Ag/Cu alloy NPs) in nylon 6 provided a fast procedure for fabricating a colorimetric probe for the detection of Ni^{2+} in water samples. The electrospun nanofiber composites responded to Ni^{2+} ions but did not suffer any interference from the other metal ions. The effect of Ni^{2+} concentration on the nanocomposite fibers was considered and the "eye-ball" limit of detection was found to be 5.8 µg/mL. Lastly, the third probe was developed by covalently linking an imidazole derivative; 2-(2'-Pyridyl)-imidazole (PIMH) to Poly(vinylbenzyl chloride) (PVBC) and nylon 6 nanofibers by post-electrospinning treatments using a wet chemical method and graft co-polymerization technique, respectively. The post-electrospinning modifications of the nanofibers were achieved without altering their fibrous morphology. The color change to

red-orange in the presence of Fe^{2+} for both the grafted nylon 6 (white) and the chemically modified PVBC (yellow) nanofibers was instantaneous. The developed diagnostic probes exhibited the desired selectivity towards the targeted metal ions.

Table of contents

Abbreviations and symbols

β-CD	βeta cyclodextrin
μg	Microgram
au	Arbitrary units
AIBN	Azobisisobutyronitrile
AAS	Atomic absorption spectroscopy
AgNPs	Silver nanoparticles
ASV	Anodic stripping voltammetry
AuNPs	Gold nanoparticles
BP	Benzophenone
CDI	1,1'-Carbonyldiimidazole
CHEF	Chelation enhanced fluorescence
CHEQ	Chelation enhanced quenching
CHNX	Carbon, hydrogen, nitrogen, and halogens or sulfur
CT	Charge transfer
CuNPs	Copper nanoparticles
DBU	1,8-diazabicyclo[5.4.0]undec-7-ene
DMF	*N,N*-Dimethylformamide
DMG	Dimethylglyoxime

EDTA   Ethylene diamine tetraacetic acid

EDX   Energy dispersive x-ray spectroscopy

EPA   Environmental Protection Agency

F   Fluorescence intensity in the presence of quencher

F_0 Fluorescence in the absence of quencher

F3GA   Cibacron blue

FTIR   Fourier transformer infrared spectroscopy

GFAAS   Graphite furnace atomic absorption spectroscopy

GSH   Glutathione

h   Hour

HS   High spin

HSAB   Hard and soft bases and acids

IC   Intersystem crossing

ICP-ES   Inductively coupled plasma emission spectrometry

ICP-MS   Inductively coupled plasma mass spectrometry

ICT   Internal charge transfer

ISA   Excited state absorption,

ISC   Inter system crossing

Ksv   Stern-Volmer constant

LOD   Limit of detection

LOQ	Limit of quantification
LS	Low spin
MeOH	Methanol
nm	Nanometer
NMR	Nuclear magnetic resonance
ns	Nanoseconds
NPs	Nanoparticles
MWNT	Multiwall carbon nanotube
PAA	Poly(acrylic acid)
PAN	Pyridylazo-2-naphthol
PET	Photoinduced electron transfer/ Polyethylene terephthalate
PIMH	2-(2′-Pyridyl)-imidazole
PM	Pyrene methanol
PVBC	Poly(vinylbenzyl chloride)
PVB	Poly(vinylbenzyl)
PVC	Poly (vinyl chloride)
R^2	Correlation coefficient
RSD	Relative standard deviation
SA	South Africa
SCO	Spin crossover

SEM	Scanning electron microscope
t	Ton
TEM	Transmission electron microscope
TXRF	Total reflection X-Ray fluorimetry
UV	Ultraviolet
w/v	Weight by volume
WHO	World Health Organization

List of figures

List of schemes

List of tables

Chapter 1 Background

1.1 Introduction

The conservation and protection of the environment is essential for the health of both humans and other organisms. Environmental pollution is becoming a global concern. Experts estimate that industrial processes introduce daily up to a million different pollutants into the atmosphere and the aquatic environment [1]. Toxic metal ions are the most significant environmental pollutants found in water bodies, thus raising concerns regarding the long-term effects of metal ion exposure on human health and natural ecosystems. The toxicity of metals has led to the urgency for the development of methods for detection, quantification and their removal from the environment.

1.2 Toxic heavy metal ions in the environment

Heavy and transition metal ions play important roles in many biological and environmental processes [2, 3]. Depending on the abiotic environment and/or the organisms of interest, the physiological, ecological and toxicological effects of these ions are usually strongly structure-specific, i.e. they depend on the species [4, 5]. The biological efficacy of a single species for instance, if it acts as an essential (trace) element or as an acute toxin, is critically determined by its concentration in the respective medium and the uptake paths of an organism [6]. Metal ions such as Zn^{2+}, Cu^{2+}, Ni^{2+} and Fe^{2+}/Fe^{3+} are fundamentally involved in biochemical reactions at the trace level (<1 mM), e.g. in catalysis, transport or biosynthesis. However, at concentrations greater than 1 mM, accumulation of the ions in an organism could lead to unhealthy interactions in biochemical redox processes. For instance, interaction of the metal ions can lead to the inhibition of enzyme activity or nephrotoxicity [7]. In fact pollution by heavy metal ions remains one of the greatest environmental risks to date [8]. Heavy metal detection continues to be a priority as high

levels of metals have been isolated from soil and drinking water because of their extensive applications in industrial and domestic processes.

1.3 Sources of metal contamination

Heavy metals have been used by humans for thousands of years. Although several adverse health effects of heavy metals have been known for a long time, exposure to metals continues. The concentration of heavy metals is even increasing in some parts of the world, particularly in developing countries, although emissions have declined in most developed countries over the last 100 years [9]. Metals are being brought into the environment by human activities which started more than 4000 years ago with mineral exploitation [10]. Consequently, the human activities have influenced and modified natural cycles (Fig. 1.1).
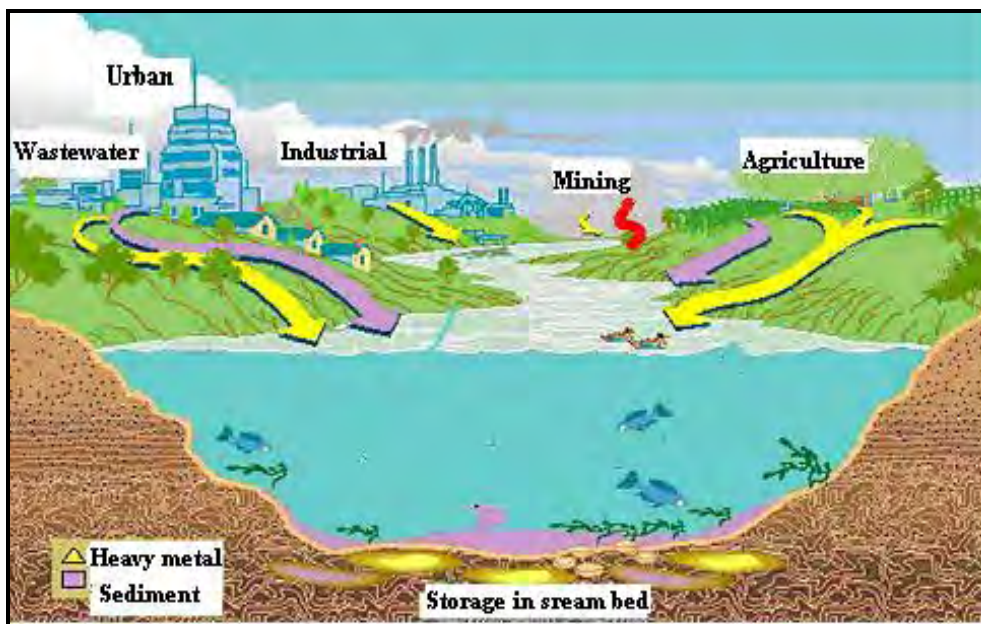
Figure 1.1: Sources of heavy metal pollution for the aqueous system [11].

Unprecedented pollution resulted from industrialization and the increased consumption of energy. The combustion of fossil fuels has led to increased concentrations of heavy metals into the atmosphere and the aquatic environment. Crude oil, for example, contains 3.4 ppm mercury and the firing of coal results in the worldwide emission of 2.4×10^4 t of lead per year [2]. Because of their non-biodegradable nature, high solubility in water and their potential to accumulate in different body parts; metals cause serious side effects to human health.

1.4 Toxicity of metal ions

Metal ions show a large tendency to form complexes, especially with nitrogen, sulphur and oxygen containing ligands of biological matter [12]. Their toxicological effects can be explained by the interactions which lead to changes in the molecular structure of proteins, through breaking of hydrogen bonds and subsequent formation of strong and stable chemical bonds (Fig. 1.2). The hydrogen atoms or the methyl groups of proteins are

replaced by the poisoning metal and the enzyme is thus inhibited from functioning, whereas the protein-metal compound acts as a substrate and reacts with a metabolic enzyme.
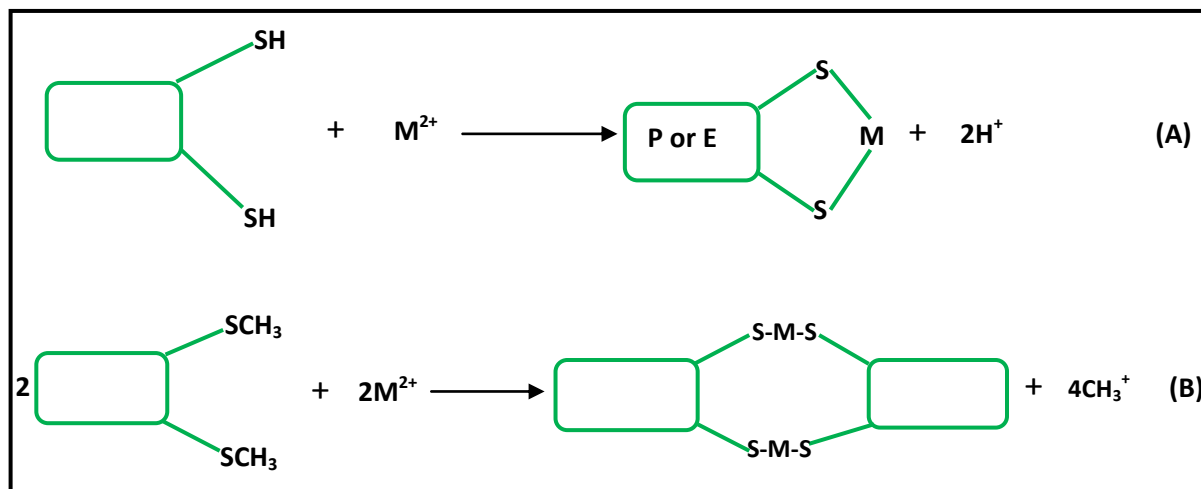
Figure 1.2: Biochemistry of heavy metal toxicity; (A) Intramolecular bonding (B) Intermolecular bonding; P = Protein; E = Enzyme; M = Metal [10].

Acute poisoning is rarely observed and usually, it results from suicidal activities or accidents. Chronic toxicity is much more relevant and is caused by repeated exposure over long periods of time. Mutagenic, carcinogenic or teratogenic effects have been described for some heavy metals [2]. Besides the fact that mercury, cadmium and arsenic are highly toxic, some heavy metals such as iron, copper, zinc, manganese, cobalt, nickel, tin, and selenium are essential to many organisms. These elements, along with amino acids, fatty acids and vitamins are required for normal biochemical processes such as respiration, biosynthesis and metabolism [13]. An undersupply of the so-called trace metals leads to deficiency, while oversupply results in toxic effects [1].

For instance nickel is an essential element to biota for its biological functions; it is required to take part in various enzyme activities such as hydrogenases, superoxide dismutases,

acetyl-coenzyme, carbon monoxide dehydrogenases, and catalytic processes [14]. However, the concentration of nickel needed by the body is very little, an excess of nickel ion in an organism may cause adverse health effects like dermatitis, allergy, carcinogenesis and even cell death and therefore its determination is of tremendous interest [14]. In accordance with toxicity data and scientific studies, the World Health Organization (WHO) recommends standards and guidelines for heavy metals in drinking water. The recommended standards and guidelines set by WHO are summarized in Table 1.1.

Table 1.1: WHO standards and guidelines for heavy metals in drinking water [15].

Metal	WHO (mg/L)
Cd	0.003
Cu	2
Pb	0.01
Hg	0.006
Ni	0.07
Fe	2

1.5 Nickel

Nickel (Ni) is the 24th most abundant element in the Earth's crust, comprising about 3% of the composition of the earth. It is the 5th most abundant element by weight after iron, oxygen, magnesium and silicon. It is a member of the transition series and belongs to group VIII B of the periodic table along with iron, cobalt, palladium, platinum and five other elements. Nickel is a naturally occurring element that can exist in various mineral forms. As a member of the transition metal series, it is resistant to corrosion by air, water and alkali, but dissolves readily in dilute oxidizing acids [16, 17].

1.5.1 Occurrence and sources of nickel

Natural nickel is a mixture of five stable isotopes although nineteen other unstable isotopes are known. It can exist in several different oxidation states, the prevalent oxidation state under environmental conditions is Ni (II), nickel in the +2 valence state. Other valences (-1, +1, +3, and +4) are also encountered, though less frequently [1, 16, 18]. Nickel and nickel compounds have many industrial and commercial applications. Nickel metal and its alloys are widely used in the metallurgical, chemical and food processing industries, especially as catalysts and pigments. The nickel salts of greatest commercial importance are nickel chloride, sulphate, carbonate, nitrate, hydroxide, acetate and oxide [19, 20].

Nickel is one of many trace metals widely distributed in the environment, being released from both natural sources and anthropogenic activities, with input from stationary and mobile sources. It is present in the air, water, soil and biological material. Natural sources of atmospheric nickel levels include wind-blown dust, derived from the weathering of rocks and soils, volcanic emissions, forest fires and vegetation. Nickel finds its way into the ambient air as a result of the combustion of coal, diesel oil and fuel oil, the incineration of waste, sewage, and miscellaneous sources [18-23].

Environmental sources of lower levels of nickel include tobacco, dental or orthopaedic implants, stainless steel kitchen utensils and low-cost jewellery [21, 24]. Tobacco smoking is another, significant, source of non-occupational exposures to nickel. It has been estimated that each cigarette contains nickel in a quantity of 1.1 to 3.1 μg and that about 10-20% of the nickel inhaled is present in the gaseous phase. According to some reports [25], nickel in tobacco smoke may be present in the form of nickel carbonyl, a form which is extremely hazardous to human health. Pipe tobacco, cigarettes and other types of tobacco products do not greatly differ from one another in the content of nickel [22, 25].

1.5.2 Nickel in water

Drinking water generally contains nickel at concentrations less than 10 µg/L, assuming a daily intake of 1 L of water and a level of 5-10 µg/L, the mean daily intake of nickel from water for adults would be between 5 and 10 µg. Tests conducted in the USA revealed that, 97% of the 2053 drinking water samples tested had nickel concentrations below 20 µg/L and 80% of the samples had less than 10 µg/L. In exceptional cases, values up to 75 µg/L were found and those as high as 200 µg/L were recorded only in the nickel ore mining areas. The incidence of health impairments due to higher nickel intakes in drinking water is extremely rare [26].

The concentration of nickel in cold and hot water depends on the quality of the water pipes as well. According to research carried out in Warsaw, Poland by Prystupa and Rudzki, in the case of metal pipes, the level of nickel in hot water was higher than in cold water. However, where PVC pipes were used, nickel concentration was higher in cold water than in hot water [27]. Soft drinking water and acidic beverages may dissolve nickel from pipes and containers. Leaching or corrosion processes may contribute significantly to oral nickel intake, occasionally up to 1 mg/day. In another study, nickel concentration in screened households' drinking water decreased significantly after 10 minutes of flushing in the morning from an average of 10.79 µg/L to 7.23 µg/L, respectively [20, 28]. The major sources of trace metal pollution in aquatic ecosystems, including the ocean, are domestic wastewater effluents (especially As, Cr, Cu, Mn and Ni) and non-ferrous metal smelters (Cd, Ni, Pb and Se).

Nickel is easily accumulated in biota, particularly in the phytoplankton or other aquatic plants, which are sensitive bio-indicators of water pollution. It can be deposited in the sediment by processes such as precipitation, complexation, adsorption on clay particles and via uptake by biota [22, 29, 30]. In lakes, nickel is predominant in its ionic form and in association with organic matter. In rivers, nickel is transported mainly as a precipitated coating on particles and in association with organic matter [29]. Like many heavy metals nickel has the ability to bioaccumulate along the food chain and cause toxicity. Therefore its

quantification and removal is essential. Like nickel, iron is also considered as an essential element in biological systems but if its concentration exceeds the normal level it may become a potential health hazard.

1.6 Iron

Iron is the most abundant of the heavy metals in the Earth's crust and the most widely used than any of the others. Metallic iron is obtained from the refining of iron ore. It has enormous applications ranging from small tools to big structures [31, 32]. Iron exists in oxidation states of 2 and 3 in a variety of rocks and soil minerals and it is an essential trace element in biological systems [33]. The oxidation states of iron, Fe(II) and Fe(III) are much closer together in stability when compared with other transition elements having oxidation states of 2 and 3. As a result of the stability, ferrous and ferric solutions can readily be inter-converted by the use of mild oxidizing or reducing agents [32]. Because of its wide spread occurrence, iron and its derivatives are widely distributed in nature.

1.6.1 Iron in the environment

Iron is a natural constituent of the environment. It is the fourth most abundant element in the Earth's crust (5.6% by mass). In natural waters, it exists in two oxidation states; Fe(II) and Fe(III). In oxygenated water, Fe(III) predominates and it readily forms hydroxide and becomes insoluble. Fe(II) when present is rapidly oxidized to Fe(III) because it is unstable in oxygenated water. Photo-reduction of Fe(III) in surface water, atmospheric deposition, and diffusion from sediments are the potential sources of Fe(II) [34-36].

The concentration of total iron in oxygenated surface water is usually more than 1 mg/L and is less in seawater. On the other hand, ground water and acidic surface drainage contain considerably higher concentrations of iron. In sea water, iron is found as dissolved

Fe(III), colloidal Fe(III) and as suspended particles. Iron can be bound in humic and fulvic acid polymers and organic particles. It can also exist in live and dead biota [37].

The concentrations of dissolved iron in the ocean are typically < 0.2 nM in surface waters and 0.7-0.8 nM in deep waters [38]. Since iron is an essential micronutrient for the growth of surface dwelling marine plankton, the very low concentration of iron in the ocean have been reported to limit phytoplankton growth in high nutrient low chlorophyll regions [39]. More than 20% of the surface oceans consist of chlorophyll waters, which support low primary production of phytoplankton despite an abundance of the major plant nutrients; nitrates and phosphates [40]. Figure 1.3 shows a schematic diagram of the biogeochemical cycling of iron in the environment. A biogeochemical cycle is the complete path a chemical takes through the four major components, or reservoirs, of Earth's system: atmosphere, hydrosphere, lithosphere, and biosphere [41]. Both iron(II) and iron(III) play a central role in the biosphere serving as an active centre in a wide range of proteins such as oxidases, reductases and dehydrases [42].
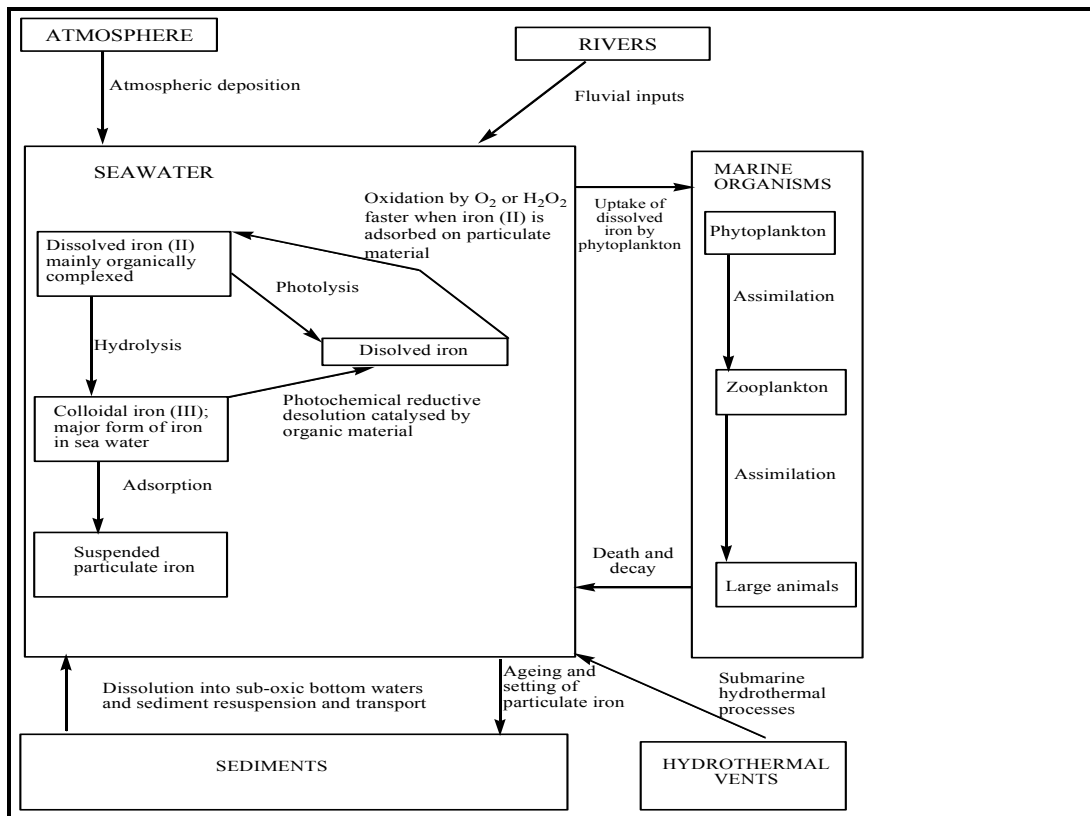
Figure 1.3: Schematic diagram of biogeochemical iron cycling in the environment [36].

1.6.2 Biological importance of iron

Iron is one of the most important elements involved in living process; it plays a central role in almost all living cells of both plants and animals. As an essential constituent of a number of proteins, iron is involved in oxygen transport or metabolism [43, 44]. In plant metabolism, iron is essential for photosynthesis, respiratory electron transport, nitrate reduction, chlorophyll synthesis and detoxification of reactive oxygen species [36]. In animals, iron is important in transport, storage and electron transfer processes [37].

Metal ions in biological systems are loosely associated with enzymes to turn on and off or modify the rate at which the enzymes work. In other cases, some metal ions are found firmly bound to the protein molecules e.g. haemoglobin in the red blood cell which is responsible for oxygen transport through the body. The binding capacity of hemoglobin to

oxygen depends on the presence of the heme group. At the center of each heme group, there is an atom of iron that is attached to four nitrogen atoms in the porphyrin ring (Fig. 1.4). Iron cannot be substituted by another metal in the heme molecule. Iron also plays a significant role in respiratory enzymes such as cytochromes that allow humans to use oxygen and is necessary for the functioning of myoglobin in muscles [45].
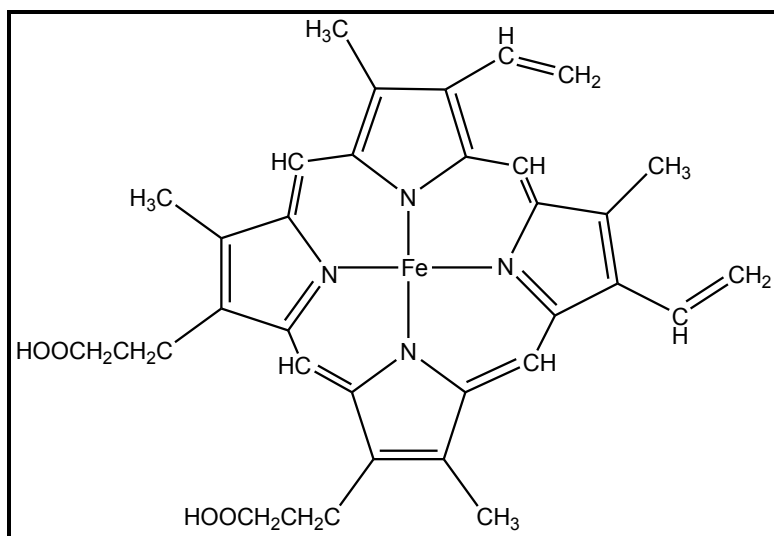
Figure 1.4: The heme complex in which Fe(II) is coordinated to four nitrogen atoms of a planar porphyrin ligand [46].

Fe(II) is required for proper transport and storage of oxygen by hemoglobin and myoglobin in higher animals. Methemoglobin and metmyoglobin are the oxidized forms of the proteins that contain Fe(III) as they cannot bind oxygen [47].

A healthy human adult body contains about 4 g of iron out of which, nearly 70% is present in oxygen carrying protein hemoglobin and myoglobin, with only 0.7% present in other intracellular proteins and enzymes. The remaining ~29% is stored [34, 48]. The average requirement of iron is 1.3 mg/day in males and non-menstruating females and 1.8 mg/day in menstruating females. Iron deficiency causes anaemia which is one of the world's most common nutritional deficiency diseases [49], and gastric mucosal atrophy [50]. At low-level

iron is an essential element in the diet but gets toxic when its concentration becomes higher [33]. Excessive intake of iron has been reported to cause siderosis and damage to organs [51], toxicity and even death [52].

Therefore, selective detection and quantification of essential and non-essential heavy and transition metal ions is of great importance in analytical, biological and environmental sciences. A number of analytical techniques approved by EPA have been in use to monitor and quantify the levels of heavy metals in the environment. While these techniques do an excellent job, only a few of them have found their way into routine analysis of heavy metals.

1.7 Conventional methods for the determination of toxic metal ions

The determination of metal ions is a challenging subject for analytical chemists based on their toxicity even at very low concentrations. In addition; their similar chemistry is complicated with respect to selectivity of the method. A variety of analytical methods fulfilling the demands are available. However, only some of them have found application in routine analysis.

Recommended procedures for the determination of metal ions in water samples include photometric methods, flame or graphite furnace atomic absorption spectroscopy (AAS, GFAAS), inductively coupled plasma emission or mass spectrometry (ICP-ES, ICP-MS), total reflection X-Ray fluorimetry (TXRF) and anodic stripping voltammetry (ASV) [1, 2, 53, 54]. While AAS and photometry are single element methods, ICP-ES, ICP-MS and TXRF are used for multi-element analysis methods, and voltammetry is an oligo-element approach. The methods offer good limits of detection and wide linear ranges, but require high cost analytical instruments developed for use in the laboratories. Furthermore, the necessary collection, transportation and pretreatment of samples are time consuming and a potential source of error [55]. However, smaller, portable and less expensive devices have been brought to the market. On the other hand, there has been an increased development of optical probes for a variety of applications. The toxicity of metal ions makes a continuous

monitoring of drinking and ground water sources necessary. Optical probes enable field monitoring and therefore could be useful alternative tools [56]. For environmental analysis, single use test-strips for various ions, including heavy metals, are commercially available [57].

Reports on the development of optical probes for heavy metals are on the increase and mainly two concepts are applied [58]. The first employs lipophilic neutral ionophores, while the second makes use of immobilized indicator dyes. Due to the nature of metal ions, their similar chemistry, nearly all probes lacked selectivity. Overcoming the limitation of selectivity has led to the development of the so-called artificial noses and tongues that rely on cross-reactive sensor arrays [59]. The schemes consist of a number of molecular recognition cavities or baskets grouped to an array format, which delivers a characteristic response that could be evaluated with chemometric tools.

1.8 Molecular recognition of metals ions

1.8.1 The principle of molecular recognition

Molecular recognition signifies the processes of specific but non-covalent binding of a guest species by an organic host molecule. Fundamentally, molecular recognition involves the interactions between molecules: i.e. bond formation, acid-base interactions, hydrogen-bonding, dipolar and multipolar interactions, van der Waals interaction and physical adsorption. Molecular recognition has its origin in the discovery of macrocyclic compounds, which were capable of selective binding of alkali ions, and is a field in supramolecular chemistry [60]. Usually, in optical probes for metal ions, the recognition process is generated by synthetic or natural receptors, so called ionophores or carriers [61, 62]. Application of the molecular cavities, or similar hosts in which ions could fit and bind selectively and reversibly, was a step forward towards the improvement of the selectivity of the probes.

Metal chelators and crown ethers are the forerunner of these types of selective host molecules. Further development led to more sophisticated organic molecules like podants, cryptands, spherands or calix(4)arenes [63]. Ionophores for metal ions take advantage of the high affinity of oxygen, nitrogen and sulfur donor atoms towards the ions. An effect that goes back to the principles of "hard and soft bases and acids" (HSAB) by Pearson [64]. Hence, Ag^+, Cu^+, Cd^{2+}, Hg^{2+} and Pb^{2+} are classified as soft acid and bind favorably to ligands containing sulfur; while the border line acids Ni^{2+}, Cu^{2+}, Co^{2+} and Zn^{2+} prefer binding to nitrogen. Figure 1.5 shows a selection of carriers bearing heteroatoms for the recognition of heavy metal ions.
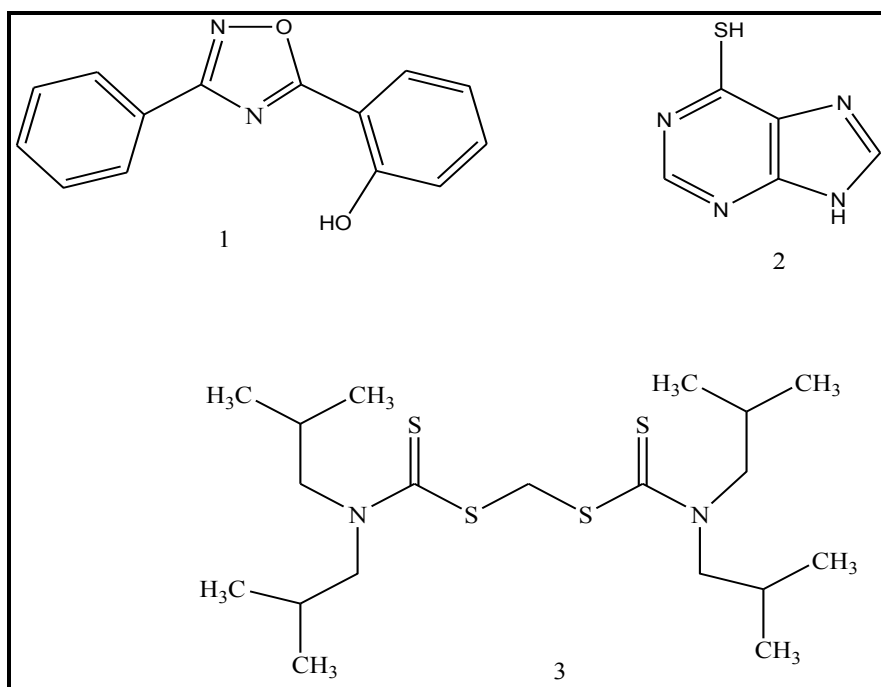
Figure 1.5: Examples of ionophores and chelators for heavy metals; 1: 2-(3-phenyl-1, 2, 4-oxadiazo-5-yl)phenol for Cu^{2+} ions 2: a purine derivative with high affinity for Hg^{2+}[65] 3: a dithiocarbamate derivative with high selectivity for Ag^+ and Hg^{2+}[66].

1.8.2 Schemes applied in molecular recognition

1.8.2.1 Probes based on chromophores and fluoroionophores

Diagnostic probes for the determination of cations based on complexation have gained popularity. A large number of metal indicators exist containing various groups with electron donating atoms for binding [67]. A prominent example is Xylenol Orange. The EDTA-type complexing agent undergoes different color changes on binding metal ions. The fluorescent counterpart calcein increases or decreases its fluorescence, besides its changes in color. To date, the field of supramolecular chemistry has brought to light new binding sites with improved selectivity. Logically, the idea of coupling the ionophores to chromophores or fluorophores emerged in the subsequent years, leading to the so-called chromoionophores and fluoroionophores [68].

Within the chromoionophores and fluoroionophores conjugates, the receptor part recognizes the ion and the chromophore/fluorophore signals the binding event by a change in its optical property. The indicator substances are often referred to as colorimetric or fluorescent probes and a variety are commercially available [69, 70]. Analytical test strips (colorimetric probes) for heavy-metal ions can provide simple and convenient procedures for on-site analysis and daily monitoring of water quality without using costly instruments. However, since the standard limit values of heavy metals in the environment and drinking water are remarkably low (ppb level), the detection limits of commercial test strips (ppm level) are insufficient to satisfy the required criteria. In addition, since they are generally prepared by soaking paper in the signaling reagent, leakage of reagent is facile, and hence reliability and sensitivity of detection are poor.

1.8.2.2 Optical probes based on dynamic quenching of fluorescence

The principle of dynamic fluorescence quenching has been widely studied. A theoretical description of fluorescence quenching is given in Chapter 2.2.1.1.4. One of the most investigated collisional (dynamic) fluorescence quencher is molecular oxygen [71]. Various

applications of quenchers have been reported [56, 72]. In the field of ion analysis, the dynamic quenching effect of halides on quinolinum and acridinium compounds is well-studied [73-75]. Approaches for the determination of chloride in blood [74], and the salinity of seawater [76], based on the effective quenching of immobilized lucigenin have been reported.

Both colorimetric and fluorescent molecular probes possessing appropriate functionalities have consistently demonstrated their potential to analyse cations, anions and neutral species, both qualitatively and quantitatively. The next chapter outlines detailed mechanisms of detection by fluorescent and colorimetric probes.

1.9 Objectives of the thesis

The overall goal of the thesis was to evaluate the potential use of electrospun nanofibers as solid supports for hosting optical probes for the detection of heavy metal ions in water. The specific aims of the thesis were;

i) To develop a fluorescent probe for the quantification of Ni^{2+} ions in water.

ii) To develop a colorimetric probe for the detection of Ni^{2+} ions based on silver-copper alloy nanoparticles hosted in electrospun nanofibers.

iii) To develop a colorimetric probe for the detection of Fe^{2+} ions in aqueous media by post-electrospinning modification of electrospun nanofibers.

Chapter 2 Diagnostic probes

2.1 Overview

This chapter presents literature review on the mechanisms, theory and examples of materials that have been used to fabricate optical probes. Also outlined in the chapter are materials such as chemo-responsive dyes, synthetic ligands and metal nanoparticles that have been used to fabricate optical probes.

2.2 Diagnostic probes for the determination of toxic metal ions

A large number of optical probes and test strips for heavy metals have been developed in the past and were extensively reviewed by Oehme and Wolfbeis [58]. More recent reports have dealt with metal indicators dispersed in plasticized poly(vinyl chloride) (PVC) [77, 78] or immobilized to ion exchange resins [79-81], and with ion exchange membranes [82]. Although extensive work has been carried out, sensing heavy metals still suffers from poor selectivity and reusability in most cases. New approaches take advantage of combinatorial methods [83] or chemometric tools [84], such as regression models or artificial neuronal networks, and gain selectivity from a response pattern of non-selective probes. The combinatorial methods run in parallel with developments in ion-selective electrodes, where chemometry has been employed for the determination of heavy metal ions [85]. The most significant methods make use of fluorescent reagents that can be quenched by metal ions or indicator dyes that can show color change in the presence of metal ions.

2.2.1 Fluorescent probes

Metal ions could have profound biological effects in animals and the environment even at extremely low concentrations, often less than 1 mg/L [14, 86, 87]. Therefore, it is important

to be able to detect transition metals at low concentrations so as to assess their impact on health and for environmental monitoring [88]. The development of such assay methods presents a significant challenge. There are many methods which are approved by the Environmental Protection Agency (EPA) to determine transition metal concentrations in drinking water [89]. While the methods do an excellent job in accurately detecting low levels of transition metals, they often require extensive sample preparation and expensive instrumentation, and thus less suited for routine analysis.

The development of other techniques having good specificity, sensitivity, as well as being inexpensive and fast is of great practical importance. One such approach that could be used to detect and quantify transition metal ions is the use of fluorescent organic probes. The fluorescence technique has added advantages over the other instrumental methods. It does not require extensive sample preparation and it is relatively fast. Intriguingly, specificity for particular metal ions can often be built into the technique. In fluorescence assays, the complexation of analyte results in either enhanced fluorescence intensity of the probe, an event that is also termed chelation-enhanced fluorescence (CHEF) or in decreased fluorescence intensity of the probe; chelation-enhanced quenching (CHEQ). For heavy metals chelation of closed shell ions, e. g. Zn^{2+} or Cd^{2+} results in CHEF, while CHEQ is usually observed with metals like; Cu^{2+}, Ni^{2+} or Hg^{2+}, due to open shell electron configuration or the heavy atom effect [90].

The most important mechanisms, signaling a recognition event of a fluoroionophore include, charge transfer (CT), photoinduced electron transfer (PET), energy transfer and excimer or exciplex formation or disappearance among others [68, 90-92]. Within intramolecular charge transfer probes, the analyte interacts directly with a ligand that is part of the fluorophore π-system. In the simplest form, the fluorophore contains an electron donating group conjugated to an electron withdrawing group able to undergo an intramolecular charge transfer on excitation by light. The intramolecular charge transfer leads to changes in the intensity of fluorescence or absorbance and consequently, simultaneous spectral shifts of absorbance or fluorescence are observed.

18

Fluorescent probes based on the PET mechanism involve, an internal red-ox reaction between the excited state of the fluorophore and another species which is able to donate or to accept an electron. The electron density of the free binding site quenches the fluorescence of the covalently linked fluorophore. In the bound state the electron density is reduced by the bound species and the quenching effect is observed. Unlike CT probes, only fluorescence intensity is affected. Therefore, a PET system can be regarded as a switch, where luminescence is switched on or off depending on the occupation of the host moieties [93]. Photoinduced energy transfer is observed for complexing bifluorophores consisting of a donor and an acceptor fluorophore, linked by a flexible spacer. Binding heteroatoms of the spacer decreases the distance between the two fluorophores and consequently, increases the efficiency of energy transfer. The transfer efficiency depends on the distance according to Förster´s theory [94].

The developments in supramolecular chemistry brought new receptors for metal ions. The ionophores linked with a fluorophore yield the so called fluoroionophores. Within the receptors, the recognition and transducing element is combined in one molecule. In literature, thiocrown ethers [95], aza-crown ethers [96], thiourea [97], thiadiazole [98], bithiazole [99], and azo derivatives [100], have been reported as recognition reagents. Most of the reagents, however, suffer from considerable disadvantages such as poor solubility, the need for an additional reagent, or, most importantly, the lack of selectivity, which makes their application difficult. Nevertheless, fluorescence is one of the most powerful transduction mechanisms that could measure chemical recognition events.

2.2.1.1 Fluorescence

Fluorescence is the emission of light by a substance that has absorbed light or any other electromagnetic radiation of a different wavelength. The light is emitted from singlet-excited states in which the electron in the excited orbital is paired (of opposite sign) to the second electron in the ground-state orbital. A return to the ground state is spin-allowed and occurs rapidly by emission of a photon. The emission rate of fluorescence is very fast;

typically 10^8 s^{-1}, so that a characteristic fluorescence lifetime is near 10 ns. Fluorescence spectral data are generally presented as emission spectra, which vary widely and are dependent upon the chemical structure of the fluorophore and the solvent in which it is dissolved [101, 102]. Processes which occur between the absorption and emission of light are usually illustrated by a Jablonski diagram [103].

2.2.1.1.1 Jablonski diagram

A typical Jablonski diagram is shown in Fig. 2.1. The ground, first and second electronic states are depicted by S_0, S_1 and S_2, respectively.
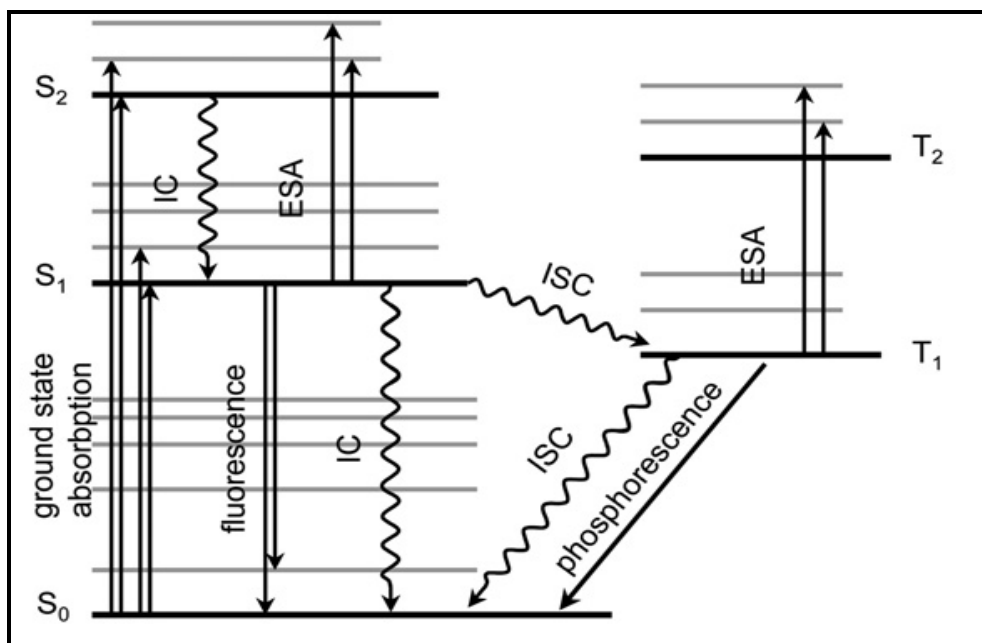
Figure 2.1: A simplified Jablonski diagram of organic dyes: IC-internal conversion, ESA-excited state absorption, ISC-intersystem crossing, fluorescence and phosphorescence [103].

At each of the electronic energy levels, the fluorophore can exist in a number of vibrational energy levels (denoted by 0, 1, and 2). Transitions between states are depicted as vertical lines to illustrate the instantaneous nature of light absorption. Transitions occur in about

10-15 seconds, a time too short for significant displacement of nuclei (Franck-Condon principle) [104]. Following light absorption, several processes usually occur including fluorescence, intersystem crossing or phosphorescence.

In fluorescence, a fluorophore is usually excited to some higher vibrational level of either S_1 or S_2. With a few rare exceptions, molecules in condensed phases rapidly relax to the lowest vibrational level of S_1. This process called internal conversion, is non-radiative and takes place in 10-12 seconds or less. A return to the ground state occurs to a higher excited vibrational ground-state level, which then quickly reaches thermal equilibrium. The consequence of emission to a higher vibrational ground state is that the emission spectrum is typically a mirror image of the absorption spectrum of the $S_0 \rightarrow S_1$ transition. Molecules in the S_1 state could also undergo a spin conversion to the first triplet state, T_1. Emission from T_1 is termed phosphorescence and is generally shifted to longer wavelengths (lower energy) relative to fluorescence. Transition from the T_1 to the singlet ground state is forbidden, and as a result, the rate constants for triplet emission are several orders of magnitude smaller than those for fluorescence. The transition from the first triplet state (T_1) to the singlet ground state is termed intersystem crossing.

2.2.1.1.2 Fluorescence technique

In fluorescence, suitable indicators which are sensitive to analyte concentrations and exhibit changes in fluorescence intensity are used as molecular recognition materials [104]. Recently, more and more attention has been paid to luminescent probes for various ions and molecules, particularly for heavy metal ions [105, 106]. Among chemosensory systems, fluorescent devices for the sensing and reporting of chemical species are currently of significant importance for chemistry, biology, and environmental science, due to the simple instrumentation, high selectivity, and direct visual perception even in very dilute solutions [107, 108]. For example, derivatives of 8-hydroxyquinoline have been used as sensitive and reliable tools to measure concentrations and fluctuations of cellular Mg^{2+} by comparing the enhancement of fluorescence with analyte concentrations [109]. Also, boradiazaindacene

as the fluorophore with 4-(bis(pyridin-2-ylmethyl)amino)-benzaldehyde was employed for intracellular emission fluorescent Cd^{2+} probe based on the internal charge transfer (ICT) mechanism [110, 111]. Other examples involve a fluorescence response system with poly[*p*-(phenyleneethynylene)-*alt* (thienyleneethynylene)]. It showed varying fluorescence "turn-on" behavior in the presence of cations including Li^+, Na^+, K^+, Mg^{2+}, Ca^{2+}, H^+, Mn^{2+}, Fe^{2+}, Co^{2+}, Ni^{2+}, Zn^{2+}, Cd^{2+} and Hg^{2+} [112].

Designing sensitive and selective fluorescent probes is a versatile and widespread approach for chemists [113-115]. The design and synthesis of fluorescent probes are mainly based on fluorescence enhancement and fluorescent quenching modes, which are obtained by employing photoinduced energy transfer, photoinduced electron transfer, enhanced spin-orbit and excited state intramolecular proton transfer [109, 116-118].

2.2.1.1.3 Modes of fluorescence detection

For transition metal ions to be detected by fluorescence there must be some observable change in the fluorescence emission by the fluorophore. There are three ways by which detection can be achieved (Fig. 2.2). The first mode is fluorescence enhancement that involves the use of a fluorophore that has little or no fluorescence in the absence of the target metal ion but becomes fluorescent or more fluorescent in the presence of the metal ion. Such an increase in fluorescence efficiency could result from conformational restriction induced upon binding [119, 120].
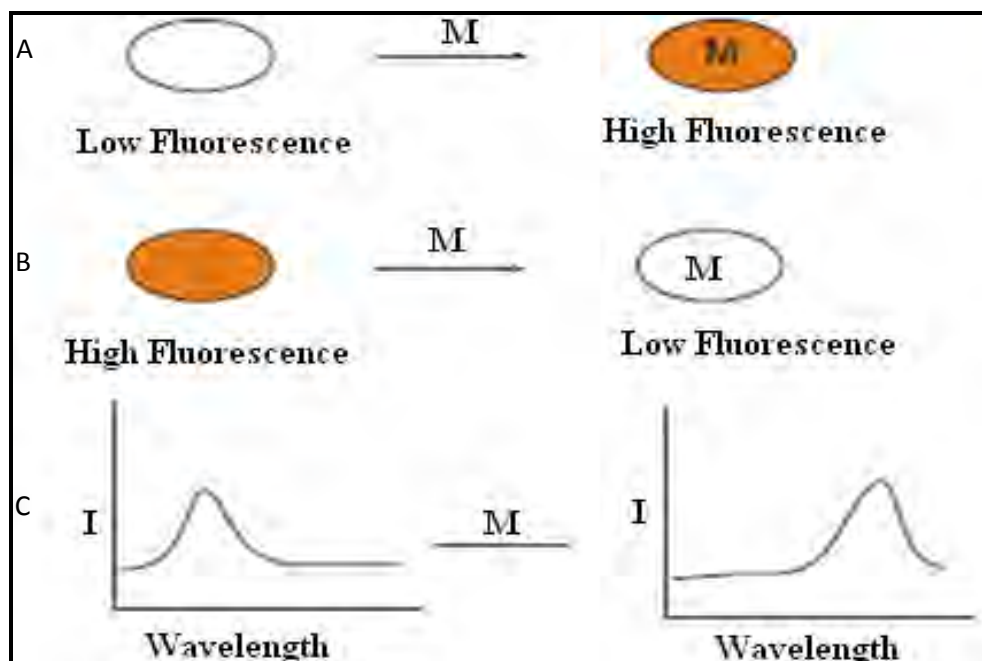
Figure 2.2: Illustration of methods of fluorescence detection where (A) represents fluorescence enhancement, (B) fluorescence quenching, (C) λ_{max} shift, I is fluorescence intensity and M = metal ion [121].

The second approach is fluorescence quenching. Fluorescence quenching involves the selection of a molecule that has a higher fluorescence in the absence of the target metal ion but, greatly reduced or no fluorescence when the target metal ion is present. Many transition metals are known to be fluorescence quenchers [122, 123], and they can quench fluorescence through energy transfer [117, 124], or electron transfer mechanisms [124]. The third approach involves a shift in the emission maximum of the spectrum depending upon whether the target metal ion is present or not [121]. Part of the thesis work was focused on the development of a fluorescent probe for nickel (II) ions in aqueous media through quenching of fluorescence.

2.2.1.1.4 Theory of fluorescence quenching

Fluorescence quenching refers to any process that decreases the fluorescence intensity of a substance. There are a wide variety of quenching processes that include; excited state reactions, molecular rearrangements, ground state complex formation and energy transfer. Quenching-based fluorescence probes utilize Stern-Volmer bimolecular quenching kinetics [125] as shown in eqns 2.1-2.3.

$$F + h\nu \rightarrow F * \qquad\qquad (2.1)$$

$$F* \rightarrow F + h\nu \qquad\qquad k_1 \qquad (2.2)$$

$$F* + Q \rightarrow F + Q * \qquad k_2 \qquad (2.3)$$

Where F is fluorophore, Q is a quencher, k_1 is the rate constant for unimolecular decay of the excited-state F*, and k_2 is the rate constant for the bimolecular quenching process by Q that can deactivate the excited state. On photoexcitation, fluorophore electron is excited from the highest occupied energy band (the π*-bond) leaving a `hole' which is the empty state in the π-bond (eqn 2.1). When the excited electron recombines with the hole, a photon is emitted (photoluminescence, eqn 2.2). Relatively, when the excited electron of fluorophore transfers to a quencher (nearby cationic electron acceptor) and the electron and the hole are separated, the luminescence is quenched (eqn 2.3). The kinetic scheme gives the well known Stern-Volmer equation (eqn 2.4)

$$I_0/I = 1 + K_{sv}[Q] \qquad\qquad (2.4)$$

Where, I_0 is the fluorescence intensity in the absence of the quencher, I is the intensity when the quencher is present, K_{sv} is the Stern-Volmer constant, and [Q] is the quencher

concentration. A linear calibration curve results for a plot of I_0/I versus [Q]. There are two basic types of quenching: static and dynamic (collisional). Both these types require an interaction between the fluorophore and quencher [126].

2.2.1.1.4.1 Collisional (dynamic) quenching

In the case of dynamic quenching the quencher must diffuse to the fluorophore during the lifetime of the excited state. Upon contact the fluorophore returns to the ground state without emission of a photon (Fig. 2.3). Collisional quenching occurs when the excited-state fluorophore is deactivated by contact with some other molecule in solution, which is called the quencher.
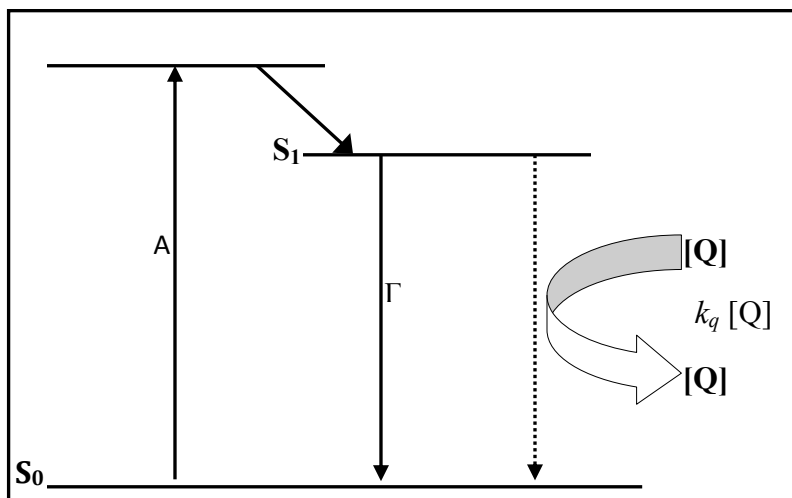
Figure 2.3: Simplified Jablonski diagram for dynamic quenching where S_0 is fluorophore ground electronic state, S_1 is fluorophore first excited state, A is absorption, Γ is radiative decay rate, kq is bimolecular quenching rate constant and [Q] is quencher concentration.

The molecules are not chemically altered in the process. For collisional quenching, the decrease in intensity is described by the ratio of the fluorescence in the absence of the quencher to the presence of quencher by the Stern-Volmer equation:

$$\frac{F_O}{F} = 1 + K[Q] = 1 + kq\tau_o[Q] \qquad (2.5)$$

Where F_0 and F are the observed fluorescence in the absence and presence of quencher respectively, K is the Stern-Volmer quenching constant, kq is the bimolecular quenching constant, τ_0 is the lifetime in the absence of quencher, and $[Q]$ is the quencher concentration. The Stern-Volmer constant is sometimes abbreviated as K_{SV} or even as K_D [101].

2.2.1.1.4.2 Static quenching

In the case of static quenching a complex forms between the fluorophore and the quencher in the ground state, and the complex is non-fluorescent (eqn 2.6).

$$\text{F + Q} \rightleftarrows \text{F-Q}$$

Fluorescent   non-fluorescent
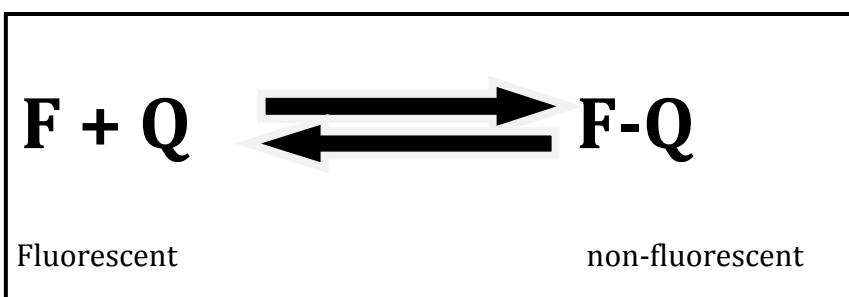
Equation 2.6: Formation of a fluorophore-quencher complex in the ground state.

The formation of the complex does not rely upon the population of the exited state. The dependence of the fluorescence intensity upon quencher concentration for static quenching is derived by consideration of the association constant for complex formation (eqn. 2.7).

$$K_s = \frac{[FQ]}{[F][Q]} \qquad\qquad (2.7)$$

Where, K_S is the fluorophore-quencher association constant, $[FQ]$ is the concentration of the complex, $[F]$ is the concentration of the uncomplexed fluorophore, and $[Q]$ is the concentration of quencher. Since the total concentration of the fluorophore, F_T is given by; $[F]_T = [F] + [FQ]$, the static quenching constant can be written as:

$$K_s = \frac{[F]_T - [F]}{[F][Q]} = \frac{[F]_T}{[F][Q]} - \frac{1}{[Q]} \qquad\qquad (2.8)$$

Equation 2.8 rearranges to:

$$\frac{[F]_T}{[F]} = 1 + K_s[Q] \qquad\qquad (2.9)$$

By recognizing the fluorescence signal in the absence of quencher, F_0 would correspond to the total concentration of fluorophore. One can substitute the fluorescence intensities F_0 and F for the total and free concentrations $[F]_T$ and $[F]$, respectively to obtain:

$$\frac{F_O}{F} = 1 + K_s[Q] \qquad\qquad (2.10)$$

Equation 2.10 is equivalent to the linear equation for dynamic quenching (eqn. 2.5).

2.2.1.1.4.3 Difference between dynamic (collisional) and static quenching

In the previous sections (2.2.1.1.4.1. and 2.2.1.1.4.2.) the mechanisms of collisional and static quenching were described. Regarding equations 2.5 and 2.9, fluorescence intensity

data are insufficient to distinguish between static and dynamic quenching. The most effective way to differentiate the two processes is to measure their fluorescence decay time, since in case of static quenching a fraction of fluorophores is removed by complex formation and this, of course, does not affect fluorescence lifetime [127, 128]. Besides investigation of the fluorescence lifetime, the static and dynamic quenching could be distinguished by recording Stern-Volmer plots at different temperatures [128].

2.2.1.1.4.4 Stern-Volmer plot

Both static and dynamic quenching can have a linear Stern-Volmer plot. Static and dynamic quenching could be distinguished from each other by their dependences on temperature, viscosity or lifetime measurements [128]. An increase in temperature leads to an increase in the diffusion constant of a quencher and will lead to an increase in collisional quenching.

In contrast, an increase in temperature would lead to a decrease in the binding constant of quencher for fluorophore and result in a decrease in quenching for a static quencher (Fig. 2.4). A linear Stern-Volmer plot is generally indicative of a single class of fluorophores that are all equally accessible to the quencher. If two fluorophore populations are present, and one class is not accessible to quencher, then the Stern-Volmer plots deviate from linearity toward the x-axis (downward) [129].
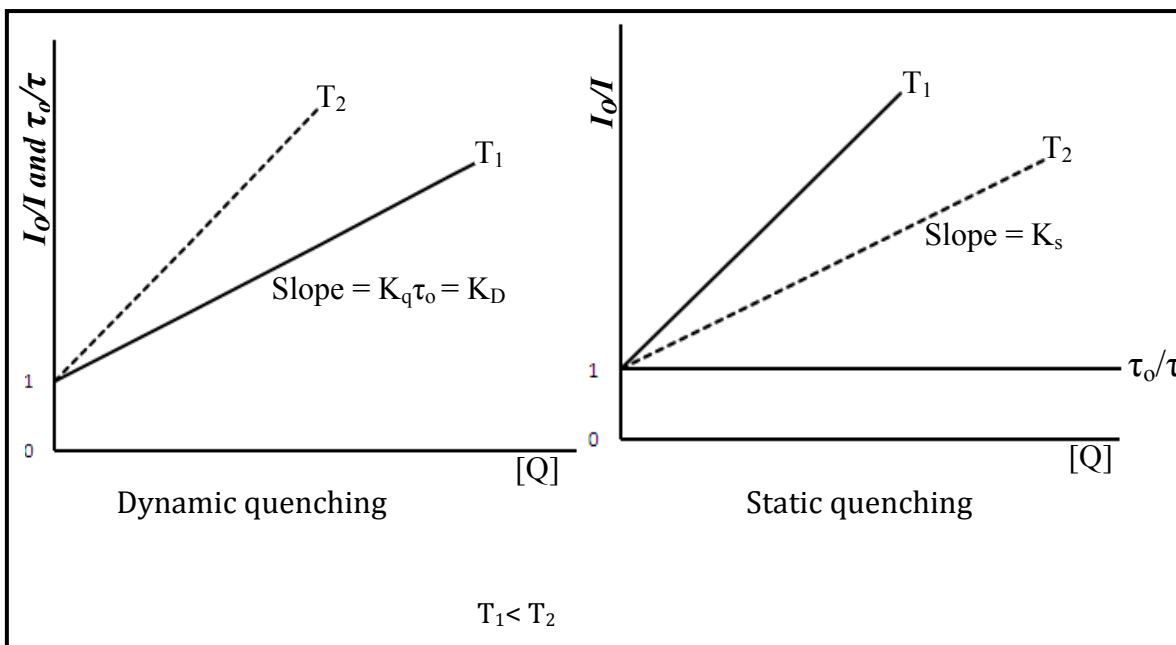
Figure 2.4: Temperature dependence on quenching constants. For dynamic quenching, $\tau_o/\tau = I_0/I$ and for static quenching $\tau_o/\tau = 1$, where τ is the fluorescence lifetime, τ_o is the fluorescence lifetime in the absence of the quencher, I_o and I is the fluorescence intensity in the absence and presence of the quencher respectively, k_q is bimolecular quenching constant, K_D is Stern-Volmer constant, K_S is the complex formation constant and [Q] is the concentration of the quenching molecule.

Another possibility for differentiating dynamic and collisional quenching is by investigating the absorption spectra of the fluorophore in the presence of the analyte. In the case of dynamic quenching the quencher must diffuse to the fluorophore during the lifetime of the excited state. Since collisional quenching has impact on molecules when on the excited state, no variation in the spectra should be observed. For static quenching, the complex has a different absorption spectrum from the fluorophore. The presence of an absorption band shift is therefore diagnostic of this type of quenching.

While fluorescence is a relatively better technique compared to the other instrumental techniques, it still requires a fluorometer or at least electricity. This renders fluorescence insufficient for online monitoring especially in resource-poor settings. Hence, there is a need to develop simpler methods that are sensitive and selective as well as capable of use by technicians preferably in the field.

Recently, colorimetric sensing of metal ions has been shown to be a less labor-intensive, alternative to techniques based on fluorescence [130]. It is well known that solid materials that change their color upon recognition of macromolecules are widely accepted for fingerprinting or conducting pregnancy tests at home [131]. The throughput of the testing was profoundly advanced by the elimination of instrumental requirements and organic solvents. The idea could be extended towards developing colorimetric probes for simple visual detection of trace environmental toxins such as toxic metal ions.

2.2.2 Colorimetric probes

Colorimetric probes could be defined as molecules of biotic and abiotic origin that bind selectively with the analyte with concomitant change in color [132-134]. Although the use of colorimetric detection method is a less advanced approach, it is gaining increased attention due to its simplicity, rapidity, high sensitivity and ease of measurement. It is simple to use in comparison with other spectroscopic methods as it can give simple visual results for "naked-eye" detection [135]. Therefore the approach is attractive as a sensing method. Colorimetric probes, as the name would suggest, are based upon the detection of an analyte-induced color change in the materials [58, 136, 137]. Hence they can overcome the limitations caused by the traditional instrumental methods because no sophisticated instrumentation or sample preparation is required in their procedures. Colorimetric probes are extremely attractive since signaling the targeted event can be visualized and thus can make on-site, real-time detection possible [138, 139]. Not only does the obvious color change of the sample make the testing direct and convenient, the linear relationship between the concentration of the analyte and the absorbance also gives steady, quantitative results [140].

2.2.2.1 Technique of detection by colorimetric probes

In colorimetric probes, the incorporation of an optical signaling moiety in close proximity to a host binding site enables the host to be used as a prototype for a target guest species as binding would perturb its electrochemical and/or photophysical properties. Hence a bathochromic or hypsochromic shift of absorption spectra or visual color change is affected by the respective increase or decrease in electron densities on the chromophore moiety (Fig. 2.5). The change in electron densities is more effectively carried out by the association of a charged analyte, i.e., cation or anion than a neutral molecule. So, most of the chromogenic probes are available for charged guests [133].
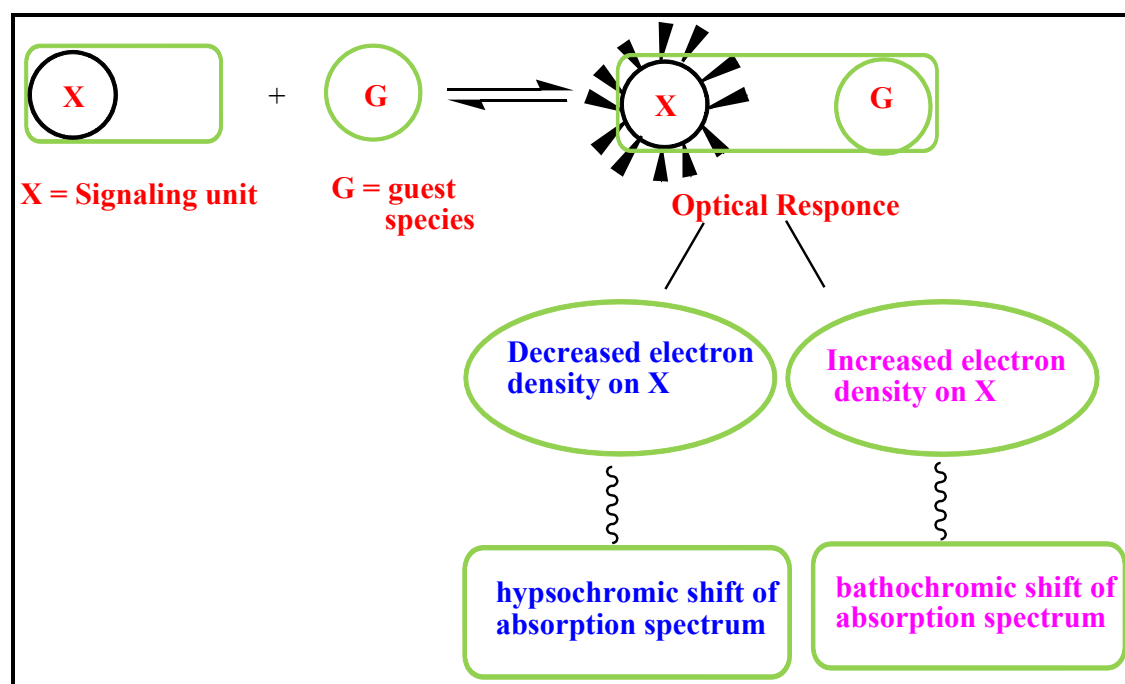
Figure 2.5: Schematic presentation of hypsochromic and bathochromic shifts in colorimetric probes [141].

Colorimetric probes seem to be very promising in the development of low cost, simple-to-use and in the field diagnostic tools for metal ions. A number of materials such as chemo-

responsive dyes, ligands and metal nanoparticles have been used for the development of colorimetric probes.

2.2.2.2 Chemo-responsive dyes

Chemo-responsive dyes are dyes that change color, in either reflected or absorbed light upon changes in their chemical environment. Consequently, chemo-responsive dyes have been utilized to develop colorimetric probes for various analytes. The consequent dye classes that display these requirements are (1) Lewis acid/base dyes (i.e. metal ion containing dyes), (2) Brønsted acidic or basic dyes (i.e. pH indicators), and (3) dyes with large permanent dipoles (i.e. zwitterionic solvatochromic dyes). Disposable colorimetric arrays of chemo-responsive dyes have been created by printing the dyes on various inert solid supports, e.g. reverse phase silica gel plates, acid-free paper, or porous membranes of various polymers e.g. nylon [142].

2.2.2.2.1 Classification of dyes

Dyes could be classified according to their chemical structures, their usage or application method. The former approach is adopted by practicing dye chemists, who use terms such as azo dyes, anthraquinone dyes, and phthalocyanine dyes. The latter approach is used predominantly by the dye user, who would speak of reactive dyes for cotton and disperse dyes for polyester. Very often, both terminologies are used, for example, an azo disperse dye for polyester and a phthalocyanine reactive dye for cotton [143].

The most appropriate system for the classification of dyes is by their chemical structure and it has many advantages. First, it readily identifies dyes as belonging to a group that has characteristic properties, for example, azo dyes (strong, good all-round properties, cost-effective) and anthraquinone dyes (weak, expensive). Second, there are a manageable number of chemical groups (about a dozen). Most importantly, it is the classification used

most widely by both the synthetic dye chemist and the dye technologist. Thus, both chemists and technologists can readily identify with phrases such as an azo yellow, an anthraquinone red, and a phthalocyanine blue [144]. Based upon their use, some dyes have been classified as indicator dyes.

2.2.2.2.1.1 Indicator dyes

As early as 1660, Boyle observed that certain plant extracts changed their color on treatment with acid or base. This effect is well known to gardeners in the case of hydrangea (hortensia): the color of its blossoms can be changed by watering it with slightly acidic or alkaline water. The first indicator dye which came into use was *litmus*, which was isolated from the orseille lichen; *Roccella tinctoria* [145]. It changes its color from red (acid) to blue (alkaline). The systematic investigation of natural colors led to the discovery of several dyes and dye classes which are able to change their color. Thus, it was found that the origin of the color of hydrangea blossoms is an *anthocyan* dye [146]. Interestingly, in nature these dyes are not always and necessarily used as indicators. The red color of roses and the blue color of the cornflower are based on the same molecule (*anthocyan*), which *in vitro* reacts as an indicator dye [147]. In the plants (*in vivo*) however, this dye does not change color. With the introduction of titration into the arsenal of analytical methods, an increasing need arose for means to detect end-points of reactions. This need stimulated the search for indicator dyes, and consequently synthesis of dyes begun. As a result, most indicator dyes are now synthetic. Synthetic dyes that have been produced as ligands for heavy metals include crown ether, cryptand and spherand structures.

In general terms, an indicator dye can be characterized as follows: (1) It shows different optical properties when the system of which it forms a part changes its status, and (2) leads to a reversible change. The first property means that the indicator molecule reacts as a part of the system. The second property in particular distinguishes indicator dyes from color forming reagents. The latter are widely used in reactions in which colors are formed by chemical or biochemical (mostly enzymatic) reactions between the analyte and added

reagents. The reactions are widely used in analytical and diagnostic test kits but are normally not reversible. The different optical properties mentioned are clearly linked to structural properties: a change in optical properties also indicates a change of molecular structure. The most important structural changes for indicator dyes are (1) Reversible transition between acid and base form of a molecule (pH indicator), (2) Reversible transition between reduced and oxidized forms of a molecule (redox indicator), and (3) Reversible transition between the free molecule and its complex with a cation (metal indicator) [148, 149].

2.2.2.2.1.2 Metal indicators

Metal indicators are organic molecules which form specifically colored soluble complexes with metal ions in aqueous media. Here, the color of the complex and of the free indicator must be different. These reactions can be used in two analytical procedures: volumetry (complexometry) and colorimetry/photometry. In both methods, the concentration of metal ions could be determined, but with different techniques. Colorimetry/photometry exploits the fact that the color intensity of the complex correlates to the metal ion concentration, at least within a certain concentration range. Therefore, sufficient indicator is added to the sample that the indicator forms a colored complex with all ions of the metal of interest in solution. The color intensity of this complex is then either compared visually against the color of reference samples (colorimetry) or the color intensity is measured at a defined wavelength with an instrument and then compared with a calibration curve (photometry). Due to different requirements of the two methods, indicators for metal determination in colorimetry/photometry and volumetry/complexometry are different (Table 2.1).

Table 2.1: Metal indicators: importance of parameters for different application areas [143].

Parameter	Colorimetry/photometry	Volumetry/complexometry
Sensitivity	Very important (detection of metals in the ppm and ppb range)	Not very important
Selectivity	Very important (ideally, an indicator detects only one metal)	Important
Complex stability as a function of time	Very important (ideally hours to days)	Not too important (hours)
Complex stability against other reagents	Important	Must be lower compared to titrants
Color difference between free and complexed indicator	Less important photometry, Quite important (colorimetry)	Very important

The main challenge with metal indicators is selectivity. Most of them form complexes with more than one metal. But selectivity can be improved by optimizing the reaction conditions either by addition of buffers or masking reagents. Nevertheless, researchers have developed many selective reagents in the last four decades that could form complexes only with specific metals.

2.2.2.2.1.2.1 Chemical structures of metal indicator complexes

The complexes formed by the metal indicator and the metal ions contain an electron donor and an electron acceptor part. If the donor molecule (ligand) contains two or more atoms with donor properties, the complex is known as a *chelate*. Most organic complexing agents can be regarded as *bidentate* ligands (they contain two donor atoms) and form five- or six-

membered chelate rings. The electron-donating atoms in these chelates include oxygen, nitrogen, and sulfur. The other part of the molecule may vary and the difference can significantly influence its binding characteristics. For instance both diacetyldioxime and 1,10-phenanthroline contain the same donor atom configuration (Fig. 2.6).

Diacetyldioxime (dimethylglyoxime)   1,10-phenanthroline
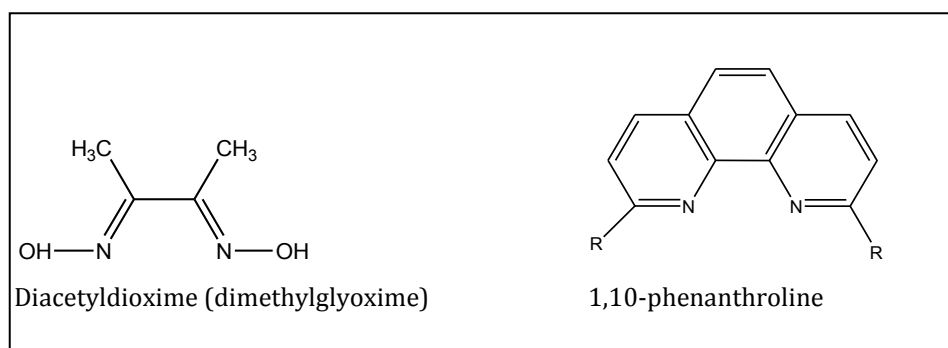
Figure 2.6: Examples of organic complexing agents.

While diacetyldioxime is highly specific for nickel and palladium, if the same donor atom configuration is incorporated into a heterocyclic system, as in the phenanthroline, the ligand becomes specific for copper and iron. The selectivity can be directed by choice of the substituent R in the molecule: if $R = H$, the ligand is specific for iron; with $R = CH_3$, and/or C_6H_5, the ligand is copper-specific. Some of the metal indicators have been reported in literature as reagents in photometric or visual test kits for the detection of metals [57]. These molecules act like color-forming reagents but are still indicators and they can be referred to as chemo-responsive dyes. Apart from natural and synthetic dyes that have been used to fabricate colorimetric probes, nanotechnology has brought in more fascinating materials**.**

Nanotechnology, nanoscience, nanostructures, nanoparticles are now some of the most widely used terms in materials science literature. But why are nanoscale materials and processes so attractive? From the point of view of the general public, nanotechnology appears to be the fabrication of miniature machines, which would be able to travel through the human body and repair damaged tissues, or supercomputers small enough to fit in a

pocket. However, nanostructured materials have potential applications in many more areas, such as biological detection, controlled drug delivery, low-threshold lasers, optical filters and colorimetric probes among others. Nanoparticles (NPs) are one of the most important class of nanomaterials owing to their unique properties hence wide applications.

2.2.2.3 Nanoparticles

Nanoparticles are defined as any material with at least one dimension in the 1-100 nm range. The shape may vary (it does not have to be spherical) and the materials include metals, semiconductors, polymers and carbon based materials [150]. A recent review by Zamborini *et al.* covered the use of NPs in measurement science showing their various applications in the traditional disciplines of analytical chemistry, including spectroscopy, electrochemistry, and separations, as well as in several sensor technologies [151]. One amazing class of nanomaterials that has been widely explored is the metal nanoparticles. The optical properties of these nanoparticles are spectacular and, therefore, have promoted a great deal of excitement during the last few decades. In fact, it is relatively easy to find examples of the use of metal nanoparticles (maybe not deliberately) as decorative pigments since the time of the Romans.

2.2.2.3.1 History of metal nanoparticles

Metal nanoparticles have been in use for a long time, for example, Lycurgus Cup, which displayed unique colors, as well as the Damascus steel, which was used to make swords [152, 153], became renowned [154], because of (1) its extreme strength, (2) the sharpness, (3) the resilience, and (4) the beauty of the characteristic surface pattern [155, 156]. The fascinating blade story is that it could cut clean through rock and still remain sharp enough to cut through a silk scarf dropped on the blade. Many scientists tried to investigate the source of these special properties and they encountered the presence of multiwall carbon

nanotube (MWNTs) in the steel [153, 157]. The famous Glass Lycurgus Cup (Fig. 2.7) from the Romans times (4th century AD) contains silver and gold nanoparticles in approximate ratio 7:3, which have diameters of about 70 nm [158]. The presence of these metal nanoparticles gives special color display for the glass. When viewed in reflected light, for example in daylight, it appears green. However, when a light is shone into the cup and transmitted through the glass, it appears red. This glass can still be seen in the British museum.

Even though, nanoparticles were being used so many decades ago, nobody realized that the materials were in nanoscale range. But after the development of modern devices that could analyze materials in the nanoscale range, nanotechnology became an interesting subject to scientists.

Figure 2.7: The Lycurgus Cup (a) green color, if light source comes from outside of the cup (b) red color, if the light source comes from inside of the cup [159].

2.2.2.3.2 Metal nanoparticles

Metal nanoparticles are very attractive because of their size and shape dependent properties. Metal nanoparticles particularly silver and gold nanoparticles with well-controlled size have recently been the focus of great interest because of their color changes. The color changes are associated with their surface Plasmon absorption band which is dependent on a number of parameters such as the size and shape of the particle, the adsorbed species, the dielectric properties of the medium, and the distance between particles [160]. These nanoparticles have been used with great success for the detection of a range of analytes such as metal ions [161]. For color signal generation, metallic nanoparticles are particularly attractive; as they possess much higher extinction coefficients compared to organic dyes, allowing sensitive colorimetric detections with minimal material consumption [161, 162].

More importantly, metallic nanoparticles display distance-dependent optical properties [163]. For example, dispersed gold nanoparticles (AuNPs) are red in color, while aggregated ones are purple or blue. Colorimetric probes using metal nanoparticles for instance have been widely explored and have important applications in the sensitive detection of metal ions [164-166]. The metal nanoparticles based colorimetric assays do not utilize organic co-solvents, enzymatic reactions, light-sensitive dye molecules, lengthy protocols, or sophisticated instrumentation thereby overcoming some of the limitations of more conventional methods. One of the studies conducted in this thesis was the development a colorimetric probe for Ni^{2+} ions based on silver-copper alloy nanoparticles (Ag-CuNPs).

2.2.2.3.2.1 Silver and copper nanoparticles

Of the three metals (Ag, Au, and Cu) that display plasmon resonances in the visible spectrum, Ag exhibits the highest efficiency of plasmon excitation. Moreover, optical excitation of plasmon resonances in nanosized Ag particles is the most efficient mechanism

by which light interacts with matter. A single Ag nanoparticle interacts with light more efficiently than a particle of the same dimension composed of any known organic or inorganic chromophore. The light-interaction cross-section for Ag can be about ten times that of the geometric cross-section, which indicates that the particles capture much more light than is physically incident on them. Silver is also the only material whose plasmon resonance can be tuned to any wavelength in the visible spectrum [167].

Copper on the other hand costs significantly less than silver and gold, therefore, it is economically attractive. Copper nanoparticles, due to their unique physical and chemical properties and low cost preparation, have been of great interest recently. Copper nanoparticles have great applications in heat transfer systems [168], antimicrobial materials [169], super strong materials [170], sensors [171], and catalysts [172]. The key to metal nanoparticles colorimetric sensing platform is the control of their dispersion and aggregation behavior. To control the inter-particle distance, several stabilizing and capping agents have been used to direct the growth of nanoparticles during synthesis.

2.2.2.3.2.2 Stabilization and functionalization of metal nanoparticles

Because of their small size, nanoparticles have a very high surface area to volume ratio resulting in high reactivity and the need for stabilization. When nanoparticles are not stabilized they will generally undergo a process known as "Ostwald Ripening". Ostwald Ripening describes the tendency for smaller particles to merge into one another until one large particle remains [173]. To avoid aggregation, various stabilizers have been used.

For further application of metal nanoparticles, attaching the molecular recognition motifs (i.e. functional groups) of interest to the nanoparticle surface has to be readily achieved. Most importantly, they must not bind non-specifically to each other or to anything else present in the system under investigation. In addition, introducing multiple functionalities would be of great value, as it provides more flexibility for multiplexing in analytical applications and new tools to control the bottom-up assembly of nanostructures.

Functionalization and stabilization of nanoparticles has been extensively explored [174, 175].

Though inorganic species and small organic ligands are indispensable tools for stabilization of nanoparticles, synthetic polymers have also played a role as a stabilizer. Previously, stabilizing agents were low-molecular organic compounds (carbonic acids, alcohols, amides) and natural polymers (gelatin, agar-agar, starch, cellulose and so on). At present, synthetic polymers are more frequently employed. Synthetic polymers solve the limitations of nanoparticle stabilization and introduction of a polymer ingredient into the nanocomposite [176].

2.2.2.3.2.2.1 Synthetic polymers and organic ligands as stabilizing agents

As stabilizing agents for nanoparticles, polymers provide several possible advantages over small molecule ligands. Because polymers consist of multiple repeating units, each of which can display ligand functionality, they have a much greater potential degree of multivalency and also allow for the ready incorporation of multiple types of ligand functionality [177, 178]. While small molecule ligands typically require very strong affinities for nanoparticle surface sites to ensure nanoparticle stability, the multivalency of polymer ligands enables the use of other ligating species e.g., pyridines which can bind metal ions [179]. For environmental applications, surface functionalization of metal nanoparticles is essential to apply them for selective detection of a specific heavy metal.

The developments in the fields of fluorescence and colorimetric techniques have seen the emergence of immobilized signaling molecules into solid supports [180]. Solid state fluorescent probes can be obtained by the incorporation of the fluorophores or chromophores to an ion permeable matrix. Three general methods are widely applied, namely physical, electrostatic and covalent immobilization [56]. The proper choice of a solid support is very important and is governed by parameters such as suitability for dye immobilization, mechanical stability, and permeability for the analyte [181]. Furthermore,

immobilization may shift spectra, *pKa* values, fluorescence lifetimes and dynamic ranges, as well as binding or quenching constants of the indicators. For this reason, various support materials for their immobilization have been employed [182]. The next chapter gives a detailed literature review of some of the solid supports that have been used for the immobilization of optical probes.

Chapter 3 Support materials for the incorporation of optical probes

3.1 Overview

Chapter 3 presents background information on the solid materials that have been used to incorporate signaling reagents. The emphasis is on the use of electrospun polymeric nanofibers as support. The chapter is therefore divided into three sections: (1) Solid supports for diagnostic probes, (2) Polymers as supports for diagnostic probes, and (3) Techniques for producing nanofibers. The chapter also outlines some methods that can be used to post-functionalize polymeric electrospun nanofibers in order to achieve the desired selectivity.

3.2 Solid supports

Solid state optical probes (diagnostic probes) are usually obtained by immobilizing the signaling reagents on solid supports. Several different support materials including lipophilic polymers and plasticizers, hydrophilic polymers, ionic polymers, sol-gel glass and molecularly imprinted polymers have been used for the preparation of diagnostic probes [182-187]. The choice of solid support and incorporation of the indicator into the support has significant impact on the performance of the probes in terms of selectivity [188], sensitivity, response time and stability [189]. Table 3.1 gives a summary on the use of solid supports in designing diagnostic probes.

Table 3.1: Solid supports used in designing diagnostic probes.

Type of probe	Solid support used	Fields of applications	Special features	Ref.
Colorimetric	Polyacrylonitrile (PAN)	Detection of Hg^{2+}, Pb^{2+}, Cd^{2+}, Zn^{2+}, Ni^{2+} and Cu^{2+}	Ethylenediamine immobilized on PAR fibers	[190]
Colorimetric	Agarose film coated glass slide (ACGS)	pH indicator	Two dyes covalently immobilized on ACGS to form a long life probe	[191]
Colorimetric	Polyvinyl chloride	Detection Cd^{2+}, Pb^{2+} and Hg^{2+} ions	Films of polymer prepared via LB deposition and solid PVC strips anchored with probe molecular assemblis	[131]
Colorimetric	Polystyrene	Detection Fe^{3+}, Sn^{2+}, Fe^{2+} and Ag^+	Polymeric chemosensor bearing the side chain donor-acceptor chromophores	[192]
Fluorescent	Poly(acrylic acid)	Determination of Fe^{3+} and Hg^{2+}	Electrospun nanofibers with covalently linked fluorescent reagent	[193]
Fluorescent	Poly(methyl methacrylate) and ethyl cellulose	Determination of Cu^{2+}	Electrospun nanofibers of polymer blends with physically immobilized fluorescent dye	[194]
Fluorescent	Ethyl cellulose	Determination of Hg^{2+}	Electrospun nanofibers with physically immobilized fluorescent dye	[195]

Because their chemical and physical properties may be tailored over a wide range of characteristics, polymers find use in sophisticated electronic measuring devices such as diagnostic probes. During the last 15 years, polymers have gained tremendous recognition in the field of artificial sensors with the goal of mimicking natural sense organs. Polymer membranes have the advantage of being rapidly penetrated by analytes and in contrast to glass-immobilized materials. Furthermore, they can more easily be fabricated and handled.

3.2.1 Polymers as supports for optical probes

Polymers are commonly used in optical probes as inert supports for indicator dyes to keep the molecules apart and allow for exposure to analytes and to maintain the peculiar optical properties of the sensitive dyes. Polymers impregnated with solvatochromic dyes or fluorophores are a common practice in the development of diagnostic probes where they have been used to detect the presence of a large number of different volatile compounds [196]. Nonetheless, in the applications, the polymeric matrix is limited to retain the indicator in place and to favor the diffusion of analyte molecules to the sensing molecules. However, the polymer properties may affect the characteristics and performances of the signaling reagent as well as the resulting optical probe [197].

Polymers are convenient due to the fact that they can easily be processed into small particles and thin films that can be deposited onto optical fibers [198], and waveguides [199, 200] for fabrication of optical probes. The presence of polymers in current technology is based on the enormous possibilities to tailor their chemical and physical characteristics. The properties include the chemical reactivity of polymers that could be altered to cope with different kinds of interactions and bind a large number of chemical compounds with controlled properties [201]. Suitable chemical functionalization can also efficiently orient their properties towards certain classes of chemicals to achieve high selectivity.

Polymers used in the development of diagnostic devices either participate in the sensing mechanism or they are used to immobilize the component responsible for analyte sensing. The use of polymers for different physical, chemical and biochemical sensing applications was reviewed by Adhikari and Majumdar [202]. During the last two decades, chemical indicators have been immobilized in polymeric matrices mainly by simple impregnation [203], by doping [204], or by covalent attachment [205]. Other strategies such as electrostatic layer-by-layer assembly have also been used [206].

3.2.1.1 Incorporation of chemical indicators into polymer matrix

3.2.1.1.1 Physical incorporation of chemical indicators into polymers

Physical entrapment of the dyes in the polymer matrix is the simplest method for immobilization of dyes and indicators into polymer materials. Indicators (which can be dyes or ligands) statically immobilized on solid supports such as ion exchangers [184, 185], are easy to fabricate although they suffer from numerous disadvantages such as; swelling, hysteresis, dye leaching and inhomogeneity of the material. Nevertheless, the method is widely used for the preparation of sensitive thin films or microspheres [207, 208]. Polymeric thin films with embedded organic dyes are also very often immobilized on the tip of optical fibers to perform the sensing measurements [209].

The specific incorporation of fluorescent probes in polymers has been recently reviewed by Bosch *et al.* [210]. Entrapment of organic dyes and transition metal complexes onto polymers has also been used to design probes for sensing O_2 [208, 211]. Yang and co-workers recently reported the immobilization of pyrene-labeled metalloporphyrins in a plastized poly(vinyl chloride) (PVC) membrane for the sensing of imidazole derivatives such as histidine [212]. Approaches based on dye-doped thin films have been used in the analysis of organic vapors [213-215], the detection of metal ions [216-218], and the determination of pH [219, 220]. It could be the reason as to why such materials have rarely been incorporated into commercial instrumentation despite their ease of preparation. In general these methods produce unstable materials because leaching of the signaling reagents limits their use for prolonged monitoring. Therefore efforts have been shifted to procedures such as covalent attachment of the ligands to the polymer backbone to prevent leaching.

3.2.1.1.2 Covalent attachment of chemical indicators to polymers

Covalent attachment comprises indicators (can be dyes, ligands or metal nanoparticles) covalently bonded to supports such as polymer, cellulose or glass [221, 222]. Covalently immobilized dyes, in contrast to the physically adsorbed or entrapped dyes, do not suffer from leaching or hysteresis and exhibit long lifetimes [182]. Hence they have the advantage of being used many times and re-usability efficiency of a material could be an important component in cost reduction in analytical procedures.

Better selectivity and rapid measurements have been achieved by replacing classical sensor materials with polymers involving nanotechnology and exploiting either the intrinsic or extrinsic functions of polymers. The advent of nanotechnology has been a major boost in the research area of polymer based solid state optical probes as it opened up possibilities for a new class of materials that could be used. Polymers can be transformed into nanoscale structures for example nanofibers which can offer enhanced responses and rapid procedures for solid phase measurement.

3.3 Nanofibers

Nanofibers have many fascinating properties such as remarkable strength, high surface energy, high surface reactivity, and high thermal and electric conductivity [223]. Nanomaterials may exhibit unique mechanical, optical, magnetic and electronic properties as a result of their nanoscale dimensions. Various techniques have been employed to fabricate polymeric nanofibers and these include; drawing, template synthesis, phase separation, self-assembly and electrospinning [224].

3.3.1 Techniques for producing nanofibers

Polymer nanofibers, possessing high surface area to volume ratio, have great potential for applications in a wide variety of fields, including high performance filtration, chemical

sensing and biomedical engineering [225-227]. There are several methods currently being used for micron- and sub-micron-scale fiber formation.

Conventional mechanical fiber drawing is one of the most mature methods. Even though high throughputs can be achieved using the method; the resulting fibers are typically ~10-100 μm in diameter [228]. To obtain sub-micron fibers, an additional fiber redraw step, commonly used in optical fiber industry, would have to be employed [229]. Melt blowing is another promising technique that has been shown to be capable of producing nanofibers in a single stage. However, due to the underlying driving mechanism, the attenuation rate is essentially slow, and thus numerous very small orifices are required to obtain nanofibers with significant throughput [230]. Another approach to produce polymer nanofibers in a single stage is electrospinning [225-227].

Electrospinning provides a simple and versatile method for generating ultrathin fibers from a rich variety of materials that include polymers, composites and ceramics. While the electrospinning process still suffers from low throughput, relatively high attenuation rates can be achieved with some process modifications [231]. The modifications eventually result in increased throughputs thus positioning electrospinning as an attractive candidate to address the industrial demand.

3.3.1.1 Electrospinning

Electrospinning of polymeric materials into well-defined fiber mats has received significant interest in the recent past. The high specific surface area and small pore sizes of electrospun nanofibers make them attractive candidates for a wide variety of applications. For instance nanofibers with a diameter of 100 nm have a ratio of geometrical surface area to mass of approximately 100 m^2/g. Nanofibers provide a connection between the nanoscale world and the macro-scale world, since the diameters are in the nanometer range and the lengths are in kilometers. Therefore, current emphasis is to exploit such properties and focus on determining appropriate conditions for electrospinning various

polymers and biopolymers for eventual applications. The properties of electrospun nanofibers qualifies them for applications such as, composite reinforcement, protective shields in fabrics, in multifunctional membranes, biomedical structural elements (scaffolds used in tissue engineering, wound dressing, drug delivery, artificial organs), structures for nano-electronic machines and platforms for hosting optical probes among others.

Specifically, electrospinning technique has been found to be a unique and cost-effective approach for fabricating large surface area mats for a variety of sensor applications [193, 232-236]. Wang *et al.* reported that the sensitivities of electrospun nanofiber to detect Fe^{3+} and Hg^{2+} are 2 to 3 orders of magnitude higher than those obtained from thin film sensors [193]. Since there is increasing need to develop highly sensitive solid-state diagnostic probes for toxic metal ions [237-241], electrospinning seems to provide the simplest approach to produce nanofibers.

Electrospinning is a process in which static voltages are used to produce an interconnected membrane-like web of fibers in the diameter range of 10-1000 nm [242]. Electrospinning is a very promising and versatile technique as it facilitates the production of multifunctional nanofibers from various polymers, polymer blends, sol-gels, composites and ceramics. Formation of nanofibers through electrospinning is based on the uniaxial stretching of a viscoelastic solution. To understand and appreciate the processes that enable the formation of various nanofiber assemblies, the principles of electrospinning and the different parameters that affect the process have to be considered. Unlike conventional fiber spinning methods like dry-spinning and melt-spinning, electrospinning makes use of electrostatic forces to stretch the solution as it solidifies. Similar to conventional fiber spinning methods, the drawing of the solution to form the fiber would continue as long as there is enough solution to feed the electrospinning jet. Thus without any disruption to the electrospinning jet the formation of the fiber would be continuous [243]. Electrospinning is an old technique. It was first observed in 1897 by Rayleigh and studied in detail by Zeleny in 1914 [244].

3.3.1.1.1 Brief history of electrospinning

Although the process of electrospinning has been known for over 90 years and the first patent was issued to Formhals in 1934 (US Patent, 1-975-504), polymeric nanofibers produced by electrospinning became a topic of great interest in the past few years. Reneker and Chun, who revived interest in electrospinning technology in the early 1990s, showed the possibility to electrospin a wide range of polymer solutions in 1996 [245]. Larrondo and Manley had performed similar work on polymer melts in 1981 [246]. In general, electrospinning is applicable to a wide range of polymers like those used in conventional spinning, i.e. polyolefin, polyamides, polyester, acrylic as well as bio-polymers like proteins, DNA or polypeptides. Currently, there are two standard electrospinning setups, vertical and horizontal. With the expansion of the electrospinning technology, several research groups have developed more sophisticated systems that can fabricate more complex nanofibrous structures in a more controlled and efficient manner.

3.3.1.1.2 Electrospinning set-up

The research groups working on electrospinning have adopted different orientations for the polymer feed. Some have simply decided on placing the capillary vertically, letting the polymer fluid to drop with help of gravity and placing the collector underneath [247]. At times the capillary can be tilted at a defined angle to control the flow [248]. In other cases, the capillary is placed horizontally [249], and a pump is used to initiate the droplet, the pump was also used in vertical feeding [250]. The electrode on the other hand can be inserted either in the polymer solution or placed onto the tip of the capillary if a syringe with a metal needle is used.

The collector is usually a plane metal sheet or a grid that can be covered with a fabric. Kim and Reneker used a different set-up in their work on polybenzimidazole (PBI) [251]. In fact, they used a rotating cylinder covered with a grounded aluminium sheet. In the work by Theron *et al.* an electrostatic field assisted assembly technique was described, combined

with an electrospinning process used to position and align individual nanofibers on a pointed and grounded wheel-like bobbin [252]. The bobbin was able to wind a continuously as-spun nanofiber at its tip-like edge. The alignment approach resulted in polyethylene oxide (PEO)-based nanofibers with diameters ranging from 100 to 300 nm and lengths of up to hundreds of microns. Electrospinning is a unique approach using electrostatic forces to produce fine fibers from polymer solutions or melts and the fibers thus produced have a thinner diameter and a larger surface area than those obtained from conventional spinning processes.

3.3.1.1.3 Electrospinning process

In the electrospinning process a charged liquid polymer solution is introduced into an electric field. The liquid polymer solution is dispensed via a needle attached to a syringe at a voltage between 0-40 kV and is deposited on a grounded conductive material (aluminum foil) located at a distance from the needle tip. The polymer is ejected from a needle with an inner diameter (ID) between 0.5-1.5 mm. The ejected polymer solution forms a continuous nanofiber when the electrical force (due to the high voltage potential of the polymer solution) overcomes the surface tension. At this point the pendant droplet of the polymer solution at the tip of the needle is deformed into conical shape, typically referred to as Taylor cone (Fig. 3.1). If the voltage surpasses a critical value (depends on the chemical composition of the polymer solution), the electrostatic force overcomes the surface tension and a fine charged jet is ejected. After the jet flows away from the droplet in a nearly straight line, it bends into a complex path as other changes in shape occur, during which electrical forces stretch and thin it by very large ratios. After the solvent evaporates solid nanofibers are left [253]. The electrospinning process has been extensively documented using a variety of fiber forming polymers [235, 254]. In order to carry out electrospinning, there are parameters/variables that play significant roles in the process and the resultant fiber morphology.
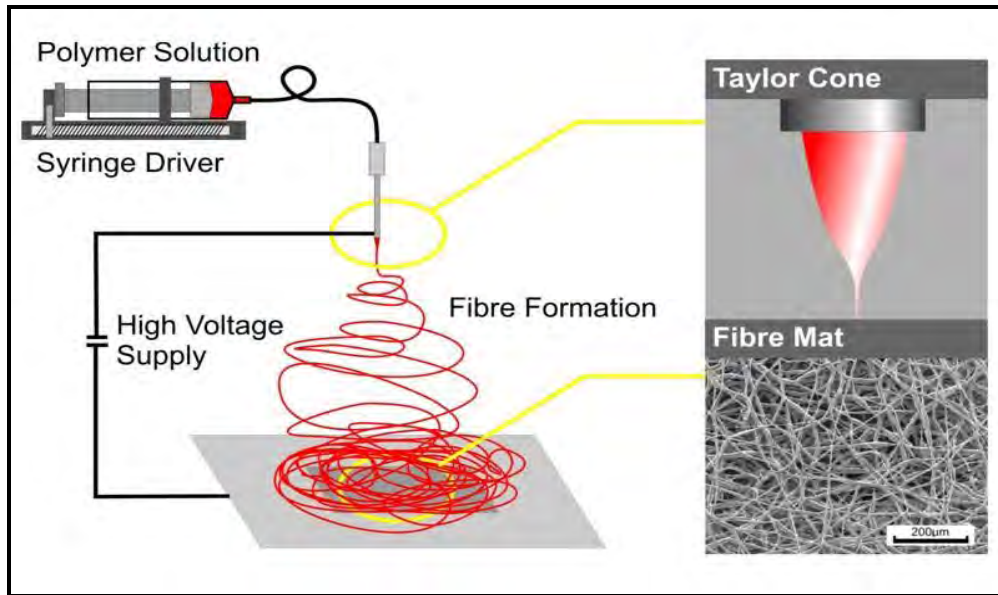
Figure 3.1: Typical electrospinning set-up [255].

3.3.1.1.4 Electrospinning process parameters

The following parameters and processing variables affect the electrospinning process:

(1) System parameters such as molecular weight, molecular-weight distribution and structure (branched or linear) of the polymer and solution properties (viscosity, conductivity and surface tension).

(2) Process parameters such as electric potential, flow rate and concentration, distance between the capillary tip and collector, ambient parameters (temperature, humidity and air velocity in the chamber) [256].

For instance, the polymer solution must have a concentration high enough to cause polymer entanglements yet not so high that the viscosity prevents polymer motion induced by the electric field. The solution must also have a surface tension low enough, a charge density high enough, and a viscosity high enough to prevent the jet from collapsing into droplets before the solvent has evaporated. Morphological changes can occur upon decreasing the distance between the syringe needle and the collector. Increasing the

distance or decreasing the electrical field decreases the bead density, regardless of the concentration of the polymer in the solution. Applied field can in addition influence the morphology of the nanofibers, creating a variety of new shapes on the surface.

Deitzel *et al.* systematically evaluated the effects of two important processing parameters: spinning voltage and solution concentration on the morphology of electrospun nanofibers [257]. They found that the spinning voltage is strongly linked to the formation of beaded fibers, and their measurements could be used to signal the onset of the processing voltage at which the density of beaded fibers increase considerably.

Solution concentration has been found to strongly influence the fiber size, with fiber diameter increasing with increasing solution concentration. In addition, electrospinning from solutions of high concentration has been found to produce a bimodal distribution of fiber sizes, reminiscent of distributions observed in the droplet generation process of electrospraying. Moreover it was found that electrostatic effects influence the macro-scale morphology of electrospun fabrics and may result in the formation of heterogeneous or three-dimensional structures [258].

In recent years, many research groups have paid more attention to altering the chemical compositions of electrospun nanofibers in order to cope with different kinds of interactions and bind a large number of chemical compounds with controlled properties.

3.3.2 Functionalization of polymer nanofibers

The extensive research activities on electrospun polymer nanofibers are encouraged by their great potential for many applications. However, most of polymer nanofibers are chemically inert and do not have any specific functions. For the applications to be successful the electrospun polymer nanofibers must be modified with desired functionalities. Chemical functionalization of electrospun nanofibers can be done by:

(1) Attaching the functional component before preparing the solution for electrospinning.

(2) Adding functional components to the solution for electrospinning so as to obtain nanofibers containing a variety of compositions.

(3) Post-electrospinning treatments (surface modification of nanofibers).

3.3.2.1 Surface modification of polymeric nanofibers

Polymers very often do not possess the surface properties needed for specific applications. In most cases, the mechanically strong and chemically stable polymers have inert surfaces both chemically and biologically. Likewise, those polymers having active surfaces usually do not possess excellent mechanical properties which are critical for their successful application.

In general, special surface properties with regard to chemical composition, hydrophilicity, roughness, crystallinity, conductivity and lubricity are required for the success of these applications. Due to this predicament, surface modification of electrospun nanofibers without changing their bulk properties has been a typical research topic for many years, and is still receiving extensive studies due to many new applications of polymeric materials. Common surface modification techniques include treatments by; coating, radiation with electromagnetic wave, electron beam, ion beam [259], chemical vapor deposition (CVD), gas oxidation, metallization, chemical modifications use wet-treatment and surface grafting polymerization [260, 261] among others.

3.3.2.2.1 Graft copolymerization

Among the surface modification techniques, surface graft copolymerization has surfaced as a simple, useful, and versatile approach to improve surface properties of polymers for a wide variety of applications. Surface grafting has several advantages;

(1) Ability to modify the polymer surface to have very discrete properties through the choice of monomers.

(2) Ease and controllable introduction of graft chains with exact localization of graft chains to the surface without affecting its bulk properties.

(3) Covalent attachments of graft chains onto a polymer surface assuring long-term chemical stability of the introduced chains.

For most of the chemically inert polymers, surface grafting can be achieved via inducing methods such as; photo-induced grafting (UV-induced grafting), thermal-induced grafting, ozone-induced grafting, plasma-induced grafting and redox-grafting techniques either via "grafting-to" or "grafting-from" routes [262]. Among the methods, UV-induced surface graft polymerization is particularly attractive due to its low cost, easy operation and mild reaction conditions. Additionally, UV graft polymerization has been reported to improve surface performance of the substrate without affecting its bulk properties [263]. The general scheme of how the surface of polymer can be grafted is shown in Fig. 3.2.
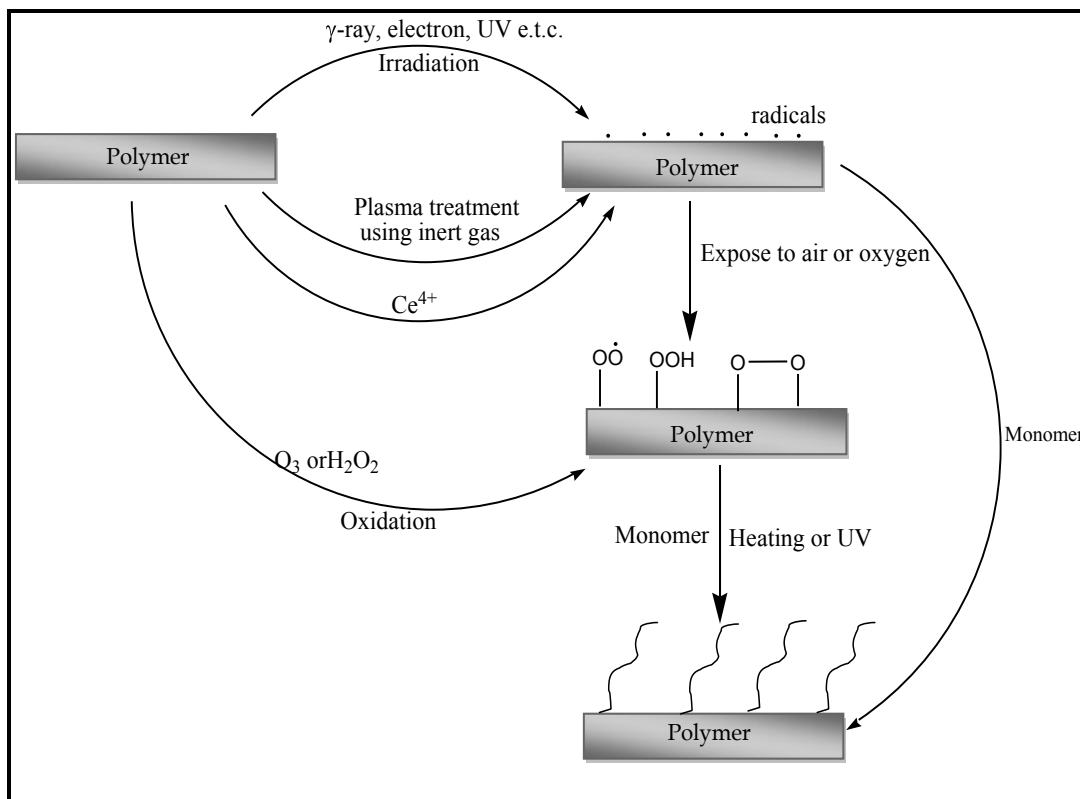
Figure 3.2: General scheme of graft copolymerization on polymer surfaces [224].

3.3.2.1.1.1 Radiation-induced graft copolymerization

Radiation induced graft co-polymerization is the irradiation of the polymer surfaces (substrates) with a high energy source such as UV and eventually grafting a monomer on the surface. Absorption of high-energy radiation by the substrate induces excitation and ionization. The excited and ionized species are the initial reactants for a series of complicated reactions to give free radicals, which can cause monomers to polymerize. The substrate is typically brought into contact with the solution containing the monomer, so that the radicals produced on the substrate can instantaneously initiate the copolymerization of the monomer.

In addition to producing radicals, exposure of polymers to radiations can also lead to other chemical reactions and physical changes, which may have both detrimental and beneficial

consequences in determining the end-uses of the polymers. It is beneficial in the sense that it could cause cross-linking. Grafting on the surface of the polymers on the other hand may cause chain scission (breaking of bond) as well hence damaging the polymer. A fair number of cross links often improve the physical properties of polymers while scission processes usually produce negative effects, resulting in materials which are weak [224].

Apart from the surface graft co-polymerization method, chemical treatment has also been reported as another simple way of introducing desired chemical functionalities onto the surfaces of electrospun nanofibers.

3.3.2.1.2 Chemical treatment

Some polymer surfaces contain functional groups such as hydroxyl, carboxyl, amine and ester. Such polymers can be modified directly by chemical treatment. Chemical modification involves the introduction of chemical species to a given surface in order to create a surface which has desired chemical and physical properties.

Chemical reactions can be carried out at sites that are susceptible to electrophilic or nucleophilic attacks. Structures such as benzene rings, hydroxyl groups, double bonds, halogens and ester groups qualify for such attacks. Polyester like Polyethylene terephthalate (PET) and Poly(caprolactone) (PCL) can be treated by amine compounds to introduce amino groups through the aminolysis of the ester groups [264]. Cellulose surface contain hydroxyl groups and can be modified with many electrophilic agents such as cibacron blue F3GA [265], via the reaction between the hydroxyl groups and the electrophilic agents.

Wet chemical oxidation treatments are also commonly employed to introduce oxygen-containing functional groups (such as carbonyl, hydroxyl, and carboxylic groups) at the surface of the polymer. This can be conducted using gaseous reagents or with solutions of vigorous oxidants. The oxygen-containing functional groups lead to increased polarity and

the ability to form hydrogen bond, which in turn results in the enhancement of wettability and adhesion.

The next chapter outlines the reagents, instrumentation and experimental aspects of the research work.

Chapter 4 Experimental

4.1 Overview

This chapter presents the experimental aspects of the studies that were carried out in this thesis. It has been configured to provide details of the general reagents and equipments that were used as well as experimental procedures for the three components of the research work which were; (i) Development of a fluorescent probe for quantification of Ni^{2+} ions in water, (ii) Colorimetric probe for the detection of Ni^{2+} ions based on silver-copper alloy nanoparticles hosted in electrospun nanofibers, (iii) Colorimetric probe for rapid detection of Fe^{2+} ions in aqueous media.

4.2 General materials and reagents

Poly(acrylic acid) (PAA) (Mw = 50000 g/mol), Nylon 6 (Mw = 10 000), pyridylazo-2-naphthol (PAN), Pyridine-2-aldehyde 99%, Azoisobutyronitrile (AIBN) (was recrystallized from THF just before use), 1,1'carbonyldiimidazole (CDI), 4-vinylbenzyl chloride (90%), 1,8-diazabicyclo[5.4.0]undec-7-ene (DBU), Glyoxal solution (40% weight in water), $NaBH_4$, glutathione (GSH), certified reference material (Iron, Ferrous 1072) and all inorganic salts ($NiCl_2.6H_2O$, $CoCl_2.6H_2O$, $CrCl_3.6H_2O$, $CuCl_2.6H_2O$, $FeSO_4.7H_2O$, $Cd(NO_3)2.4H_2O$, $Zn(NO_3)_2.H_2O$, $Pb(NO_3)_2$, $Al_2(SO4)_3.15H_2O$, $AgNO_3$), were of analytical grade and were used as obtained from Sigma Aldrich (St. Louis, MO USA).

Formic acid (90%), Glacial acetic acid (100%), Ethanol, Diethyl ether, Ethyl acetate, *N,N*-Dimethylformamide (DMF) (was distilled over nitrogen at reduced pressure), Tetrahydrofuran (THF), Potassium hydroxide (KOH) and Sodium hydroxide (NaOH), 25% ammonia solution were obtained from Merck Chemicals (Wadeville, South Africa).

Sodium dihydrogen phosphate ($NaH_2PO_4.2H_2O$) and Potassium hydrogen phthalate ($C_8H_5KO_4$) were obtained from Saarchem Analytic (Krugersdorp, South Africa). All experimental manipulations and data collections were performed at room temperature unless otherwise stated. Standard solutions were freshly prepared by dissolving known quantities of metal salts in deionized ultrapure water obtained from a Millipore system.

4.3 Instrumentation and measurements

4.3.1 Characterization techniques

In this thesis, the characterization techniques described were used to confirm the successful formation of products in cases where synthesis was done and the morphology as well as elemental composition. The rest other characterization techniques were used to study the optical properties of the diagnostic probes that were developed. Characterization instruments used in this work are briefly described below.

4.3.1.1 Elemental analysis

Elemental analysis or "EA" almost always refers to CHNX analysis; the determination of the mass fractions of carbon, hydrogen, nitrogen, and heteroatoms (X) (halogens, sulfur) of a sample. This information is important to help determine the structure of an unknown compound, as well as to help ascertain the structure and purity of a synthesized compound. Elemental analyses were performed with Vario Elementar Microtube ELIII (Hanau, Germany) after drying the samples.

4.3.1.2 Fourier transform infrared spectroscopy (FTIR)

Fourier Transform Infrared Spectroscopy provides information about the chemical bonding or molecular structure of materials, whether organic or inorganic. The technique works on the fact that bonds and groups of bonds vibrate at characteristic frequencies. The specimen's transmittance and reflectance of the infrared rays at different frequencies is translated into an IR absorption plot consisting of reverse peaks. FTIR spectra were recorded on a Perkin Elmer Spectrum 100 ATR (attenuated total reflection)-FTIR spectrometer.

4.3.1.3 Nuclear magnetic resonance spectroscopy (NMR)

NMR spectroscopy is one of the principal techniques used to obtain physical, chemical, electronic and structural information about molecules due to either the chemical shift, Zeeman effect, or the Knight shift effect, or a combination of both on the resonant frequencies of the nuclei present in the sample. It is a powerful technique that can provide detailed information on the topology, dynamics and three-dimensional structure of molecules in solution and the solid state. ^{1}H and ^{13}C NMR spectra were collected on Bruker Avance 400 MHz spectrometer and reported relative to tetramethylsilane (δ 0.00).

4.3.1.4 Transmission electron microscopy (TEM)

Transmission electron microscopy is the most useful imaging techniques for nanoparticles. In case of transmission electron microscopy (TEM) a beam of electrons is transmitted through an electronically transparent specimen interacting with the atoms to produce one image. Due to the small *de Broglie* wavelength of electron image, atomic resolution is possible to be captured by TEM. To obtain TEM image, the sample is required to be dispersed on TEM grids (carbon coated copper grid or molybdenum grid). For this work,

TEM images were recorded by a JEOL-JEM 2010 electron microscope operating at 100 Kv and a JEOL JEM 2100 LaB6, working in STEM and HAADF (High Angle Annular Dark Field Mode). Samples for TEM were prepared by placing a drop of colloidal sample or nanofiber mat on carbon coated copper grid and dried at room temperature.

4.3.1.5 Scanning electron microscopy (SEM)

In SEM the area of the sample to be analyzed is targeted by a narrowly focused electron beam which can be swept across the surface of specimen to form image or may target one place only to analyze particular position. The image is produced due to the interaction of the electron beam with atoms at or near the surface of the samples. SEM can also produce very high resolution images (1 to 5 nm). SEM specimens are required to be conductive at the surface to avoid accumulation of electrostatic charge at the surface. For imaging non-conductive specimens, the specimen surface is coated with a thin film of conducting metal like gold. For this work the morphology of the nanofiber mats were studied by the Tescan (TS5136ML) Scanning Electron Microscope (SEM) operating at an accelerated voltage of 20 kV and a JEOL JSM-7001F Field Emission Scanning Electron Microscope operating at 2 kV after gold sputter coating.

4.3.1.6 Energy dispersive x-ray spectroscopy (EDX)

Chemical characterization and elemental analysis of nanometer scale particles can be done by EDX/EDS. This analysis is based on the analysis of x-rays emitted by the matter in response to interaction between electromagnetic radiation and matter. As each element has unique atomic structure and can emit unique x-rays, elemental composition can be detected by analyzing the emitted x-rays. EDX/EDS for compositional characterization of nanoparticles is usually integrated with TEM or SEM. The elemental contents of the surface

modified nanofibers were determined by Environmental Scanning Electron Microscopy (SEM/ESEM-EDAX-QUANTA 200) operating at an accelerated voltage of 20 kV.

4.3.1.7 UV-vis absorption spectroscopy

In this technique a beam of light of wavelengths in the visible and ultraviolet region passes through the specimen and its intensity before and after interacting with a sample is measured to determine the light transmitted through or absorbed by the sample. For metal nanoparticles absorption peaks can be correlated to their surface plasmon resonance peak. Absorption peaks can also indicate type of bonds in a given molecule. For this work, electronic absorption spectra were recorded on a Perkin Elmer Lambda 25 UV/VIS spectrophotometer in a quartz cell (1 cm).

4.3.1.8 Fluorescence microscopy

In fluorescence microscopy, images are taken based on the fluorescence property of samples. The sample is usually first tagged with a fluorescent molecule and excited by light with excitation energy required for the fluorophores. The fluorescence emission from the specimen is collected through an emission filter to separate the emitted light from the illumination light. Only a single fluorophore can be imaged at a time. For this work, fluorescence images were taken with a DMLS fluorescence microscope. The excitation source was a high-voltage mercury lamp and light with a wavelength between 470-570 nm was emitted with the help of an optical filter.

4.3.1.9 Fluorescence spectroscopy

In this type of fluorescence electromagnetic spectroscopy, fluorescence intensity from sample is analyzed. The sample is excited using a particular wavelength of light and emitted fluorescence emission of a lower energy is detected. For this work, emission spectra were recorded on Varian Cary Eclipse spectrofluorometer in a quartz cell (1 cm). The spectrofluorometer was equipped with xenon discharge lamp (75 kV), Czerny-Turner monochromators and an R-928 photomultiplier tube with manual or automatic voltage controlled using the Cary-Eclipse software.

4.3.1.10 Electrospinning set-up

The electrospinning set-up consisted of a polypropylene 25 ml syringe and a 21 gauge, 90° blunt end stainless steel needle that was clamped horizontally on a syringe pump. The metal electrode and the collector plate were made of copper. The grounded static collector plate was covered with aluminum foil. The stainless steel needle was connected to the tip of the syringe via polytetrafluoroethylene (PTFE) tubing. The anode of the high voltage power supply was connected to the needle. All polymer solutions were delivered by a syringe pump at controlled flow rates. Electrospinning was carried out at room temperature (25 °C). The typical electrospinning set-up used in this study is shown in Fig. 4.1.
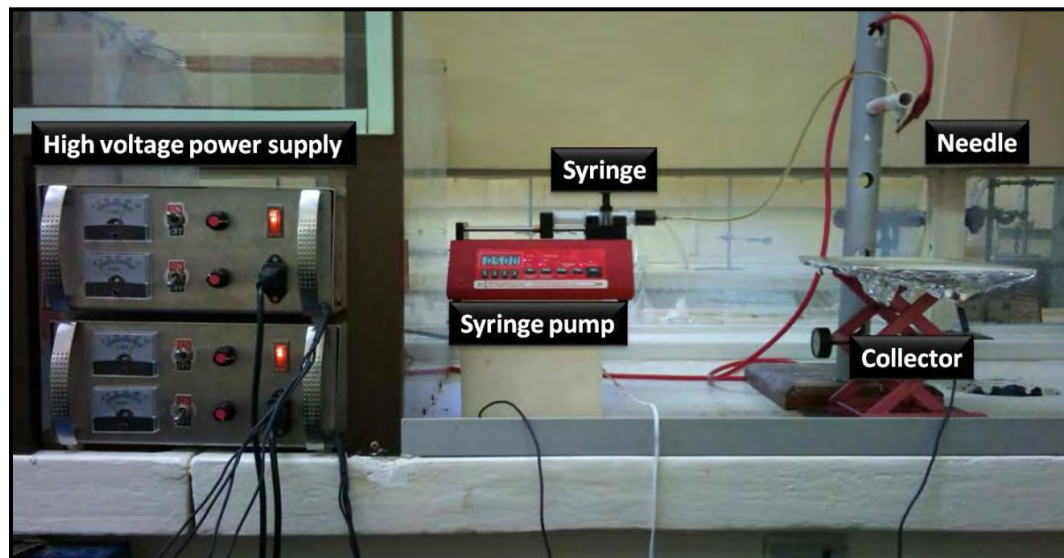
Figure 4.1: The electrospinning set-up that was used for the fabrication of nanofibers for the thesis.

4.4 Development of a fluorescent probe for the determination of Ni²⁺ ions in water

4.4.1 Synthesis of fluorescence pyridylazo-2-naphthol-poly(acrylic acid) (PAN–PAA)

A solution of 1, 1'-carbonyldiimidazole (CDI), (0.34 g, 2.1 mmol) and a catalytic amount of 1, 8-diazabicyclo [5.4.0]undec-7-ene (DBU) in 10 mL of (dimethylformamide) DMF were added to a solution of poly(acrylic acid) (PAA) (1.5 g, 20.8 mmol) in 40 mL of DMF. After stirring the solution at 70 °C until the evolution of carbon dioxide subsided (15 min), a solution of 1-(2-pyridylazo)-2-naphthol (PAN) (0.52 g, 2.08 mmol) in 15 mL DMF was added and the solution was stirred at 70 °C for 18 h. The solution was slowly transferred with vigorous stirring into diethyl ether to precipitate the polymer. After filtration, the obtained solid was washed extensively washed with ether and acetone and dried in a vacuum oven for 24 h at 25 °C.

4.4.2 Fabrication of fluorescence electrospun nanofiber

A solution for electrospinning was prepared by dissolving 6.6 wt% PAN–PAA in 1:4 (v/v) water-ethanol solvent system and stirred overnight to obtain a homogeneous solution. After loading the polymer solution into a 10 mL glass syringe, the syringe was mounted on a programmable syringe pump (New Era, NE-1000). The solution was pumped at a flow rate of 1 mL/h through a steel needle of internal diameter 0.584 mm. Nanofibers were collected on glass slides which were covered with masking tape and only the targeted area (0.5-2.5 cm) exposed for deposition to occur. This system was mounted on aluminium foil and the collection was carried out for 8 min. The distance between the needle tip and the collector was 15 cm and the voltage applied at the needle tip was 8.75 kV. In order to improve the insolubility of the fiber mat in an aqueous medium, the electrospinning solution with cross-linker was prepared with the addition of β-cyclodextrin at 20 wt% of the product. After the deposition process, fibers were heat treated at 120 °C for 20 min to cross-link the films.

4.4.3 Fluorescence measurements

In order to perform fluorescence measurements, the glass slides containing electrospun nanofiber layers were placed in 1 cm quartz cuvettes which were filled with various metal salt solutions. The cuvette was placed in the sample holder of the spectrofluorometer, samples were illuminated at an excitation wavelength of 500 nm and the emission was scanned from 510 to 640 nm, while the detector voltage was maintained between 600 and 650 V.

4.4.4 Performance of fluorescence measurements

In fluorescence data collection, the 5 mL aliquots of nickel ion stock solutions (ranged 0.1‑1.0 μg/mL) were added into optical cell containing glass slide coated with the fluorescent nanofiber (Fig. 4.2). The data, corresponding to the average of three determinations, were fitted by a standard least-squares treatment and the Stern-Volmer equations were evaluated. The procedure for examining the influence of other metal ions on fluorescence quenching of Ni^{2+} was essentially the same. For this instance, sensing nanofiber was exposed to several metal cations at higher equivalence with or without fixed concentration of nickel ion. A custom-made certified reference material for groundwater (SEP-3) purchased from Inorganic Ventures (Christiansburg, USA) was used to validate the analytical procedure. Repeatability of the method was evaluated by comparing the signals obtained from three determinations of the reference material.
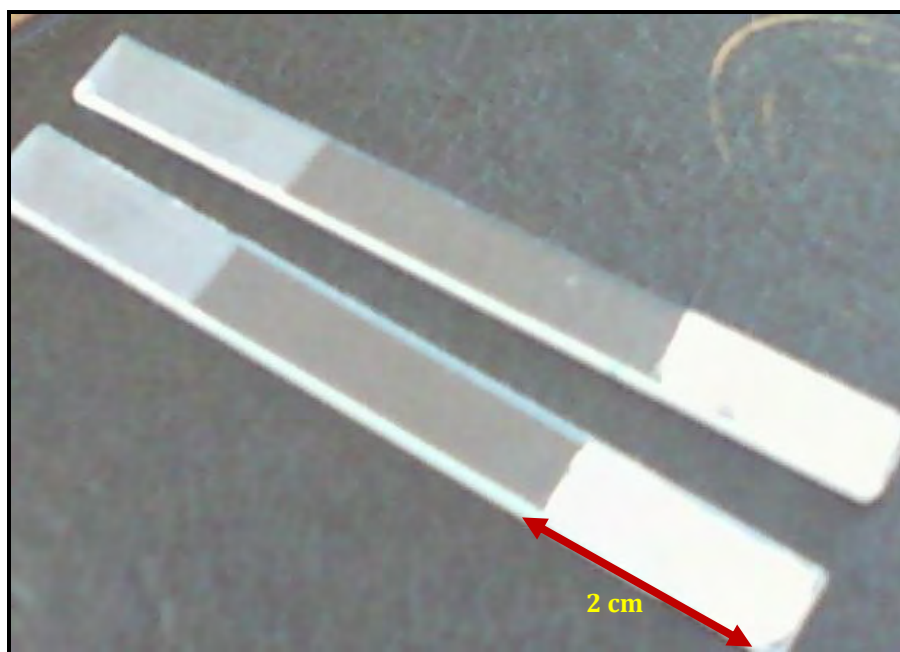
Figure 4.2: Photograph of glass slides coated with fluorescent nanofibers.

4.4.5 Preparation of buffers

Buffer compositions were calculated according to Perrin [266]. This calculation is based on the Henderson-Hasselbalch equation (buffer equation), and allows the calculation of; buffer composition at a defined pH, buffer concentration and ionic strength. The buffer solutions used were potassium hydrogen phthalate-hydrochloric acid (pH 2.2-4.0), potassium hydrogen phthalate-sodium hydroxide (pH 4.5-5.9) and sodium dihydrogen phosphate-sodium hydroxide (pH 6.0-8.0). The pH of the solutions were monitored by use of a digital pH-meter; A Jenway 3510 pH meter (London, UK) calibrated with standard buffers of pH 7.00 and 4.00 at 21±1 °C.

4.4.6 Regeneration studies

The whole regeneration process included destabilization of the bond formed between nickel cation and the indicator by immersing the fiber in 0.1 M HCl solution, modulating the pH value to 7.0 using 0.1 M NaOH and putting the probe back into the Ni^{2+} ion solution. After each time, the used test strip was dipped into HCl for 1 min to desorb the Ni^{2+} ions, conditioned in NaOH for 2 min and washed with fresh deionized water.

4.5 Colorimetric probe for detection of Ni^{2+} ions based on silver-copper alloy nanoparticles hosted in electrospun nanofibers

4.5.1 *In situ* synthesis of glutathione-stabilized silver/copper alloy nanoparticles

Nylon 6, silver nitrate, copper sulfate, $NaBH_4$ and glutathione were used as electrospinable polymer, silver precursor, copper precursor, reducing agent and stabilizer respectively. Nylon 6 pellets were dissolved in a mixture of acetic acid and formic acid in the ratio of 1:1

to make a solution with a concentration of 15 wt/wt%. The mixture was stirred with a magnetic stirrer for 1 h until the lumps of the nylon 6 pellets were broken and well dispersed. 10.5% of $AgNO_3$ and $CuSO_4$ in the mole ratio of 1:1.96 were then added to the nylon 6 solution. The mixture was allowed to stir for an hour after which, 1.5×10^{-3} moles of $NaBH_4$ were added to this mixture. After stirring for about 5 min 22.8% of GSH was added. The percentage weight of the salts and the capping agent were calculated based on the weight of nylon 6.

4.5.2 Fabrication of electrospun nanocomposite fibers

The homogenous nanocomposite solution was loaded into a 10 mL plastic syringe. The syringe was then mounted on a programmable syringe pump (New Era, NE-1000). The solution was delivered at a flow rate of 0.3 mL/h through a steel needle of 0.584 mm internal diameter. Nanofibers were collected on an aluminum foil collector with the distance between the needle tip and the collector of 12 cm and the applied voltage at the needle tip was 22.5 kV. The electrospun fiber mats were cut into uniform strips and without any further treatment the strips were placed in the various test solutions.

4.5.3 Preparation of standard solutions

Nickel (II) stock solution (0.1 M) was prepared by dissolving 23.77 mg $NiCl_2.6H_2O$ in 100 mL volumetric flask with deionized water. The other metal ion solutions were prepared from their sulphate, nitrate or chloride salts. Ag^+, Cu^{2+}, Zn^{2+}, Cd^{2+}, Pb^{2+}, Fe^{3+}, Co^{2+}, Mn^{2+}, Cr^{3+}, Ni^{2+}, Ca^{2+}, Na^+ and Mg^{2+} salts were dissolved to prepare stock solutions with concentrations of 0.1 M. The prepared stock solutions of the metal ions were directly used in the measurements.

4.5.4 Performance testing of the probe

Standard solutions of various metal salts were prepared by appropriate dilution of their stock solutions with double-distilled deionized water. Aliquots (5 mL) of the standard solutions were measured out in a sample vial and the strips of electrospun fiber mats were placed in these solutions.

4.6 Colorimetric probe for the rapid detection of Fe^{2+} ions in aqueous media

4.6.1 Synthesis of 2-(2'-pyridyl)-imidazole (PIMH)

2-(2'-pyridyl)-imidazole was synthesized following the literature procedure described by Gerber *et al.*, [267]. Briefly, a solution of 10.70 g of pyridine-2-aldehyde (0.10 mol) in 10 mL of ethanol was mixed with 20 mL of a 40% aqueous glyoxal solution at 0 °C. Immediately, 30 mL of an ice-cold 20% aqueous ammonia solution was added, and the yellow-brown solution was stirred at 0 °C for 30 min, and then allowed to stir overnight at room temperature. The ethanol was then boiled off, and the residue was extracted several times with 50 mL aliquots of diethyl ether. The ether was evaporated using a rotary evaporator, and the yellow solid crystals were re-crystallized from ethyl acetate. These were filtered and dried under vacuum.

4.6.2 Synthesis of poly(vinylbenzyl chloride) (PVBC)

Poly(vinylbenzyl chloride) was produced by free-radical polymerization of 4-vinylbenzyl chloride (10 mL, 70.9 mmol) in toluene (2 mL) using azobisisobutyronitrile (AIBN) (0.05 g, 0.3 mmol) as the initiator. The reaction mixture was heated at 70 °C under nitrogen gas for 12 h. The polymer obtained was dissolved in THF and precipitated with methanol, filtered

and air dried. ^{1}H NMR (CDCl$_3$) δ (ppm): 1.4-1.7, (−CH$_2$ and −CH main chain), 4.4-4.6, Ph-CH$_2$-Cl, 6.4-7.1, (−CH benzyl ring).

4.6.3 Synthesis of 4-vinylbenzyl-2-(2′-Pyridyl)-imidazole

Potassium hydroxide (2.88 g, 0.05 mol) was added to a solution of 2-(2′-Pyridyl)-imidazole (7.2 g 0.05 mol) in acetone. To this, 4-vinylbenzyl (7.63 g, 0.05 mol) was added dropwise. The reactants were refluxed, with stirring at 50 °C for 5 h. After which, the solvent was evaporated using a rotary evaporator and the product dissolved in dichloromethane, and washed with water to remove the water soluble KCl. Anhydrous MgSO$_4$ was used to dry the product and dichloromethane was removed by the rotary evaporator to obtain a yellow oil. ^{1}H NMR (CDCl$_3$) δ (ppm): 5.1-5.9; (vinyl CH$_2$), 6.5-6.7; (vinyl CH).

4.6.4 Preparation of standard solutions

Iron (II) stock solution (0.1 M) was prepared by dissolving 2.78 g FeSO$_4$.7H$_2$O in 100 mL volumetric flask using 0.2 M of concentrated H$_2$SO$_4$ and deionized water. The other metal ion solutions were prepared from their sulphate, nitrate or chloride salts. Ag$^+$, Cu^{2+}, Zn^{2+}, Cd^{2+}, Pb^{2+}, Fe^{3+}, Co^{2+}, Mn^{2+}, Cr^{3+}, Ni^{2+}, Ca^{2+}, Na$^+$ and Mg^{2+} salts were dissolved to prepare stock solutions with concentrations of 1.0×10^{-3} M, the synthetic ligand was dissolved in the mixed solution of EtOH: H$_2$O (*V/V* = 10:90) to give the stock solution (1 mg/mL). The prepared stock solution of the metal ions and ligand were directly used in the spectroscopic measurement.

4.6.5 Optimization of the pH of PIMH-Fe(II) complex

The buffer solutions used were potassium hydrogen phthalate-hydrochloric acid (pH 2.2-4.0), potassium hydrogen phthalate-sodium hydroxide (pH 4.5-5.9) and sodium dihydrogen phosphate-sodium hydroxide (pH 6.0-8.0). In each case, a mixture containing 0.34 mg of Fe(II), 5.0 ml of the suitable buffer and 6.0 ml of PIMH solution were taken and the volume was adjusted to 20.0 ml with Millipore water. The experiment was repeated with buffers of different pH values from 3.0-8.0.

4.6.6 Determination of the absorbance of Fe(II)-PIMH with different Fe(II) concentrations

The absorbance of the different Fe(II)-PIMH compositions were determined with a UV spectrophotometer. This was carried out in triplicates for each composition. From the values, a plot of absorbance against concentrations of Fe(II) was constructed. Statistical methods were then used to determine the limit of detection (LOD), limit of quantification (LOQ), standard deviation, regression and equation of the calibration curve.

4.6.7 Preparation of calibration curve

A series of Fe(II) standard solutions having concentrations ranging from 0 to 3.5 μg/mL were prepared. In each case, an appropriate volume of the stock solution of iron (II) standard was mixed with 4.0 ml of the buffer (pH 6.0) followed by the addition of 2 mL of PIMH solution. The pH of the mixtures was brought to 6.0 by using either NaH_2PO_4 or NaOH solutions and the volume was adjusted to 20.0 mL with Millipore water.

4.6.8 Interference evaluation

Evaluation of chemical interferences was conducted by repeating Fe(II) analysis in the presence of each of the interfering species at different concentration levels, and comparing the results with a measurement of a blank solution containing iron with no interfering substance. The interferences were studied by analyzing samples after adding between 2-25 µg/mL of each interfering ion into a fixed concentration (2.0 µg/mL) of Fe(II). All the solutions were prepared according to the standard preparation procedures already described.

4.6.9 Fabrication of nanofibers by electrospinning PVBC

A solution for electrospinning was prepared by dissolving the polymer to make a 40% (wt/v) in 1:1 (v/v) DMF/THF solvent system and the mixture was stirred for 3 h to obtain a homogenous solution. After loading the polymer solution into 10 mL glass syringe, the syringe was mounted on a programmable syringe pump (New Era, NE-1000). The solution was pumped at a flow rate of 0.8 mL/h through a steel needle of 0.584 mm internal diameter. Nanofibers were collected on a stationary collector covered with aluminum foil. The distance between the needle tip and the collector was 12 cm and the applied voltage was 15 kV.

4.6.10 Fabrication of nanofibers by electrospinning nylon 6

A homogenous solution of nylon 6 was prepared in a mixture of formic and acetic acid in the ratio of 1:1 to make concentration of 16% wt/v. After stirring the mixture for 5 h, it was loaded into a 10 mL plastic syringe. The syringe was then mounted on a programmable syringe pump (New Era, NE-1000). The solution was pumped at a flow rate of 1 mL/h through a steel needle of 0.584 mm internal diameter. Nanofibers were collected on an

aluminum foil collector with the distance between the needle tip and the collector of 10 cm and the applied voltage at the needle tip was 20 kV.

4.6.11 Post-functionalization of PVBC nanofibers with PIMH

A strip of approximately 14 cm x 6 cm of the PVBC nanofiber mat measuring 0.65 g was cut out. The strip was placed into a 20 mL methanol solution of PIMH (5.0 g, 0.035 mol) in a 50 mL flask along with KOH (3.93 g, 0.07 mol). The contents were heated and stirred gently at 40 rpm for a period of 5 days at 40 °C. Afterwards, the fibers were rinsed in methanol. Finally, the fibers were cleansed with diethyl ether in a Soxhlet extraction system and dried at room temperature, under reduced pressure for 12 h.

4.6.12 Photo-grafting procedure

The nylon 6 nanofibers were cut into strips (5 cm wide and 5 cm long) and then dried in an oven at 50 °C. The monomer solution with varied concentrations in the range between; 0.3–4.0% (w/v) were prepared in MeOH as the solvent. The concentration of the initiator (benzophenone) was varied between 0.1–0.4% (w/w). Weight of the initiator was calculated based on the weight of the monomer. One piece of nylon 6 nanofibers was placed in a Pyrex glass tube containing 15 mL solution of the initiator; this tube was purged with nitrogen gas to eliminate oxygen and then sealed.

The tube was exposed to ultraviolet light under controlled conditions. The light source was a 400-W high-pressure mercury lamp, and the glass tubes were rotated and revolved simultaneously around the light source at a distance of 10 cm for 30 min. After which, a solution of the monomer in MeOH was added to the tube and the contents placed back in the oven for grafting to take place. After the grafting reaction, the nylon 6 nanofibers were removed from the glass tubes, washed with hot water, and then extracted with MeOH for 6

h in a Soxhlet extraction system to remove unreacted monomer and homopolymer. The nanofiber mat was then dried at 50 °C to a constant weight. The degree of grafting was calculated from the weight gain.

Chapter 5 Results and Discussion

5.1 Development of a fluorescent probe for quantification of Ni^{2+} ions in water

5.1.1 Choice of fluorescent Indicator

A variety of fluorescent reagents such as fluorescein and rhodamine dyes for the determination of heavy metals, in particular nickel ions, have been described in literature [268]. In the search for a specific indicator for the development of a fluorescent probe, 1-(2-pyridylazo)-2-naphthol (PAN) (Fig. 5.1), was identified as a fluorescent reagent that could selectively respond to nickel (II) ions in aqueous samples. For fluorescent applications, the indicators need to meet some criteria: (1) should have a sufficiently large change in the fluorescence (enhancement or quenching) in the presence of the analyte, (2) a large Stokes shift, (3) high fluorescence quantum yields, (4) high photostability, and (5) should be easy to immobilize into a solid support.

1-(2-pyridylazo)-2-naphthol was found to fulfill most of these requirements. It is one of the most sensitive reagents among heterocyclic azo compounds for determining metal ions. It has been reported to possess exceptionally high selectivity for nickel(II) [269]. 1-(2-pyridylazo)-2-naphthol is commercially available and did not require any chemical modification for the application presented. Neither its absorbance nor emission maxima were affected by pH changes between 5 and 8. Finally, it had a reactive hydroxyl group which makes its incorporation into a polymer backbone easy.
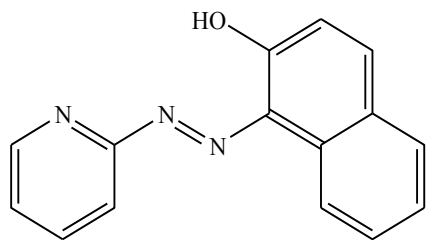
Figure 5.1: Structure of 1-(2-pyridylazo)-2-naphthol.

5.1.2 Choice of the polymer support

Poly(acrylic acid) (PAA) was chosen as the polymer support in the work. The choice of PAA was driven by the fact that it possess high molecular weight hence could be transformed into nanofibers through the process of electrospinning. Secondly PAA contains carboxylic acid groups that could allow the formation of ester bonds with the alcohol group of 1-(2-Pyridylazo)-2-naphthol. Consequently, covalent attachment of the signaling reagent onto the back bone of the polymer was achieved.

5.1.3 Synthesis of pyridylazo-2-naphthol-poly(acrylic acid)

A two-step synthesis using 1,1'-carbonyldiimidazole (CDI) as a coupling agent provided an effective route for the preparation of the fluorescent pyridylazo-2-naphthol-poly(acrylic acid). In this reaction scheme, the carboxylic acid groups were activated by reacting them with CDI (1) to form an imidazolide (2) (Fig. 5.2). In the activation step, partial protonation of the imidazole nitrogen led to the formation of an activated species which was then attacked by the carboxylate. Without isolation, the imidazolide was reacted immediately with pyridylazo-2-naphthol in the presence of a base (1,8-diazabicyclo[5.4.0]undec-7-ene (DBU)) to give the required ester (Scheme 5.1). The method is very effective and has been followed in the preparation of picolinyl ester derivatives from epoxy [270], and fatty acids [271]. An important advantage of the method was that the byproducts; carbon dioxide and

imidazole were readily and quantitatively separated from the reaction product by a simple washing procedure.
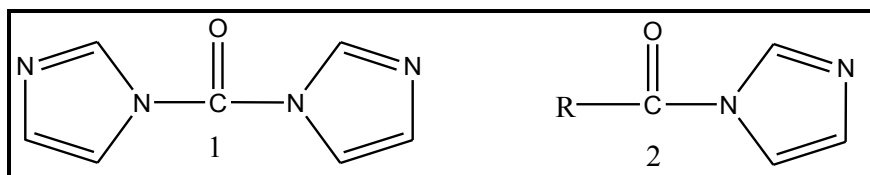
Figure 5.2: Chemical structures of; (1) CDI and (2) imidazolide intermediate.
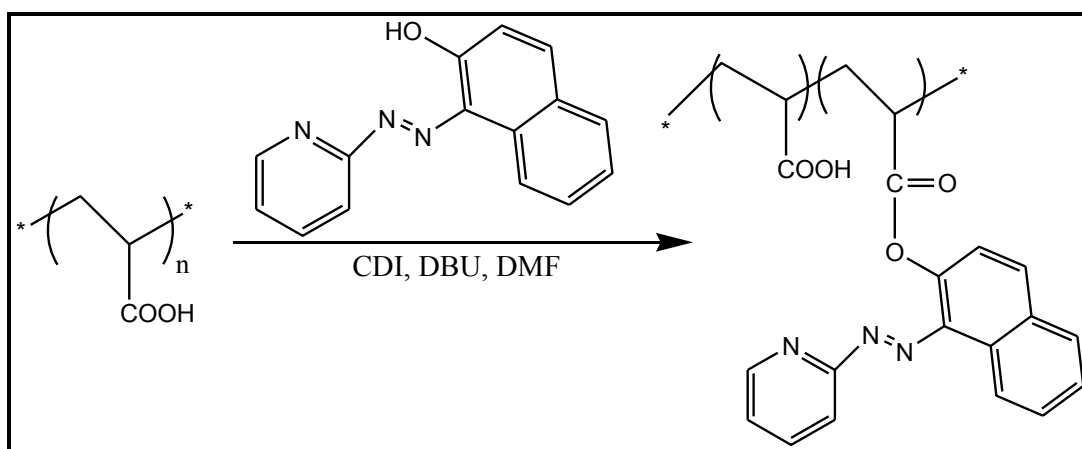
Scheme 5.1: Synthesis of fluorescent functionalized polymer of 1-(2-Pyridylazo)-2-naphthol and poly(acrylic acid) (PAN-PAA).

5.1.4 Characterization of fluorescent PAN-PAA

The obtained product was characterized by IR spectroscopy. The FTIR spectra (Fig. 5.3) confirmed the successful immobilization of 1-(2-Pyridylazo)-2-naphthol onto poly(acrylic acid). In the spectrum of the polymer, a strong band corresponding to C=O stretching band appeared at around 1699 cm^{-1} but disappeared in the spectrum of PAA-PAN. This along with the appearance of a new peak at 1737.07 cm^{-1} was an indication that an ester bond had been formed between the hydroxyl groups of PAN and carboxylate groups of PAA. The

formation of the new covalent bonds between the indicator and support materials prevented the indicator from leaching-out and afforded electrospinable material for transformation into nanofiber mat for direct solid phase measurement of nickel ions in water.
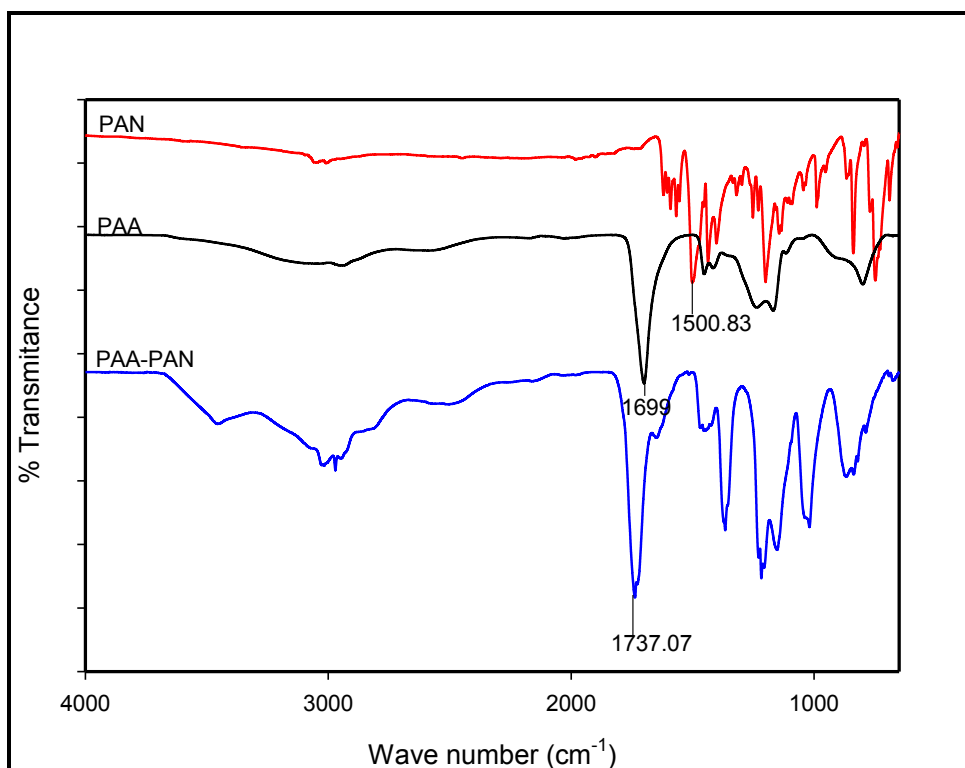
Figure 5.3: Infrared spectra of new fluorescence polymer PAN–PAA, PAN and PAA.

5.1.5 Stokes shift of the fluorescent pyridylazo-2-naphthol-poly(acrylic acid)

PAN has been shown to be one of the most sensitive reagents among heterocyclic azo compounds for determining nickel ion [269]. Most fluorescent dyes show a difference between the absorption and emission maximum. Emission is shifted to a longer wavelength, which means a loss of energy. This "bathochromic" shift is called Stokes shift [272, 273]. The main reason for this could be seen from the Jablonski diagram (Figure 2.1).

The absorption from S_0 to S_1 is normally from the lowest to the higher vibrational levels (Franck Condon Principle) [104], followed by a fast decay to the lowest vibrational state of S_1. From here fluorescence occurs mainly to higher vibrational levels of S_0, which leads to loss of energy compared to absorption.

The fluorescent electrospun nanofiber PAN-PAA exhibited distinct and well-defined emission peak as shown in Fig. 5.4. Previously, the intrinsic absorbance of PAN had been reported to be 470 nm [269], comparing this with absorbance maximum of the new PAN functionalized molecule, there was a slight shift to 479 nm. This could be due to the fact that PAN was linked to a polymer through a covalent bond unlike in the previous reports where it was used as a free molecule. The emission maximum of the complex occurred at 557 nm which was indicative of a good Stokes' shift (78 nm). With the incorporation of PAN into PAA, the rate of self-quenching of PAN, as a result of site isolation was greatly reduced and this resulted in a remarkably improved fluorescence efficiency and sensitivity of the system.
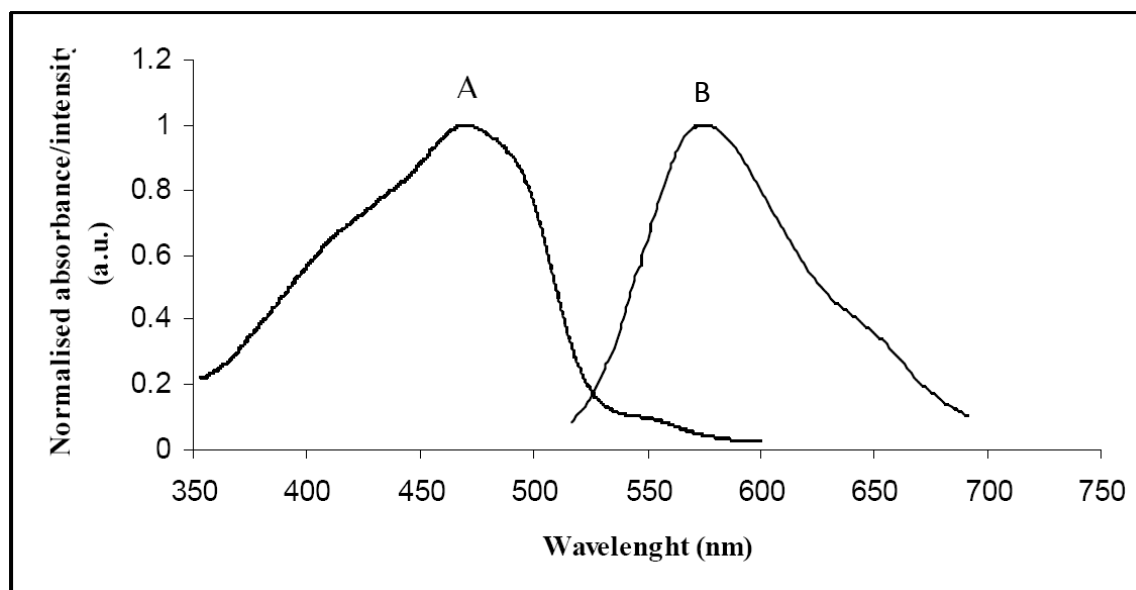
Figure 5.4: UV absorption (A) and fluorescence emission (B) spectra of PAN–PAA.

5.1.6 Fabrication of fluorescent PAN-PAA nanofiber

To obtain the optimal electrospinning conditions, several operational parameters were investigated including voltage, working distance and flow rate. Within the tested range (5-15 kV voltage, 10-20 cm working distance and 0.5-1.5 mL h^{-1} flow rate), the optimal electrospinning parameters which gave bead-free nanofibers (Fig. 5.5), prepared from 6.6 wt% solution were 8.75 kV voltage, 15 cm working distance and 1 mL h^{-1} flow rate.
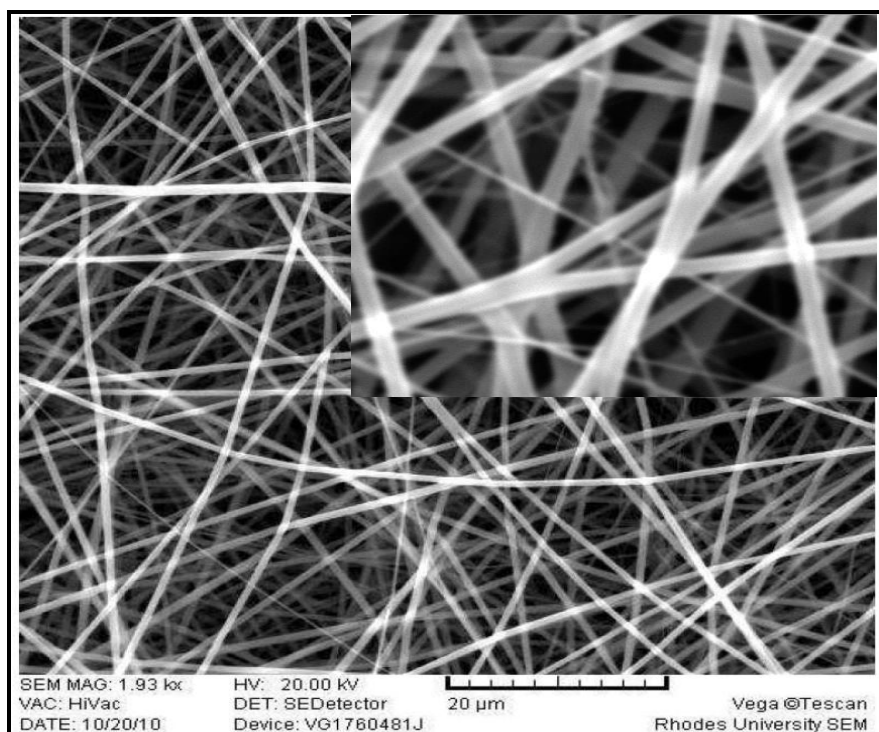
Figure 5.5: SEM image of fluorescent functionalized electrospun PAA–PAN nanofibers (Inset shows image of cross linked fibers, average fiber diameter range was 230-800 nm).

The fibers obtained were very soluble in water and even heating the fiber mats at 120 °C for 30 minutes did not change their solubility in water. Since their application was intended to be carried out in water samples, this posed a challenge. Therefore, there was need to render the nanofibers water insoluble. In this regard, a cross linker was used with the aim to form covalent bonds with the free carboxylic acid groups in the product.

Cross linking could be performed by chemical reactions that are initiated by heat, pressure, and change in pH or radiation. In this case, thermally cross linkable β-cyclodextrin (Fig. 5.6) was employed as it has free hydroxyl ends that are reactive and could form ester bonds with the free carboxylic acid groups.
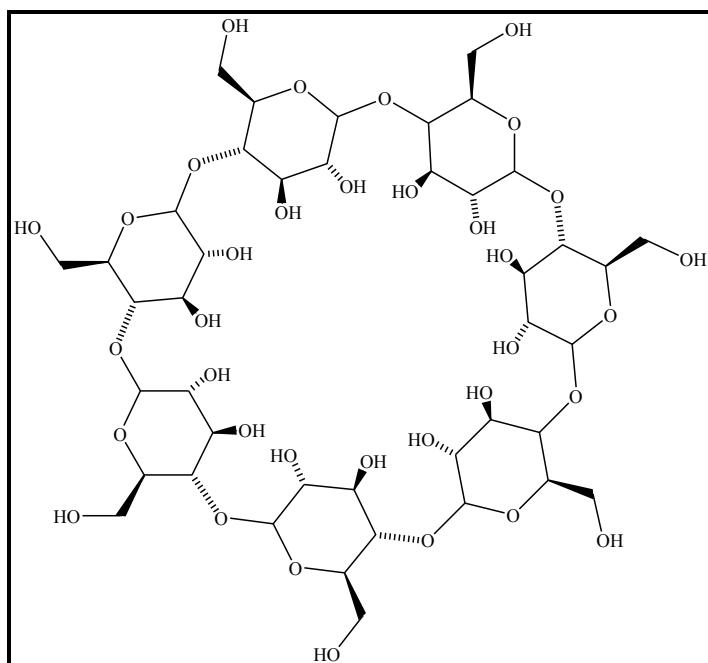
Figure 5.6: Chemical structure of β-cyclodextrin.

The suggested mechanism for this reaction indicates that it occurs in two steps [274]; in the first step; during heating, glutaric anhydride type rings could form first by the dehydration of carboxylic acid groups of poly(acrylic acid). In the second step, these 6-member cyclic anhydride rings further react with the hydroxyl groups from β-cyclodextrin (β-CD) by esterification to form the ester bonds and become water insoluble (Scheme 5.2). The cross linked PAN-PAA electrospun fibers retained their fibrous structure after a long immersion in water.

Step one;
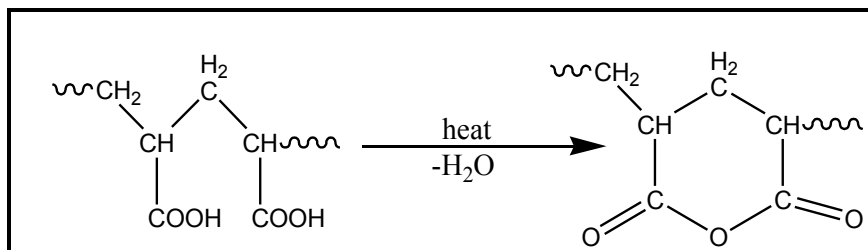
Step two;
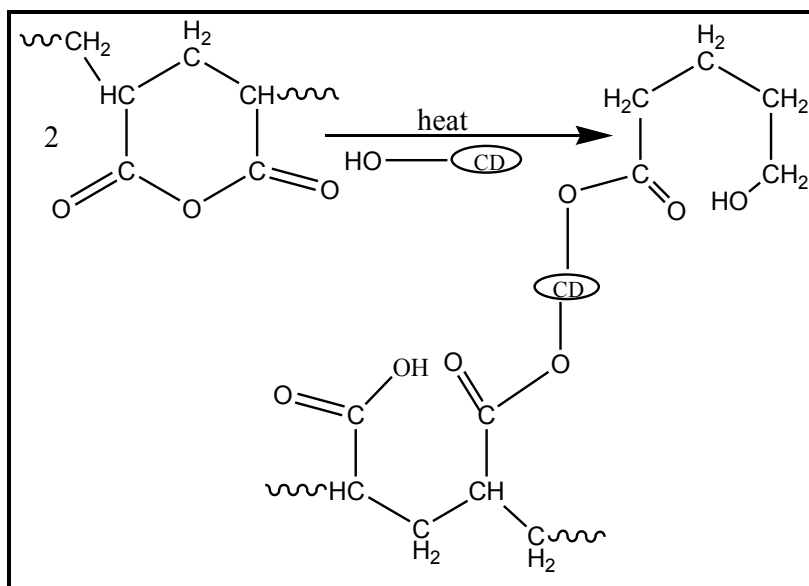
Scheme 5.2: Reaction mechanism of heat cured PAA-PAN/β-cyclodextrin at 120 ^{0}C for 20 minutes [274].

Beta-cyclodextrin was chosen as it has free hydroxyl ends that were capable of further esterification with the free carboxylic acid groups on the functionalized polymer. But a question arises regarding the possibility of coordination of metal ions by the hydroxyl groups of β–cyclodextrin. Some of the hydroxyl groups on cyclodextrin were involved in the esterification. Therefore hydroxyl groups which could be used for binding with metal ions were not directly available. However, the free ones were not expected to readily react

strongly with borderline metals like nickel in terms of hard/soft acids since the hydroxyl deprotonation occurs at high pH. More so, the binding affinity of β-cyclodextrin could only be extended through the electrostatic interaction and/or electron transfer between ligated metal and accommodated guest molecule, which in this case is the PAN-PAA. In addition, nickel (II) has a much higher affinity for the nitrogenous bases, and PAN has excellent selectivity for nickel (II) ions. So in terms of competitive binding, there would be a preference for nitrogen donor atom [275].

5.1.7 Effect of pH on the response of PAA-PAN to nickel

The fluorescence intensity versus pH plot for the PAA-PAN nanofiber (Fig. 5.7) was obtained by using the appropriate buffer and adjusting the solution pH with hydrochloric acid and sodium hydroxide while keeping the concentration of Ni^{2+} constant. It could be seen that at lower pH values, the fluorescence intensity decreased with decreasing pH value. Considering that at pH below 5.0, the protonation of receptors' nitrogen atoms of the PAN-PAA fiber could lead to a decrease in its electron donating ability and at higher pH (>8.0) value, the precipitation of metal hydroxide which decomposes to the oxide could be promoted, so the experiments were carried out at a pH range from 5.0-8.0. From the results that were obtained, it was obvious that the system could be used in a wide range of pH (5.0-8.0). In other words, there was no need for strict control of pH of the sample solution in the determination of Ni^{2+} in real samples since most water bodies exist at this range. The results however demonstrated that the functionalized polymer was affected by proton in the detection of nickel (II) ions.
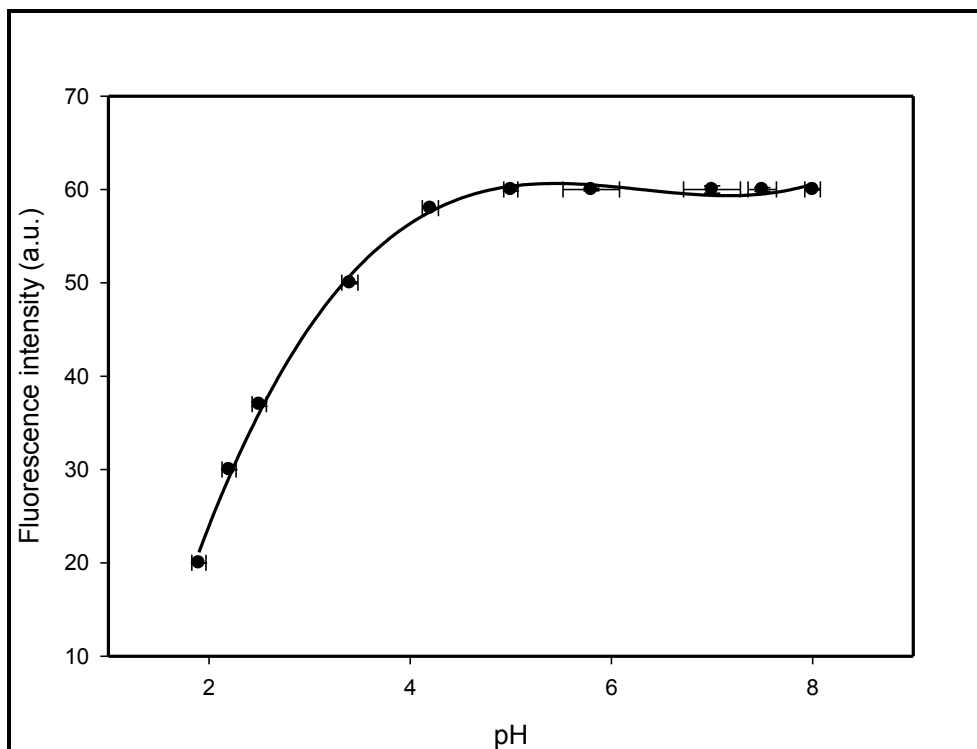
Figure 5.7: Effect of pH on the determination of Ni^{2+} with the proposed flurescent PAA-PAN system, the concentration of Ni^{2+} was 1.0 μg/mL.

5.1.8 Response of PAN−PAA nanofiber to Ni^{2+} ion concentration

In order to get clearer insight into the florescence behavior of the nanofiber, its fluorescence intensity was monitored when various concentrations of Ni^{2+} were added. It was observed that the addition of Ni^{2+} at a lower concentration of 0.1 μg/mL decreased the emission intensity drastically. When 1.0 μg/mL of Ni^{2+} was added, the fluorescence intensity decreased to less than 2%. Figure 5.8 shows the decrease of fluorescence upon addition of different concentrations of Ni^{2+}.

It was evident that the fluorescence emission intensity of the ligand decreased dramatically with increasing concentration of Ni^{2+}. The decrease in emission intensities was due to the formation of a coordination complex between Ni^{2+} ions and the N atoms of the ligand. The coordination complexes make the energy transfer possible from the excited state of the ligand to the metal ions; thus, increasing the non-radiative transition of the ligand excited

state and decreasing the fluorescence emission. The mechanism clearly involved an interaction between the metal ion and the ligand where fluorescence emission of the ligand was inhibited in this case.
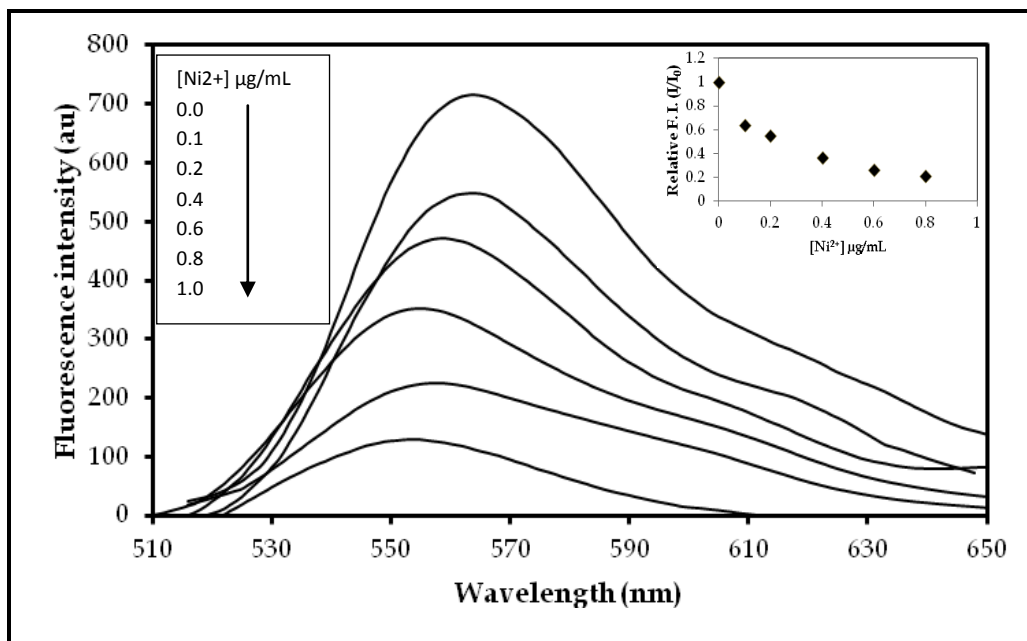
Figure 5.8: Fluorescence emission spectra of PAN–PAA nanofiber as a function of Ni^{2+} concentration. The insert shows relative fluorescence intensities (I/I_o) at 557 nm with Ni^{2+} concentration.

The relationship between the emission at 557 nm and Ni^{2+} concentrations could be deduced from the Stern-Volmer equation;

$$I_0/I = I + K_{sv}[Q] \hspace{3cm} (5.1)$$

Where, I_0 is the fluorescence intensity in the absence of quencher (Ni^{2+}), I is the intensity when the quencher is present, K_{sv} is the Stern-Vomer constant and [Q] is the concentration

of quencher. The linear range of the method was found to be 0.1-1.0 µg mL^{-1} Ni^{2+} with a correlation coefficient of $R^2 = 0.996$ (Fig. 5.9). The detection limit, based on the definition by IUPAC (DL = (3δ/S) [169], was found to be 0.07 ng mL^{-1}. The relative standard deviation (R.S.D.) for eight repeated measurements of 1.0 µg mL^{-1} Ni^{2+} was 3.9%. The K_{sv} of the nanofiber calculated from the slope of the plot was found to be; 3.69 x 10^3 mL µg^{-1} indicative of enhanced sensitivity of the detector which can be attributed to the higher surface area of the electrospun nanofibers.
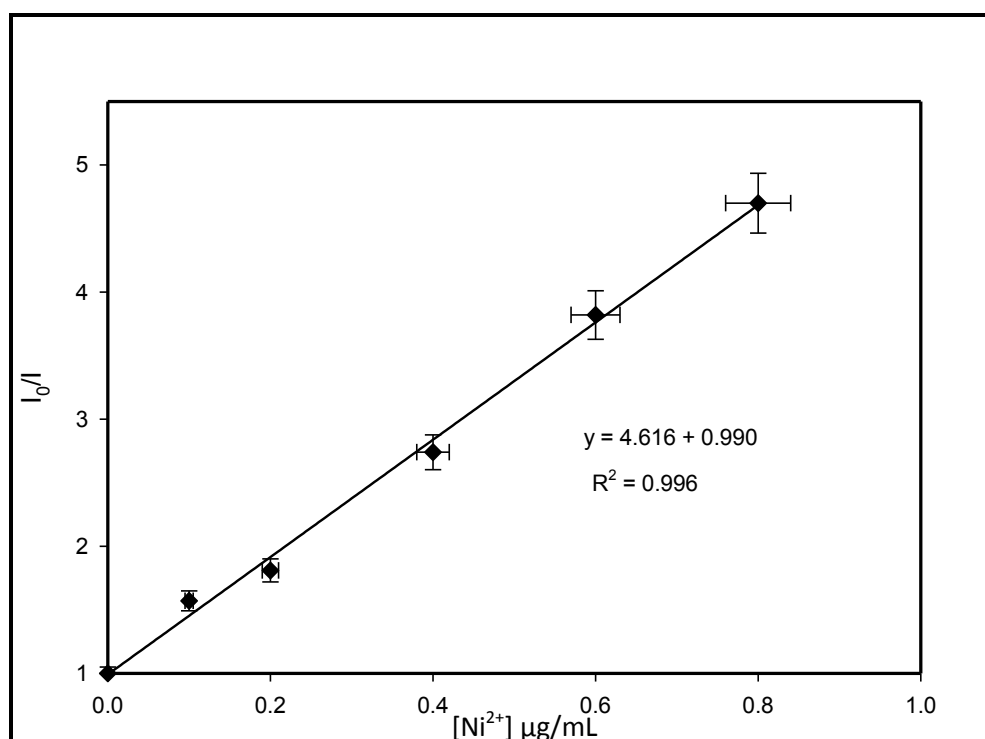
Figure 5.9: Stern-Volmer plot of fluorescence PAN–PAA nanofiber as a function of Ni^{2+} concentration.

5.1.9 Fluorescence imaging of the electrospun nanofibers

The sensitivity of the nanofiber was further visualized by fluorescence microscopy. The fluorescence images before the quenching process indicated fluorescence emission and

uniform dispersion of fluorophores, which was beneficial to the performance of the fluorescent probe. After treating the fiber mat with a 1.0 µg/mL Ni^{2+} solution, a remarkable quenching effect could be observed in the fluorescence image (Fig. 5.10).
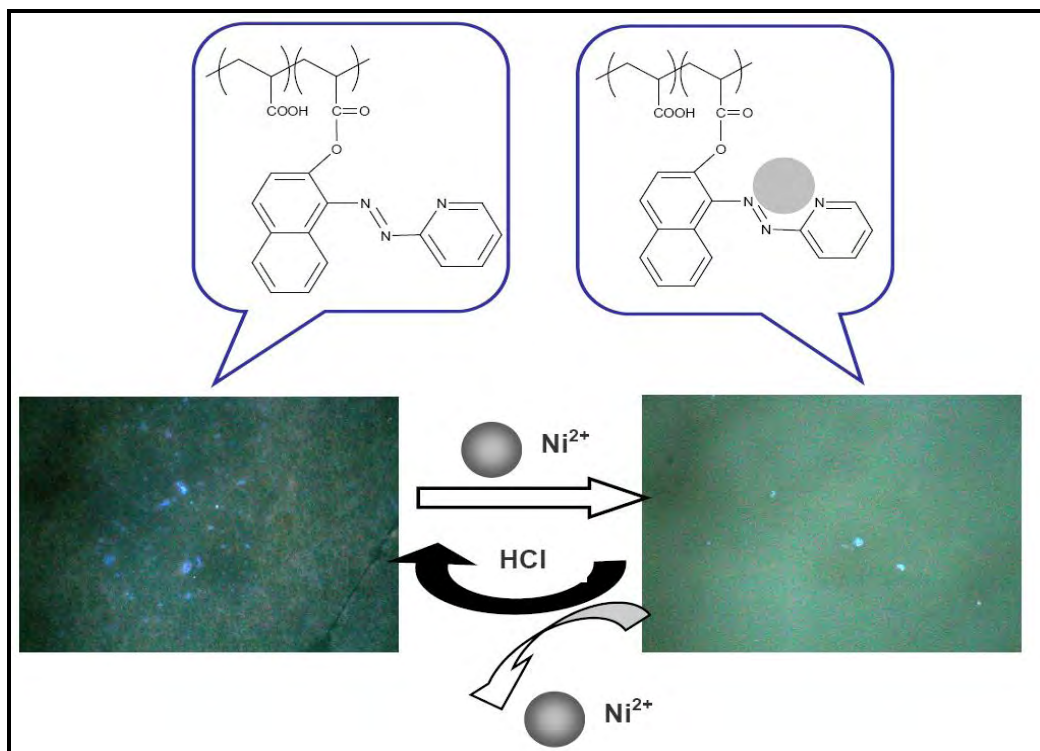
Figure 5.10: Fluorescence images of sensing electrospun PAN−PAA nanofibers before and after treating it with 1.0 µg/mL Ni^{2+} solution.

5.1.10 Mechanism of PAA-PAN quenching by Ni^{2+}

Basically, electron transfer as well as energy transfer [118, 123] and paramagnetic interactions [276], have been suggested to be responsible for the quenching of fluorescence by transition metal ions. Utilizing the Stern-Volmer mechanism, the quenching of fluorescence by metal ions could occur by at least two different mechanisms [272]. In the static quenching, on complexing of the ground state molecule with paramagnetic ion, fluorescence intensity decreases as a function of concentration of the metal ion introduced.

However, a second mechanism must involve the excited state, rather than the ground state of the fluorescent molecule (dynamic quenching). The paramagnetic metal ion causes a reduction of fluorescence intensity by inducing intersystem crossing. In an equilibrium situation, both of these mechanisms could be operating and the scenario is represented for Ni-PAN–PAA system as shown in Scheme 5.3.

$$^1(\text{Ni-PAN-PAA}) \underline{\quad\quad} (\text{IC}) \longrightarrow {}^3(\text{Ni-PAN-PAA})$$

$$h\nu \qquad (\text{PAN-PAA})_o + \text{Ni}^{2+}$$
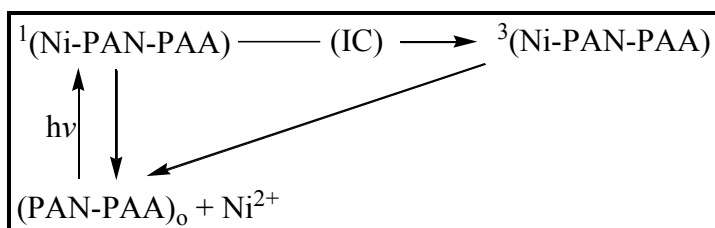
Scheme 5.3: Proposed quenching mechanism of PAN-PAA by Ni^{2+}.

Where; $(\text{PAN–PAA})_o$, $^1(\text{Ni-PAN–PAA})$ and $^3(\text{Ni-PAN–PAA})$ are ground state fluorescence molecule, first excited singlet and triplet state respectively. The rationalization is that the rate of intersystem crossing (IC) in the first excited singlet complex is enhanced by the influence of the unpaired electrons of the nickel metal ion. The first excited singlet crosses over to the triplet state, which may then undergo some type of quenching to return to the ground state.

The exact mechanism taking place in this system was not fully established since fluorescence lifetimes were not determined. But absorption spectra of PAA-PAN and PAA-PAN-Ni^{2+} were recorded. For static quenching, the complex is expected to have a different absorption spectrum from that of the fluorescent indicator. Presence of an absorption change is therefore diagnostic of static quenching. From the spectra obtained, the spectrum of the complex; PAA-PAN-Ni^{2+} was different from that of PAA-PAN (Fig. 5.11). The complex had a spectrum with absorption maxima at 509 nm with a shoulder band at 553 nm while that of PAA-PAN had a maximum absorption at 479 nm. The difference therefore, signified that the quencher had diffused into the fluorophore while in the ground state. But, the UV-

vis results only could not be conclusive without the fluorescence lifetime data since both static and dynamic quenching can be at play in a single system [127].
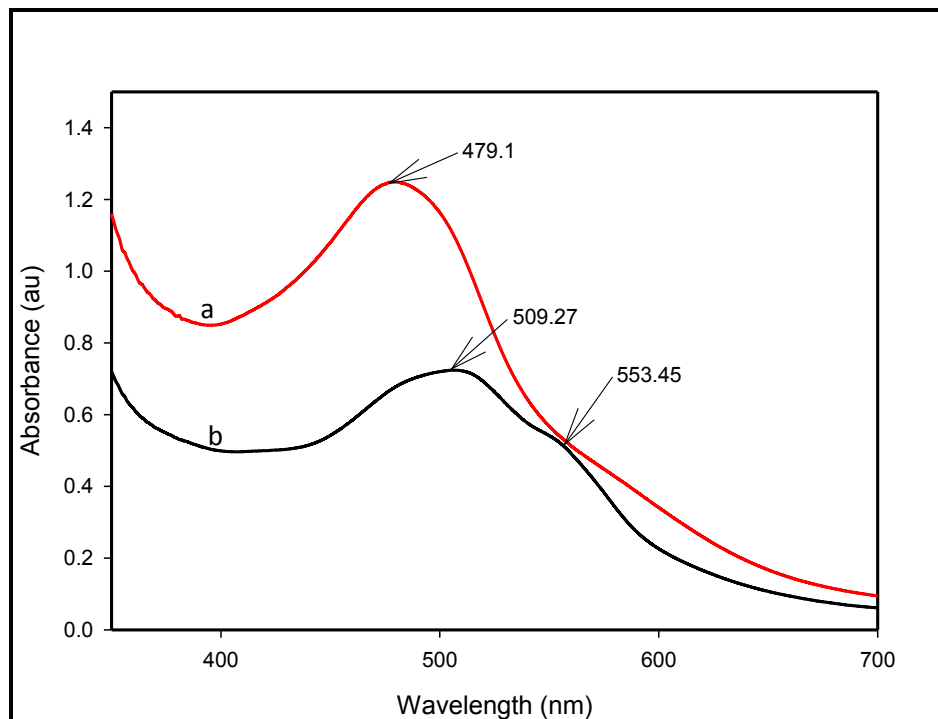
Figure 5.11: Absorption spectra of; (a) PAA-PAN (b) PAA-PAN-Ni^{2+}.

5.1.11 Selectivity of the fluorescent probe

In the design of diagnostic probes for environmental analysis, the interference due to other species in the sample normally poses a challenge to analysts. Depending on the proposed end-use of the diagnostic probe, interference from other species could limit their applications. The selectivity of metal ions could be affected by the diffusion kinetics of the metal ions into the probes and also the binding affinity of metal ions with ligands. Therefore, several commonly existing metal ions were tested.

The selective binding ability of PAN−PAA nanofiber was determined by addition of equal concentrations of various metal ions (Al^{3+}, Cr^{3+}, Fe^{2+}, Co^{2+}, Cu^{2+}, Zn^{2+}, Cd^{2+} and Pb^{2+}). PAN-

PAA nanofibers were found to have a large chelation enhanced quenching (CHEQ) effect only with Ni^{2+} among the metal ions examined with percentage quenching near 100% as shown in Fig. 5.12. In contrast, addition of other metal ions (Al^{3+}, Cu^{2+}, Zn^{2+}, Cd^{2+} and Pb^{2+}) did not show fluorescence quenching but rather enhanced the fluorescence intensity of the probe. However, Cr^{3+}, Fe^{2+} and Co^{2+} ions showed weak quenching abilities, probably due to their diamagnetic nature. In particular, the probe showed a high selectivity for Ni^{2+} in contrast to other metal ions tested in its fluorescence quenching response.
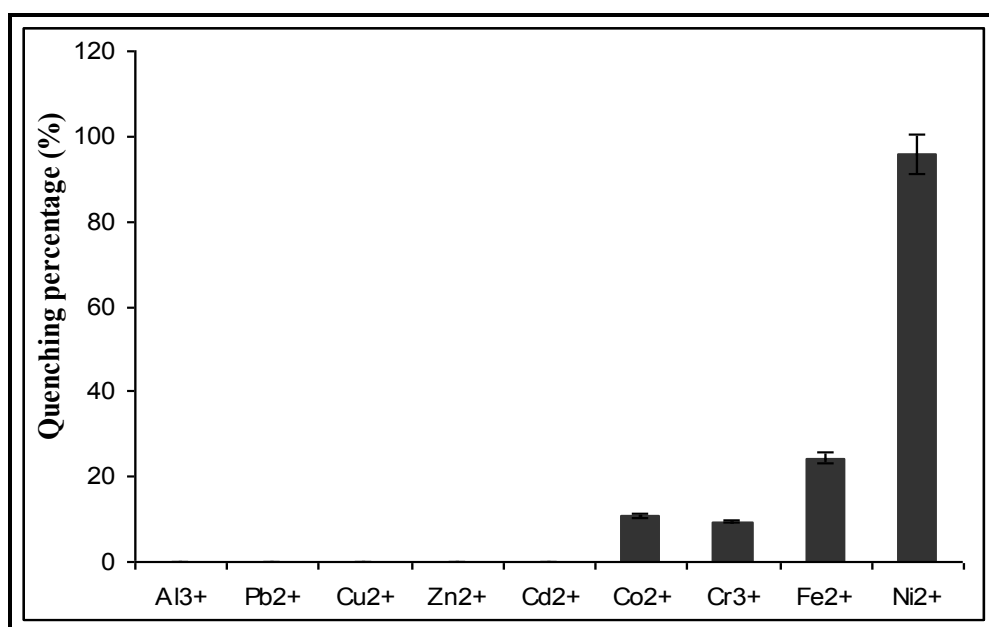
Figure 5.12: Quenching percentage ($[Io-I/Io]$ x 100 %) of fluorescence intensity of PAN–PAA nanofiber upon addition of 1.0 equivalence of metal ions.

The selectivity and tolerance of PAN–PAA for Ni^{2+} over other metal ions was further examined by competition experiments (Fig. 5.13). When 1 equivalent of Ni^{2+} in the presence of 10 equivalence of respective metal ion was introduced on the fiber, the emission spectra displayed a similar quenching near 557 nm to that of Ni^{2+} alone. The results indicated that the fluorescence quenching by Ni^{2+} was hardly affected by the co-existence of other metal ions, a characteristic which is vital to its applications in

environmental samples. When analyte solutions containing mixtures of competing species are used, the issue of selectivity becomes more important.
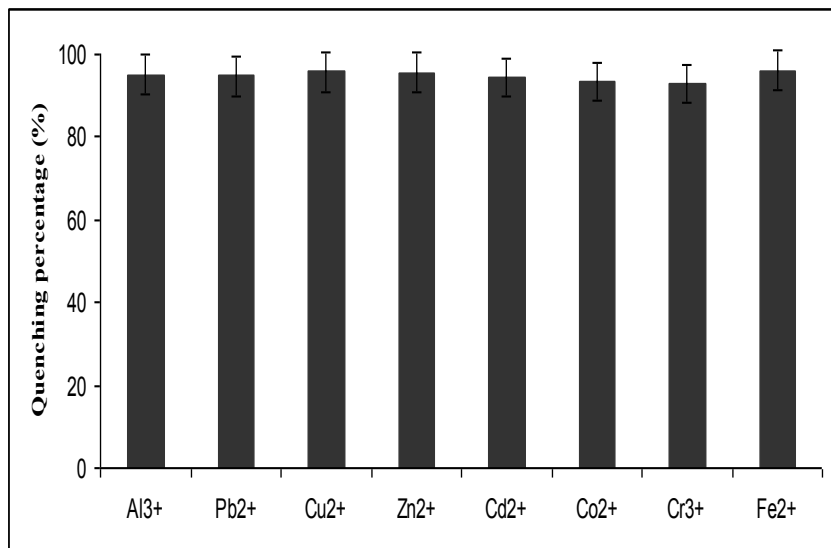
Figure 5.13: Quenching percentage ($[I_o-I/I_o]$ x 100 %) of fluorescence intensity of PAN–PAA nanofiber upon addition of 1.0 equivalent of Ni^{2+} and 10.0 equivalence of other ions.

5.1.12 Reusability of the probe

The reproducibility of a signaling response is a desirable characteristic in the design of a diagnostic probe. In fact the most attractive characteristic of the solid state probes is their regeneration efficiency because it is this parameter that would determine the cost of any analytical procedure. To investigate its reusability, the fluorescent nanofiber was used to complex Ni^{2+} through complex-stripping cycles. The stripping agent used was 0.1 M HCl. Figure 5.14 shows a profile of the fluorescence response during five sequential cycles. The nanofiber was found to be able to re-combine with Ni^{2+} for at least four times (I_4/I_1=94.8%). The subsequent decrease of the fluorescence intensity could be attributed to the effect of stripping agents on the sensing performance and little loss of the fiber during multiple regeneration experiments. However, the probe showed excellent reusability and

stability towards Ni^{2+} for at least four successive cycles. Hydrochloric acid was chosen as a simple stripping agent for the regeneration of nickel-free PAN-PAA nanofiber. This was because at pH below 5.0, the protonation of receptors' nitrogen atoms of the PAN-PAA fiber decreased its electron donating abilities.
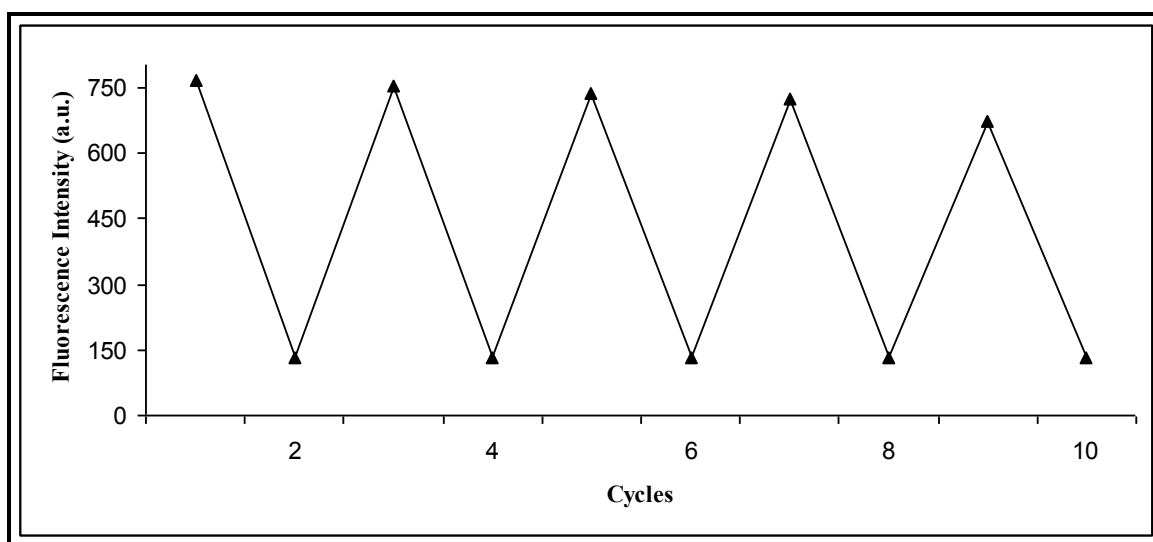
Figure 5.14: Repeated switching of fluorescence emission of the PAN–PAA nanofiber against the number of Ni^{2+} solution/eluent cycles.

5.1.13 Validation of the method

Table 5.1 gives the quality control parameters regarding the detection of nickel metal ion in aqueous solution. Accuracy of the determinations, expressed as relative error between the certified values of the reference material and the observed were $\leq 0.1\%$. The precision of these measurements expressed as relative standard deviation for eight repeated measurements of 1.0 μg/mL Ni^{2+} was also satisfactory, being lower than 4%. The limit of detection, based on the definition by IUPAC (LOD = (3δ/S) [277], was found to be 0.07 ng/mL. This LOD achieved with the PAN-PAA nanofibers was lower than 4.5 ng/mL achieved with fluorescence-based sensor from *Escherichia coli* nickel binding protein labeled with N-[2-(1-maleimidyl)ethyl]-7-(diethylamino)coumarin-3-carboxamide [278].

In addition, the LOD was significantly lower than 0.02 µg/mL nickel concentrations above which it is toxic in drinking water as established by EPA [279].

Table 5.1: Analytical quality control.

I_0/I	Certified concentration (µg/mL)	Concentration found (µg/mL)	Relative error (%)	Relative standard deviation (%)	LOD (ng/mL)	LOD[a] (ng/mL)	LOD[b] (ng/mL)
5.29	0.8980(0.007)	0.8986(0.004)	+0.0668	3.9203	0.0710	0.1	4.5

[a]Square-Wave anodic stripping voltammetry bismuth-film electrode sensing method [280].

[b]Fluorescence-based sensing system using nickel binding protein from *Escherichia coli* [279].

5.2 Colorimetric probe for detection of Ni^{2+} ions in water based on Ag/Cu alloy nanoparticle

5.2.1 Choice of the metal nanoparticles

For color signal generation, metal nanoparticles are particularly attractive; as they possess much higher extinction coefficients compared to organic dyes, allowing sensitive colorimetric detections with minimal material consumption [281]. Among the metals, gold, silver and copper are known to display plasmon resonances in the visible spectrum [282]. Metal alloy nanoparticles, on the other hand, have mainly been studied because of their catalytic effects [283]. For whichever application they are designed, colorimetric probes should be simple and robust. Even if these criteria are fulfilled, whether an assay will be used or not is decided by the availability of the reagents, their price, and their overall simplicity. We chose to use Ag and Cu because they are cheap in comparison to gold. Secondly, alloy nanostructures have been reported to offer additional degrees of freedom for tuning their optical properties.

5.2.2 Choice of the stabilizing agent

Because of their small size, nanoparticles have a very high surface area to volume ratio resulting in a high reactivity and the need to stabilize them. Glutathione (GSH) (Fig. 5.15) was used both as a stabilizing agent and a ligand that could selectively bind Ni^{2+} ions in aqueous media.
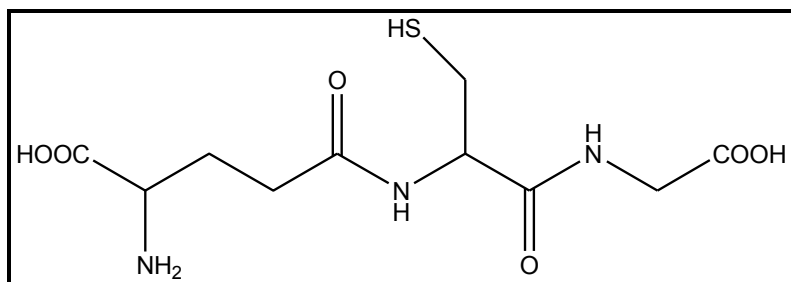
Figure 5.15: Structure of glutathione (GSH).

Glutathione is a tripeptide (-Glu-Cys-Gly) that contains a thiol (-SH) group which can easily form a covalent bond with the metal nanoparticles. Glutathione is known to protect red cells from oxidative damage when it is present in sufficiently high quantities (~5 mM) and to maintain the normal reduced state of the cell because of its antioxidant nature. Glutathione also plays an important role in the detoxification of the cell and is responsible for removing harmful organic peroxides and free radicals. It binds to toxins, such as heavy metals, solvents, and pesticides, and transforms them into a form that can be excreted in urine or bile [284].

In particular, GSH has two free -COOH groups and a -NH$_2$ group to provide a hydrophilic interface and a handle for further reactivity with heavy metals such as nickel(II) ion. GSH could bind Ni^{2+} in aqueous solution resulting in the aggregation of nanoparticles due to strong coordination bond formed between Ni^{2+} and -NH$_2$, -COOH of the functionalized glutathione modifier. The aggregation was expected to result in a significant shift in the

plasmon band and a substantial color change since metallic nanoparticles display distance-dependent optical properties [282].

5.2.3 Choice of the polymer support

Incorporation of metal nanoparticles into other materials is an attractive method of increasing compatibility for specific applications. Polymers are considered as good host materials for metal nanoparticles as well as other stabilizing agents. Nylon 6 was used as the polymer matrix firstly because of its good mechanical strength [285]. Secondly, nylon 6 has multiple nitrogen atoms on its back bone which could stabilize the metal nanoparticles during synthesis. In addition to the afore-mentioned properties, the presence of hydrogen bonds in the polymer makes it polar hence enhances its wettability when used in water samples.

5.2.4 Synthesis of glutathione-stabilized silver/copper alloy nanoparticles

One step *in situ* synthesis of the alloy nanoparticles in the polymer matrix was employed in the work. Different chemical and physical methods exist to prepare metal-polymer composites [286]. A successful preparation of nanoparticles is determined by the ability to produce particles with uniform distributions and long stability, given their tendency to rapidly agglomerate. The widely used fabrication approach is to disperse previously prepared particles in the polymer matrix [287]. This method is often referred to as the evaporation method since the polymer solvent is evaporated from the reaction mixture after nanoparticle dispersion. However, this often leads to inhomogeneous distribution of the particles in the polymer.

One solution is the *in situ* synthesis of metal particles in the polymer matrix, which involves the dissolution and reduction of metal salts or complexes in the polymer matrix [288]. *In situ* synthesis can be done by reducing the metal precursors to nanoparticles with chemicals (e.g., an aqueous solution of N_2H_5OH, potassium/sodium borohydride, radiation (e.g., UV radiation) or high temperatures. The *in situ* reduction of metal ions led to the homogeneous distribution of nanoparticles in the polymer matrix. Sodium borohydride was used as the reducing agent to produce the alloy nanoparticles within the polymer matrix (Scheme 5.4).

The choice of $NaBH_4$ was based upon the fact that, it is a strong reducing agent which did not require heating during the reaction. Secondly $NaBH_4$ has been reported to produce nanoparticles that have very small sizes [289]. The small particle sizes were of great interest in the research work since electrospinning was to be applied for fabrication of the nanocomposite fibers. This meant that the sizes had to be very small to pass through the electrospinning needle and also to blend well with the polymer.

Polymer Solution/ $AgNO_3$/$CuSO_4.5H_2O$ → $NaBH_4$ → NPs → GSH → NPs
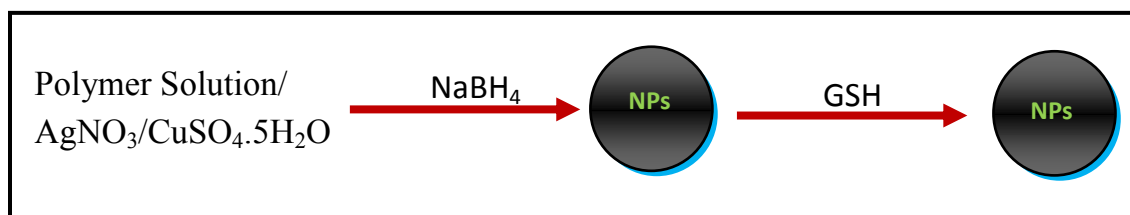
Scheme 5.4: *In-situ* synthesis of glutathione stabilized Ag-Cu alloy nanoparticles.

5.2.5 Optical properties of synthesized Ag-Cu alloy nanoparticles

UV-vis spectroscopy is one of the widely used techniques for structural characterization of nanoparticles. The absorption spectrum (Fig. 5.16) of the black silver-copper alloy colloids prepared showed a surface plasmon absorption band with a maximum at 424 nm. If silver and copper ions are reduced simultaneously in the same solution, silver-copper alloy nanoparticles are expected to be formed. The alloy formation could be concluded from the

fact that the optical absorption spectrum showed only one plasmon band and this was in agreement with what had been reported in literature [290-292]. Two bands would be expected for the case where there was a mixture of silver and copper nanoparticles. Also, the appearance of a narrow SPR absorption band at 424 nm confirmed the narrow size distribution and the well dispersed state of the alloy nanoparticles that were formed.
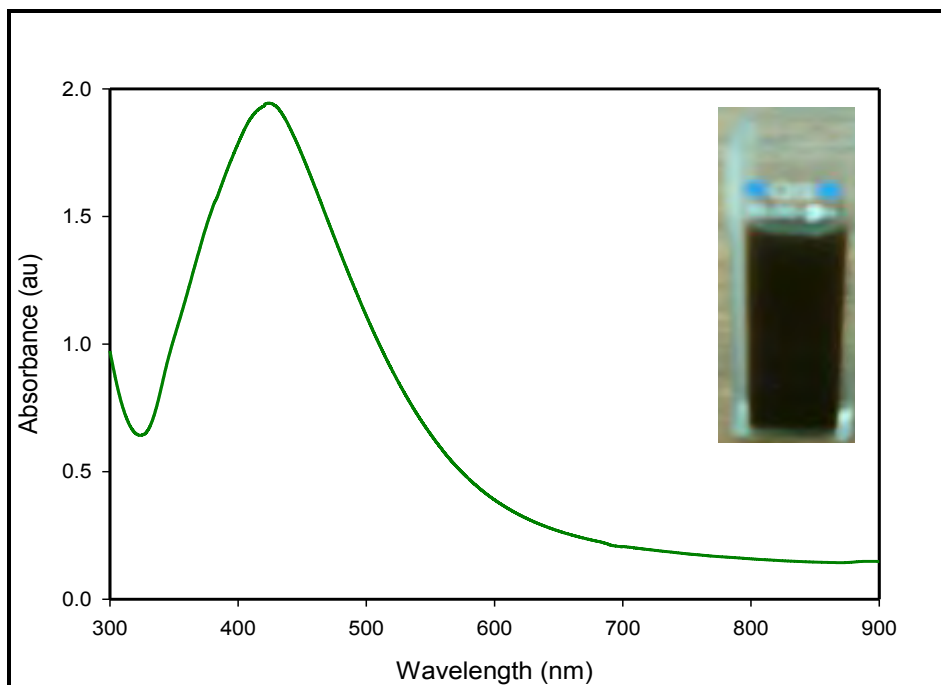
Figure 5.16: UV-vis spectrum of Ag-Cu/Nylon 6 nanocomposite solution before electrospinning.

The appearance of a single absorption band indicated that the synthesized Ag-Cu bimetallic particles were in alloy form rather than being a mixture of individual metal nanoparticles, whereas the physical mixture of synthesized Ag and Cu nanoparticles showed two absorption bands corresponding to the individual metal nanoparticles (Fig. 5.17 inset). Silver NPs alone in the polymeric solution had a strong surface plasmon resonance peak at 408 nm, while that of the Ag-Cu alloy NPs was red-shifted to 424 nm and slightly broadened which is in agreement with what had been reported [290]. In addition, the plasmon resonance absorption band of Ag NPs was stronger and sharper in comparison to

that of Cu nanoparticles which was at 551 nm, and occurred at a longer wavelength (Fig. 5.17).

The collective plasmon resonance absorption band of Ag-Cu alloy differed dramatically from that of Ag or Cu, and could easily be tuned in the UV-vis region by changing the Cu/Ag mole ratio. The notable change in the absorption spectra could primarily be attributed to a change in the dielectric function when different metal atoms were mixed. Silver has been reported to display approximately free electron behavior in the visible region, which gives rise to a sharp absorption band. Other metals, including Cu and Au, have less free-electrons, which gives rise to a broad absorption bands [293].
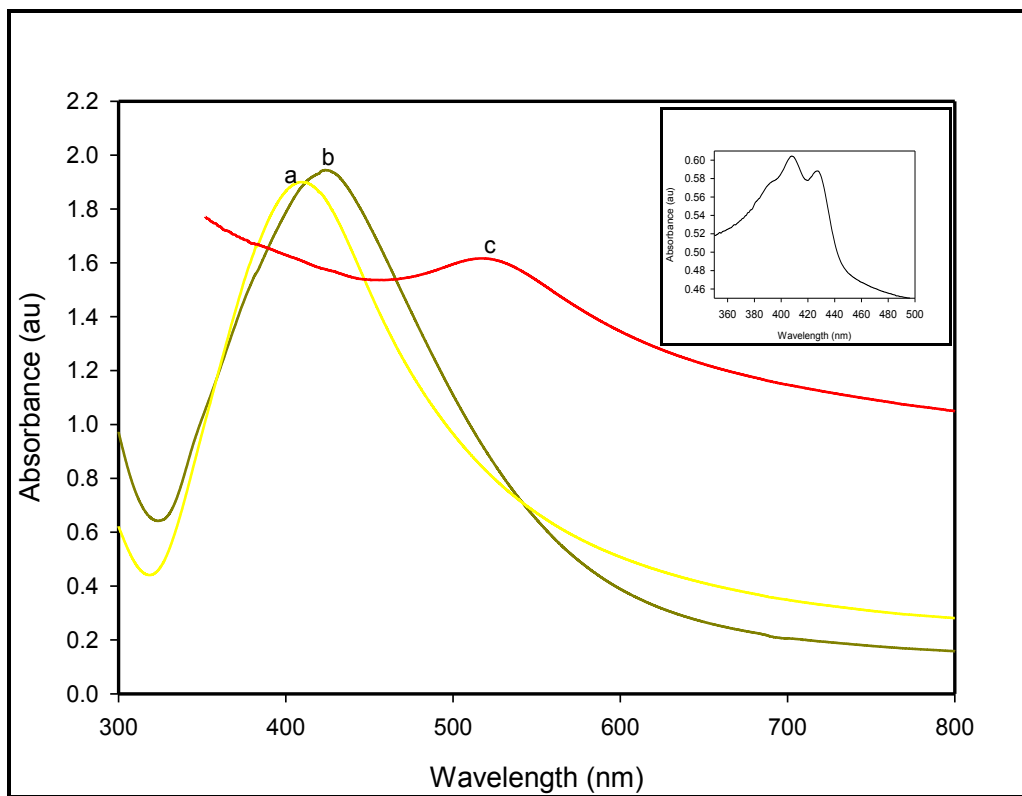
Figure 5.17: Surface plasmon absorption spectra of AgNPs (a), Ag-Cu alloy NPs (b), CuNPs only (c), inset is for the physical mixture of Ag and Cu NPs.

5.2.6 Reducing agent

The general chemical reduction reactions involve reducing agents that are reacted with a salt of the metal according to the following chemical equation:

$$mMe^{n+} + nRed \longrightarrow mMe^0 + nO_x \qquad (5.2)$$

Where, m is the number of moles of the metal ions, Me is the metal ion, $n+$ is the charge on the metal ion, n is the moles of the reducing agent, Red is the reducing agent and O is the oxidized form of the reducing agent.

In a study of metal ion reduction by borohydride system, it was reported that BH_4^- ions functions not only as a reducing agent but also as a stabilizer that prevents the nanoparticles from aggregating [294]. Adsorption of borohydride onto the surface plays a key role in stabilizing growing nanoparticles by providing particle surface charge leading to electrostatic repulsion that keeps them from agglomerating (Scheme 5.5). Therefore, there had to be enough borohydride in solution to reduce the metal ions as well and to stabilize the particles as the reaction proceeded.
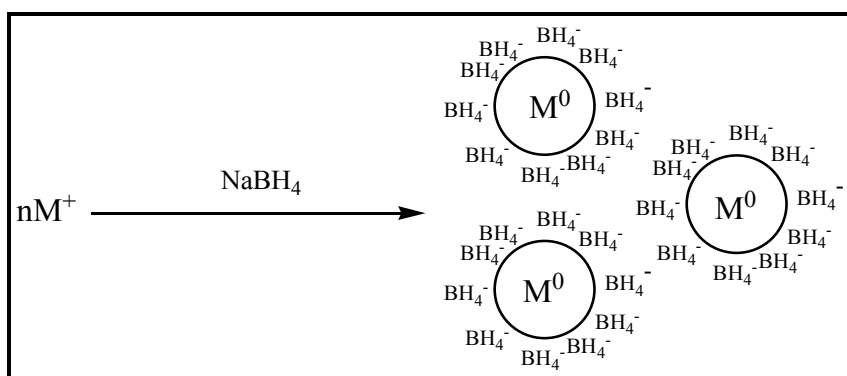
Scheme 5.5: Separation of nanoparticles by repulsive forces induced by adsorbed borohydride.

Later in the reaction however, it was observed that when the mole ratio of the salts to $NaBH_4$ was greater than 1:2.8, aggregation of the nanoparticles was observed. This could be

due to the fact that NaBH$_4$ increased the overall ionic strength of the solution leading to aggregation of the nanoparticles. Therefore, the amount of NaBH$_4$ had to be optimized. The optimal mole ratio of the total salts to sodium borohydride was found to be; 1:2.8. Below and above the optimized mole ratio, there appeared more than one peak which was also very broad (Fig. 5.18). The broad nature of the peaks could be attributed to large size distribution and probably aggregation caused by excess or less concentrations of the reducing agent.
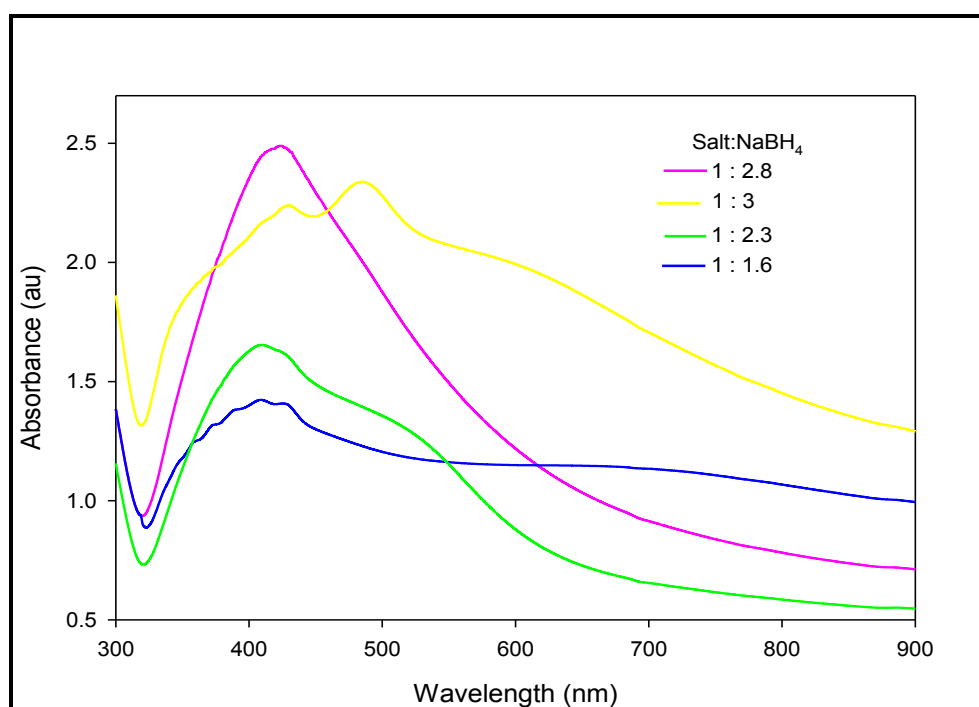
Figure 5.18: UV-vis spectra of Ag/Cu alloy nanoparticles with varying mole ratios of reducing agent.

Upon introduction of the stabilizing agent (GSH), the rather loose shell of borohydride ions on the Ag/Cu NPs surfaces could easily be displaced by other desired ligands with valuable functionalities (e.g. N and -SH groups). Molecules with electron-rich nitrogen or sulphur atoms are easily bound onto the surface of metal nanoparticles through the coordinating interactions between sulphur or nitrogen atoms with the electron-deficient surface of

metal nanoparticles. In particular, the sulphur atom of GSH exhibited much stronger binding ability/affinity to NPs than the borohydride ions. A stabilizing agent relies on electrostatic repulsion force caused by either surface charge or steric stabilization, or both to prevent nanoparticles from aggregation.

5.2.7 Characterization of GSH-Ag/Cu Alloy NPs nanofibers

The morphology of the GSH-Ag-Cu alloy nanofibers was observed using a transmission electron microscope (TEM). As shown in Fig. 5.19, glutathione stabilized Ag-Cu alloy nanoparticles having sizes between 3-6 nm were well dispersed in the electrospun nanofibers. Glutathione was used with the aim to stabilize the nanoparticles in order to prevent them from aggregation and this was successful as could be observed from the TEM image. For environmental applications, surface functionalization of nanoparticles is essential to apply them for selective detection of a specific analyte. Therefore, apart from stabilizing nanoparticles formed, GSH also served as a ligand that could selectively bind Ni^{2+} ions in aqueous media.
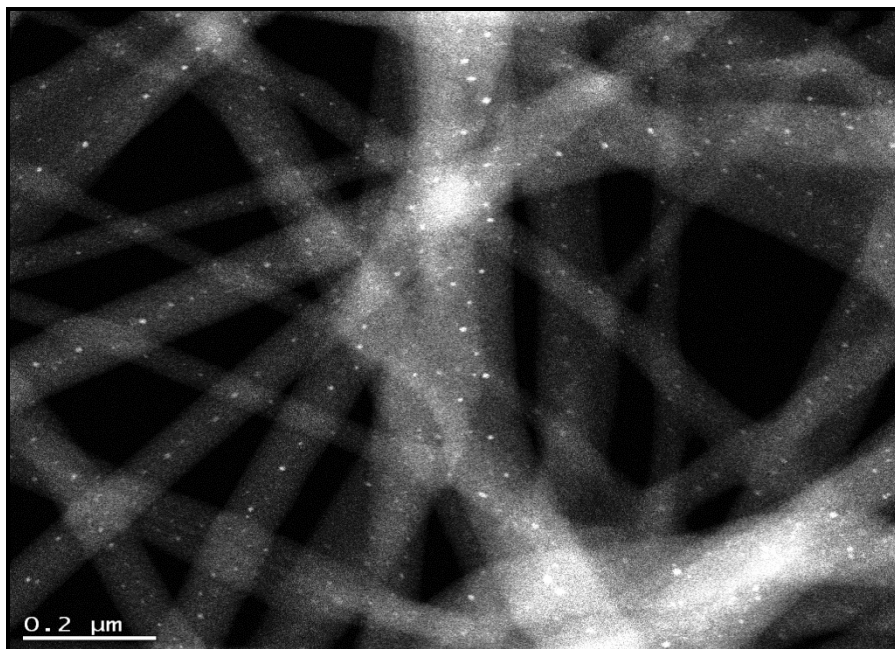
Figure 5.19: Transmission electron micrograph of Ag-Cu alloy nanoparticles in the electrospun nanofibers.

5.2.8 Metal ions recognition ability of Ag-Cu alloy nanoparticles

To investigate the metal ions recognition ability of GSH-Ag-Cu alloy NPs, metal ions (Ni^{2+}, Mn^{2+}, Fe^{2+}, Co^{2+}, Cd^{2+} and Pb^{2+}, Na^+, Cr^{3+}) of the same concentration (0.1 mol L^{-1}) were prepared and the electrospun fiber mats were cut and placed in the solutions. Deionized ultrapure water obtained from a Millipore system was used as control in this experiment. Upon interaction with various metal ions, as could be seen from Fig. 5.20, the fiber mat placed in the solution containing Ni^{2+} was discolored, while other metal ions did not discolor the mats.
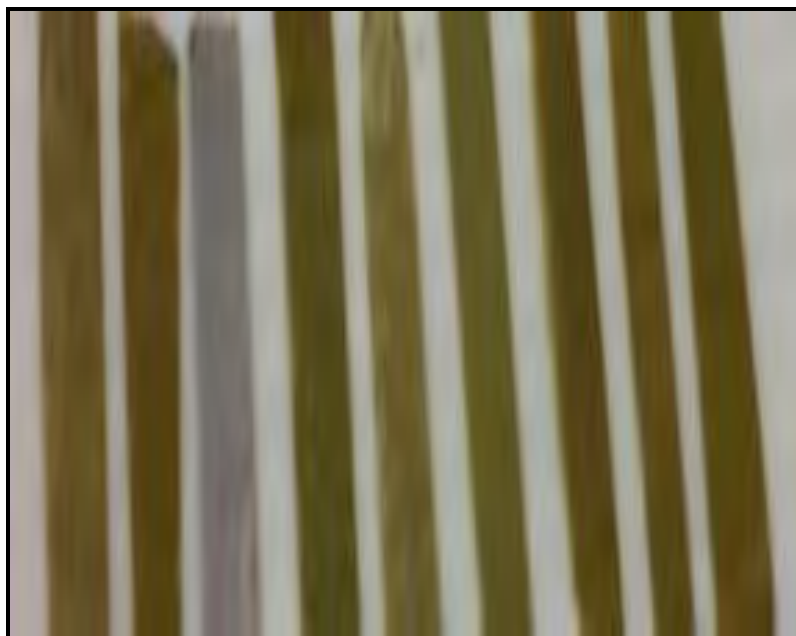
Figure 5.20: Colorimetric responses of the fiber strips to various solutions from left, H_2O, Pb^{2+}, Ni^{2+}, Fe^{2+}, Na^+, Cr^{3+}, Ca^{2+}, Mn^{2+} and Co^{2+} respectively.

Glutathione, a tripeptide containing cysteine, contains two carboxylic acid groups. Marco Bieri and Thomas Bürgi [295], reported that, at least one of these carboxylic acid groups forms an additional anchor to the metal nanoparticle surface, besides the strong metal-sulfur bond when it is used as a stabilizer. Upon interaction with the surface, part of the carboxylic acid groups also deprotonates. Ni^{2+} is known to bind well to groups or ligands containing lone pair of electrons such as -NH_2, -COOH via a coordination bond [296]. Both the terminal carboxylate groups of glycine moiety and the free -NH_2 groups from glutamate moiety were believed to be responsible in binding the Ni^{2+} center. The nanoparticles were expected to aggregate upon interaction with Ni^{2+} due to strong coordination bond between Ni^{2+} and –NH_2, –COOH of the functionalized glutathione modifier. We therefore concluded that; the carboxylic acid groups that were bound to the surface of the nanoparticles were detached and in the process the nanoparticle surface became exposed and this led to agglomeration and subsequent loss of their surface properties. Agglomeration is mainly caused by excess surface energy and high thermodynamic instability of the nanoparticle surface [289].

It must be noted that in the presence of Ni^{2+} ions, Ag/Cu alloy nanoparticles were aggregated and latter oxidized to silver and copper ions probably because GSH no longer surrounded the alloy nanoparticles. The observations were consistent with the SEM results that were obtained. The SEM images of alloy nanoparticles before and after the addition of Ni^{2+} ions are shown in Fig. 5.21. As could be seen, aggregated nanoparticles were observed in nanofibers treated with Ni^{2+} solution although it was not possible to see the nanoparticles before the nanofibers were treated with the analyte using SEM microscope. This could have been so because; they were encapsulated within the nanofibers. The discoloration was probably related to the oxidation of the aggregated nanoparticles which we believe were no longer stabilized and the consequent formation of a colorless complex between glutathione and Ni^{2+} ions.
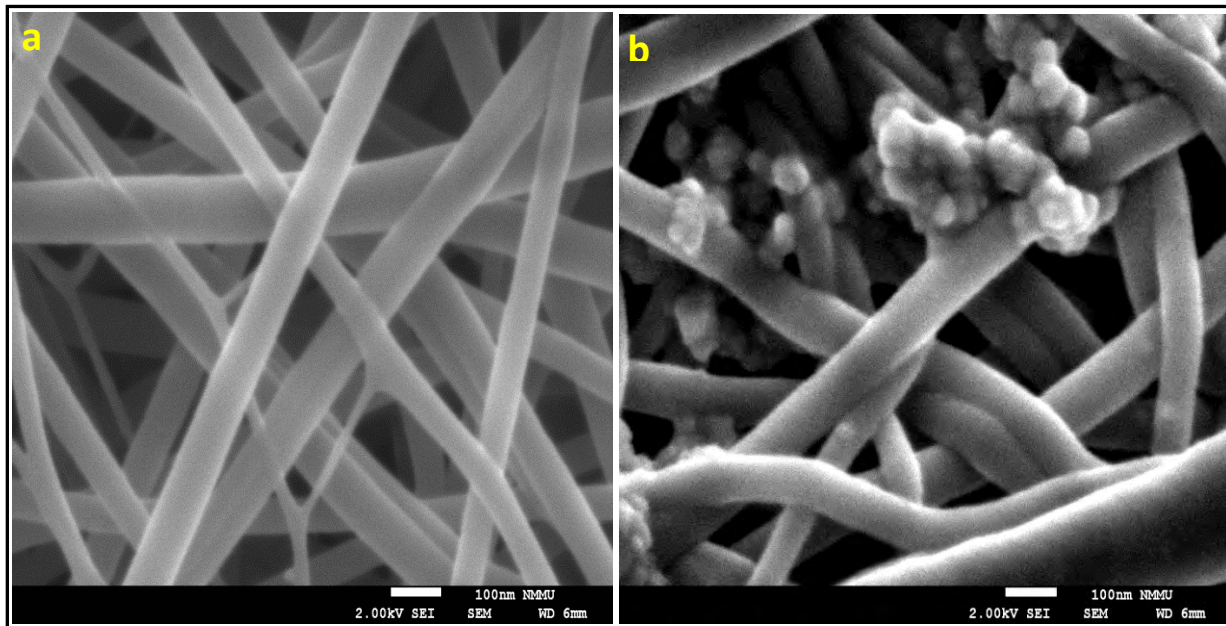
Figure 5.21: Scanning electron micrograph of Ag-Cu alloy-nylon 6 nanocomposite fibers (a) before and (b) after treatment with nickel (II) ions.

To further confirm that the nanoparticles had actually been oxidized, some crystals of nickel chloride salt were dissolved in the nanocomposite solution before electrospinning and a color change from black to blue was observed(Fig. 5.22 inset). The blue color indicated the presence of Cu^{2+} ions in the mixture while Ag^+ ions are colorless. This oxidation was further confirmed by UV-vis spectroscopy (Fig. 5.22). It could be seen that the SPR absorbance had been significantly decreased by the presence of nickel in the nanocomposite solution and that designated a considerable decrease in the concentration of Ag-Cu alloy NPs.
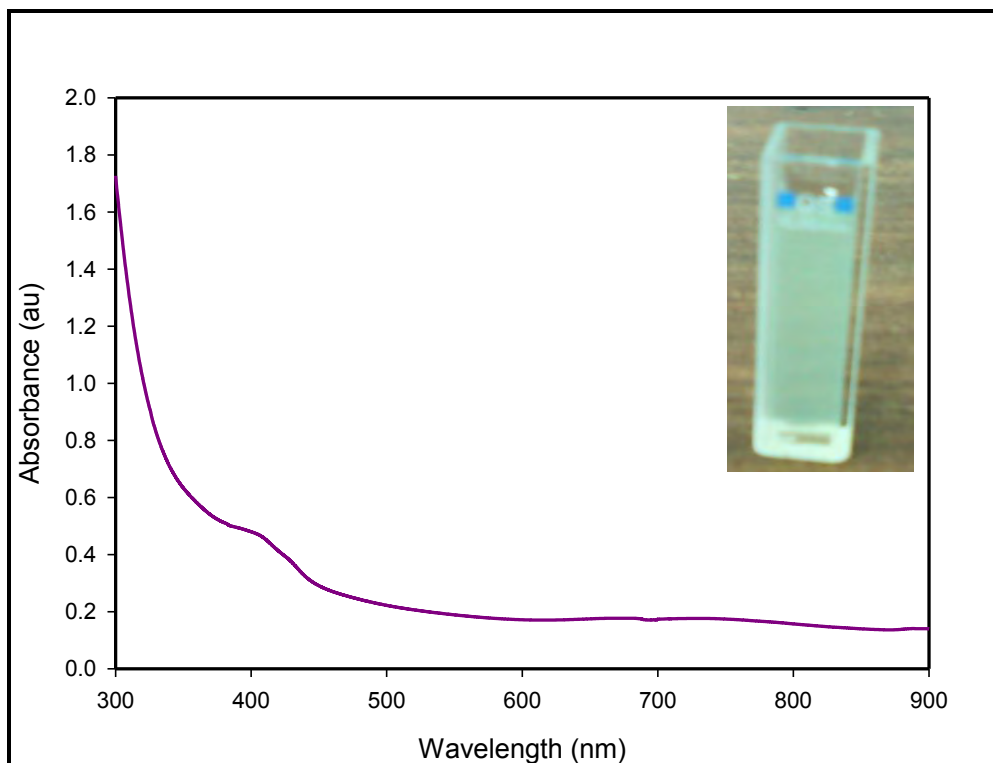
Figure 5.22: UV-vis spectra of Ag-Cu alloy nanocomposite solution incubated with Ni^{2+} ions and inset is photograph of the mixture.

In an attempt to evaluate the effect of concentration of Ni^{2+} to the color change of the nanocomposite fiber, a series of solutions of Ni^{2+} with different concentrations ranging from 0.058 μg/mL to 5.8 mg/mL were prepared and the fiber immersed into the solutions. Color changes were observed on the fibers in solutions having concentrations of 5.8 μg/mL to 5.8 mg/mL within 30 min, at the rate at which was proportional to the concentration. Below 5.8 μg/mL, the fibers changed after an overnight stay in the nickel ion solutions down to a concentration of 0.058 μg/mL.

5.2.9 Real samples analysis

The proposed method was applied in the determination of the concentration of nickel (II) ions in a water sample, tap water from the F12 research lab at Rhodes University was used.

For this purpose, the fiber strip was put in a vial containing 5 mL of tap water sample. No change in the color of the fiber strip was observed thus confirming that the concentration of Ni^{2+} in the sample was less than the limit of detection of the proposed method. The tap water was then spiked with 5.8 μg/mL of Ni^{2+} solution and the fiber mats were discolored. This result demonstrated the applicability of the colorimetric probe for detection of Ni^{2+} ion in real water samples.

5.3 Colorimetric probe for rapid detection of Fe^{2+} ions in aqueous media

5.3.1 Synthesis of 2-(2'-pyridyl)-imidazole (PIMH)

The synthesis of the ligand (PIMH) was accomplished by use of pyridine-2-aldehyde, gloxal and ammonia solutions. Synthesis of PIMH from pyridine-2-aldehyde and glyoxal in aqueous ammonia solution (Scheme 5.6) provided a direct route for the preparation of the imidazole ring of the ligand. This reaction is highly exothermic and hence must be carried out at low temperatures. This necessitated the use of ice cold glyoxal and ammonia solutions. The reaction vessel was also placed in an ice bath to maintain the needed low temperatures. The reactants were stirred in the ice bath for 30 min and then allowed to stand overnight at room temperature. Upon leaving the solution overnight, the color changed from light yellow to dark brown. A black viscous liquid was formed after evaporating the solvent with a rotary evaporator. To achieve optimum yield, extraction of the product with diethyl ether was done several times until no visible brown color was observed. The obtained yellow crystals were further purified by re-crystallization in ethyl acetate.
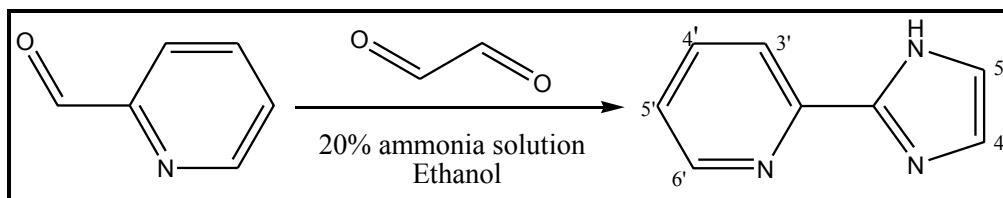
Scheme 5.6: Synthesis of 2-(2′-Pyridyl)-imidazole (PIMH) ligand.

5.3.2 Characterization of 2-(2′-Pyridyl)-imidazole

mp = 133-135 °C. Anal. Calc. for $C_8H_6N_3$ (%): C, 66.65; H, 4.20; N, 29.15. Found: C, 66.29; H, 5.30; N, 29.16. ^1H NMR (CDCl$_3$) δ (ppm): 7.19 (s, 1H, H4), 7.22-7.25 (m, 2H, H5, H5′), 7.76 (t, 1H, H4′), 8.25 (d, 1H, H3′), 8.50 (d, 1H, H6′), 12.05 (br s, 1H, NH). ^{13}C NMR (CDCl$_3$) δ (ppm): 149.29 (2C), 77.90 (4C), 77.58 (5C), 148.80 (2′), 123.45 (3′), 137.71 (4′), 120.73 (5′), 146.70 (6′). IR (ν$_{max}$/cm^{-1}): 1592, ν(C=N$_{im}$); 1567, ν(C=N$_{py}$); 3108 ν(N-H).

The successful synthesis of PIHM was confirmed by both FTIR and NMR spectroscopy. In the IR spectrum of pyridine-2-aldehyde, a strong band for the stretching frequency of the C=O appeared at 1706.74 cm^{-1} but disappeared in the spectrum of 2-(2′-Pyridyl)-imidazole (Fig. 5.23). The disappearance of the carbonyl band indicated that the reaction took place via the carbonyl group of the aldehyde. In addition to the absence of the carbonyl group in the spectrum of 2-(2′-Pyridyl)-imidazole, the appearance of the ν(C=N) at 1592.97 cm^{-1} of the imidazole moiety confirmed that the product was formed. Similarly, the C=N absorption band of the pyridine-2-aldehyde at 1582.86 cm^{-1} was slightly shifted to 1567.69 cm^{-1} upon attachment of the imidazole ring.
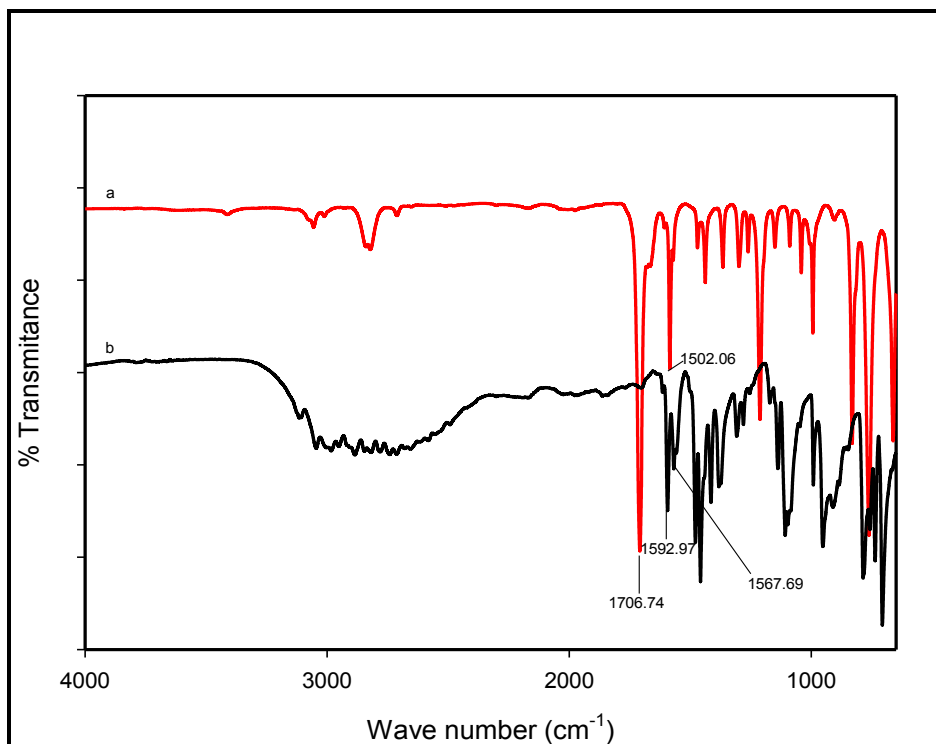
Figure 5.23: Infrared spectra of (a) pyridine-2-aldehyde and (b) 2-(2'-pyridyl)-imidazole.

The ^{1}H NMR and ^{13}C NMR spectra of 2-(2'-pyridyl)-imidazole together with the spectral assignment are shown in Fig. 5.24 and 5.25 respectively. From the ^{1}H NMR spectrum of 2-(2'-pyridyl)-imidazole, the characteristic presence of a broad singlet peak at 12.05 ppm which depicts the chemical shift of the imidazole nitrogen was a confirmation that the product was indeed formed. The ^{13}C NMR spectra of 2-(2'-pyridyl)-imidazole is shown in Fig. 5.25. The peak at 149.29 ppm was attributed to the C atom that attaches the imidazole ring to the pyridyl ring and all the other peaks were accurately assigned.
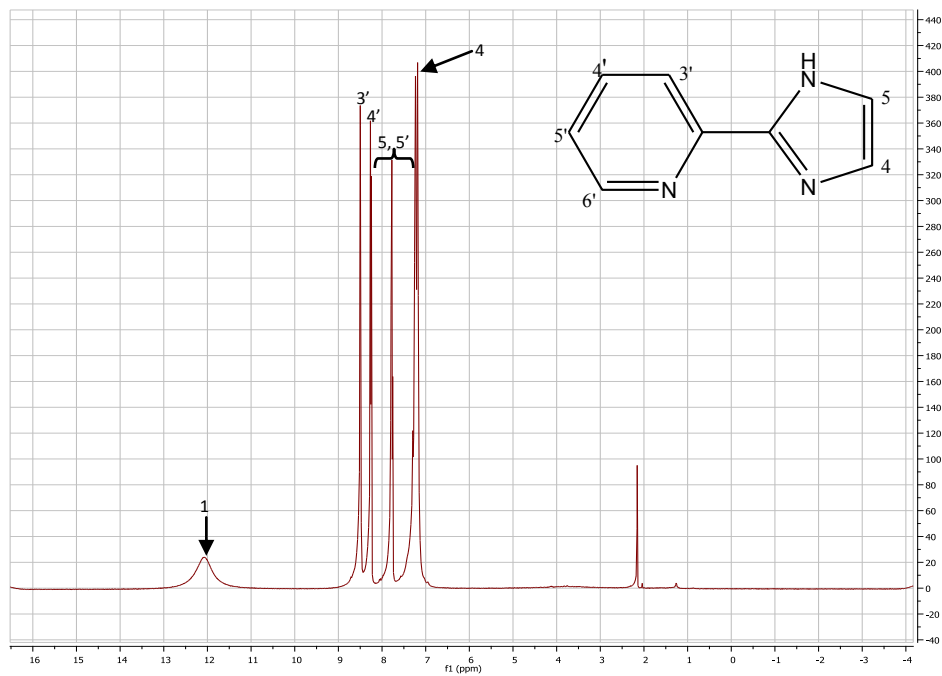
Figure 5.24: ^{1}H NMR of 2, 2'-pyridyl-1H-imidazole (PIMH) ligand recorded in CDCl$_3$.
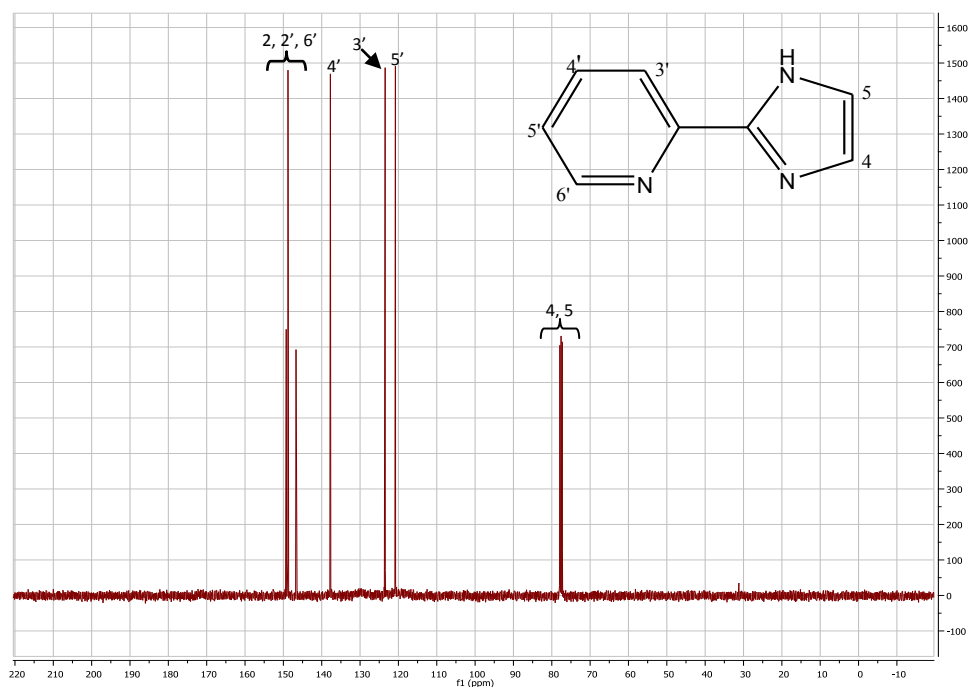
Figure 5.25: ^{13}C NMR of 2-(2'-Pyridyl)-imidazole (PIMH) ligand recorded in CDCl$_3$.

Microanalysis results further confirmed that 2-(2′-Pyridyl)-imidazole had been successfully synthesized since the expected elemental compositions were very close to those that were found (Table 5.2).

Table 5.2: Elemental composition of 2-(2′-Pyridyl)-imidazole.

Element	C	H	N
Expected Values (%)	66.65	4.20	29.19
Obtained values (%)	66.29	5.30	29.16

5.3.3 Absorption response of 2-(2′-Pyridyl)-imidazole to different metal ions

Although many sophisticated techniques are available for the determination of iron(II) at trace levels in numerous complex materials, factors such as the high cost of the analytical instruments, sample preparation and handling steps as well as expensive maintenance has made spectrophotometry to remain a popular quantification technique, particularly in laboratories in developing countries with limited budgets. UV-vis spectroscopy measures the absorption of a molecule at different wavelengths in the ultraviolet and visible spectrum caused by the excitation of electrons from the highest occupied molecular orbital (HOMO) to the lowest unoccupied molecular orbital (LUMO). Shifts in peak locations and changes in absorbance intensity can give information about the kinetics of a chemical reaction, as well as changes in optical and electronic properties.

The recognition ability of PIMH towards different metal cations was investigated by UV-vis spectroscopy. In each case, 1 mL solution of the ligand was added to 1.0×10^{-3} M of the metal ion solutions. The absorption spectrum of the ligand in the presence of Fe(II) was red shifted to the visible region (Fig. 5.26). The bathochromic shift could be attributed to spin crossover (SCO) in which is a common phenomenon in numerous compounds of Fe^{2+} (d^6). In Fe^{2+} the outer electrons could occupy all the lower t_{2g} level (low spin) or they could occupy both t_{2g} and e_g level (high spin). It is believed that the replacement of water molecules in $FeSO_4.7H_2O$ by 2-(2'-pyridyl)-imidazole molecules led to the spin transition from the high spin (HS) to low spin (LS) state of Fe^{2+}. In particular, the spin transitions between LS and HS states in SCO compounds have been reported to result in distinctive color changes [297]. When SCO occurs, it normally results in the variation of the thermal energy at the crossover, which leads to an electronic change in the d-orbital configuration and the resulting change is often observed as a color or magnetic moment change.

The variation of absorption spectra of ligand upon addition of other metal ions including Ni^{2+}, Mn^{2+}, Cr^{2+}, Co^{2+}, Zn^{2+}, Cd^{2+}, Cu^{2+}, Fe^{2+}, Fe^{3+}, Ag^+, Pb^{2+}, alkali and alkaline earth metal ions, were also recorded. As shown in Fig. 5.26, there was no significant change observed except with nickel. On addition of Ni^{2+}, the spectrum shifted to 530 nm accompanied by the appearance of a faint purple color.
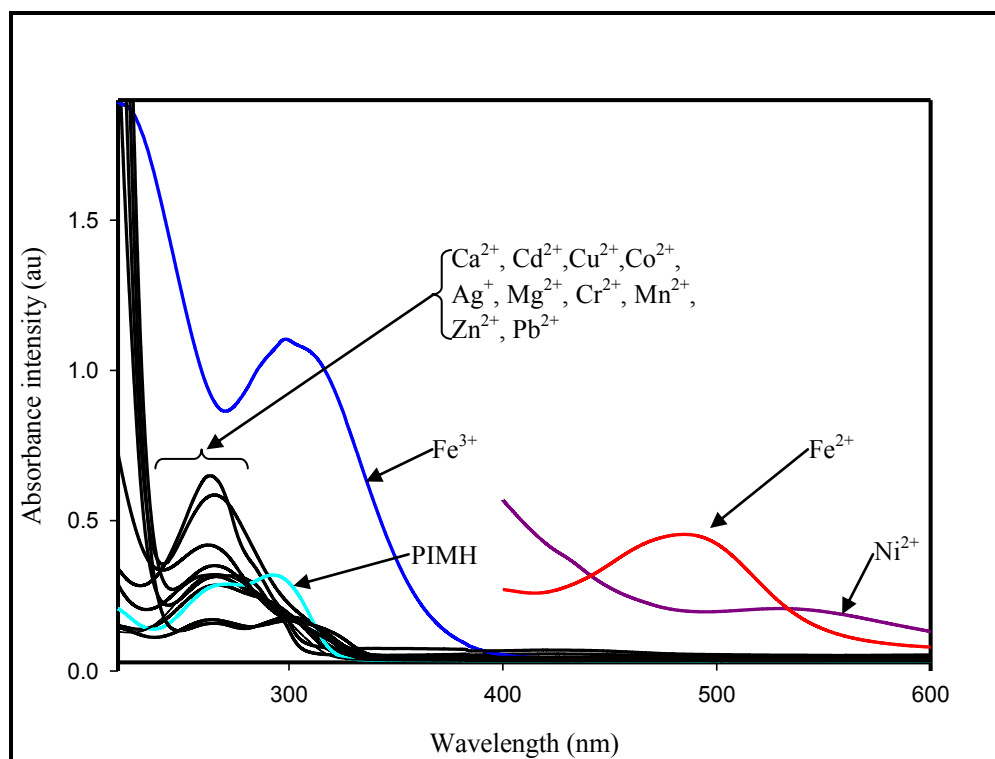
Figure 5.26: UV-vis spectra of PIMH (1 mg/mL) in water-ethanol (90:10 v/v) at pH 6 in the presence of 1 equiv of Ag^+, Zn^{2+}, Cu^{2+}, Pb^{2+}, Cd^{2+}, Ni^{2+}, Co^{2+}, Fe^{2+}, Fe^{3+}, Mn^{2+}, Mg^{2+}, Ca^{2+}, Cr^{3+}.

It could be seen that the maximum absorption of the ligand was shifted from 292 nm and 271 nm to 484 nm upon addition of Fe(II). The shift was accompanied by a visual color change from colorless to red-orange upon the addition of PIMH (Fig. 5.27). The results obtained demonstrated that PIMH had a high-binding affinity towards Fe(II). The ligand was highly suitable for use in aqueous solutions and showed high selectivity towards Fe(II) over a large number of mono-, bi- and trivalent cations tested.
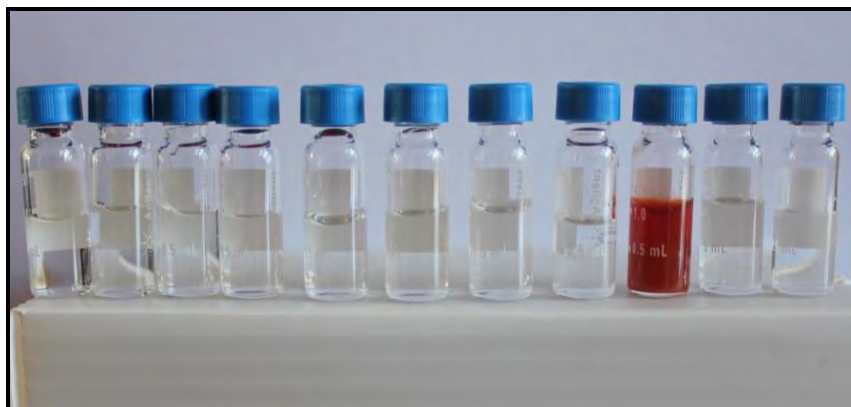
Figure 5.27: Color changes of PIMH (1 mg/mL) upon addition of PIMH alone, Mn^{2+}, Ag^+, Cu^{2+}, Fe^{3+}, Mg^{2+} Pb^{2+}, Cd^{2+}, Fe^{2+}, Ni^{2+}, Zn^{2+} (1.0 equiv) respectively.

5.3.4 Effect of pH on the color intensity of PIMH-Fe(II) complex

In order to select the optimum pH value at which maximum sensitivity occurs, the influence of the pH of the medium on the absorption spectra of Fe(II)-PIMH was studied over the pH range 3.0 to 8.0. It was observed that the absorbance intensity increased as the pH increased from 3.0, reached a maximum at pH 6.0 and started to decrease up to pH 8 (Fig. 5.28). At lower pH (< 5.0), the absorbance was lower and this could be due to the fact that PIMH could be protonated and hence reduced its chelating ability. It is important to note that at higher pH (> 6.0), there could be a probability of formation of the hydroxide ions. Hence, pH 6.0 was taken as the optimum pH value and used for further studies.
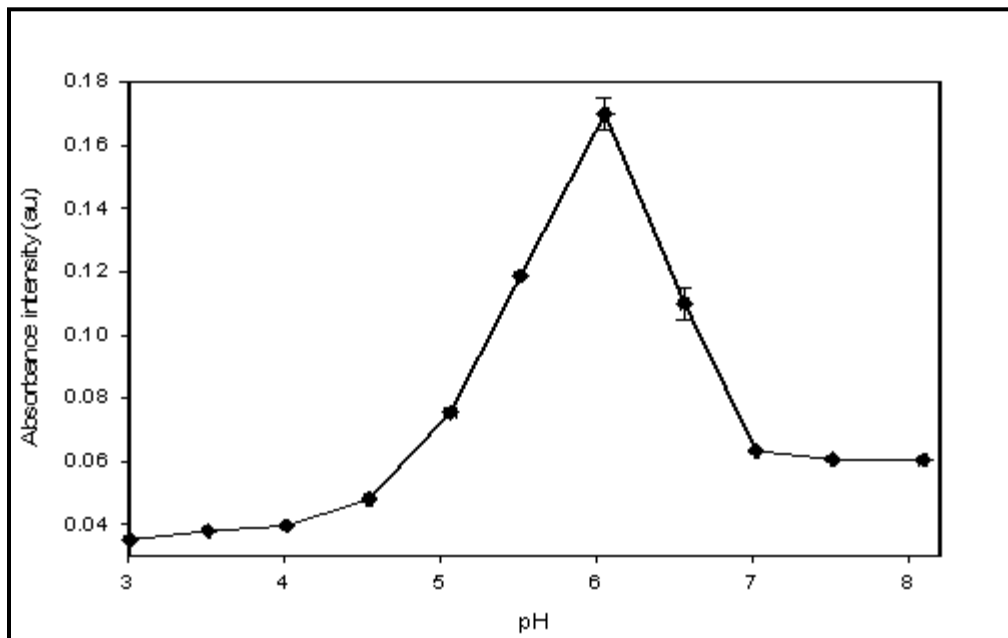
Figure 5.28: The effect of pH on the absorbance intensity of Fe(II)-PIMH complex.

5.3.5 Effect of iron(II) concentration on the absorbance intensity of Fe(II)-PIMH complex

The change in absorbance intensity as a function of increasing metal ion concentration was monitored. The increasing peak intensity at 484 nm with increasing Fe(II) concentration (Fig. 5.29) enabled quantitative determination of test samples by comparison with the calibration curve.
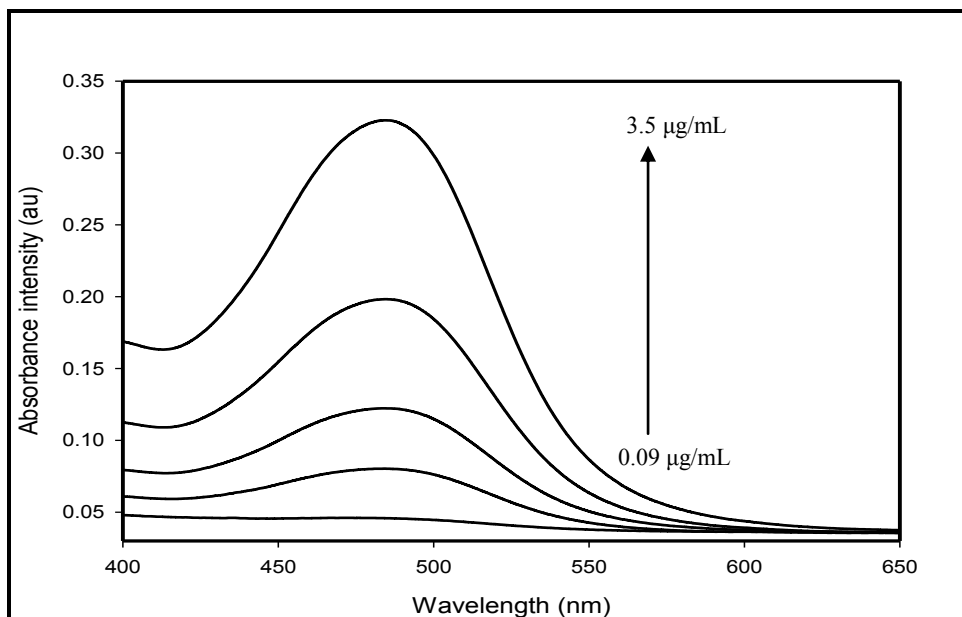
Figure 5.29: Absorption spectral changes of PIMH-Fe(II) complex with increasing concentrations of Fe(II) solution (pH 6.0).

Spectroscopic analysis in very dilute solutions is usually derived from the well known Beer's law (eqn 5.3); which gives the relationship between the absorbance of PIMH-Fe(II) complex at 484 nm and Fe^{2+} concentrations.

$$A = \varepsilon l c \qquad (5.3)$$

Where A is the absorbance intensity (arbitrary units), ε is the molar absorptivity (L mol^{-1} cm^{-1}), l is the length of the solution the light passes through (cm) and c is the concentration of the solution (molL^{-1}). A linear correlation between the concentration of Fe(II) and absorbance was observed over the range of 0.0988 µg/ mL to 3.5 µg/mL (Fig. 5.30). The ε of the method calculated from the slope of the plot was found to be 4.353×10^3 L mol^{-1} cm^{-1}.
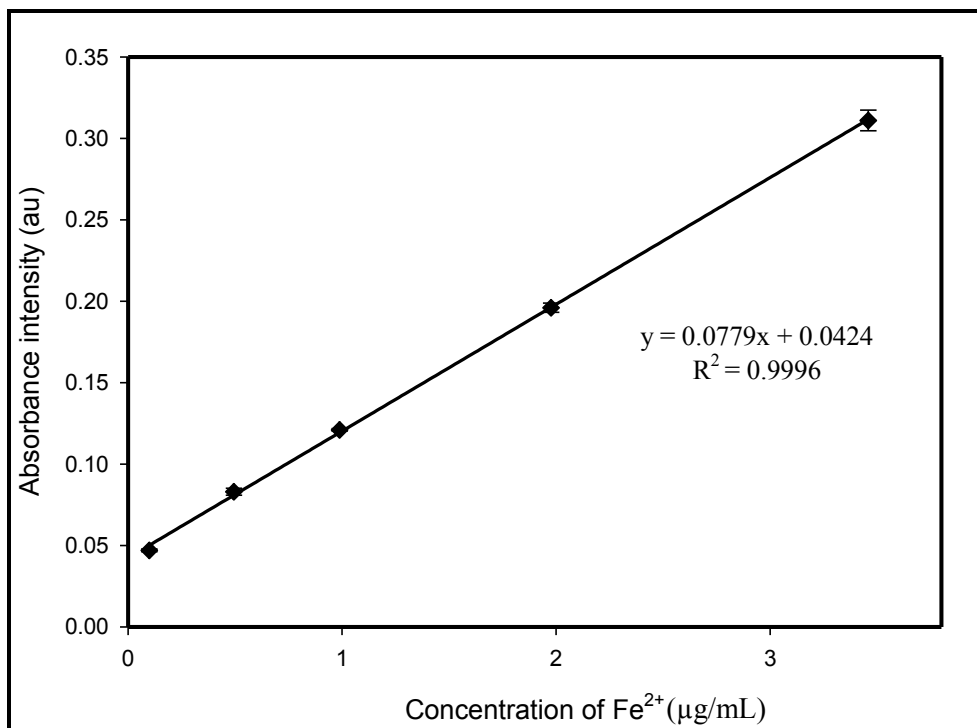
Figure 5.30: Calibration curve for the determination of Fe(II) concentration with PIMH.

5.3.6 Limit of detection (LOD) and limit of quantification (LOQ) of the method

The slope and standard deviation of the calibration curve were used to determine the LOD and LOQ of Fe(II) using the procedure. LOD is the lowest concentration of analyte in a sample which can be detected but not necessarily quantified as an exact value while LOQ is the lowest concentration of analyte in a sample which can be quantitatively determined with suitable precision and accuracy. LOD and LOQ were calculated using eqns 5.4 and 5.5 respectively.

$$LOD = 3.3\delta/s \qquad\qquad (5.4)$$

$$LOQ = 10\delta/s \qquad\qquad (5.5)$$

Where; δ is the standard deviation and s is slope of calibration curve [298]. The standard deviation was calculated from the slope of the calibration curve. The limit of detection (LOD) and limit of quantification (LOQ) of the proposed method were found to be 0.102 μg/mL and 0.309 μg/mL respectively. The method had a detection limit which is lower than the WHO guideline limit (2 mg/L) for Fe(II) in drinking water [15], and this showed that the assay was particularly very sensitive.

5.3.7 Composition of the absorbing complex

Most colorimetric analyses particularly for metal ions depend upon the formation of colored complex molecules. It is important to ascertain the molar ratio of metal to reagent in the complex. The stoichiometry of the absorbing complex could be evaluated from photometric data by different procedures. The continuous variation method attributed to Job and modified by Vosburgh and Cooper [299], as well as the mole ratio method [300], were applied to ascertain the stoichiometry of the complex.

In the continuous variation method, the total concentration of the solution (ligand + metal) is kept constant while varying the mole fractions of the ligand and the metal. While in the mole ratio method, the absorbances are measured for a series of solutions which contain varying concentrations of either the ligand or the metal but having a constant concentration of the other reactant.

From Fig. 5.31 it could be seen that, increasing the mole fraction of the ligand, led to a steady increase in the absorbance intensity of the complex and curve reached a maximum absorbance when the mole fraction of PIMH in the mixture was 0.75. The maximum absorbance gave the mole ratios corresponding to the complex formed between Fe(II) and PIMH.
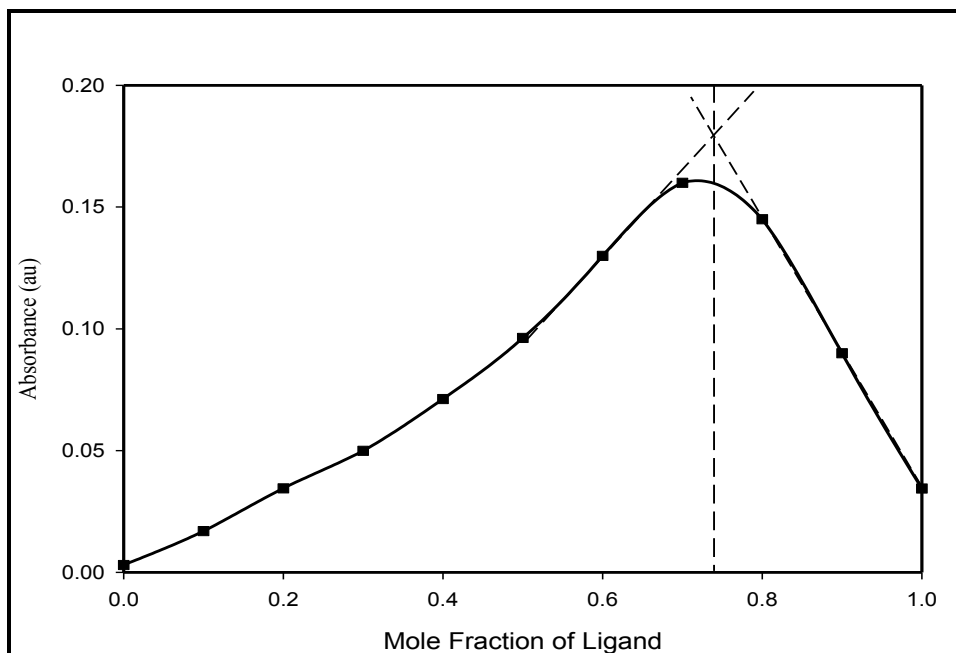
Figure 5.31: Plot of Job's method of continuous variation for determination of the stoichiometry of Fe(II)-PIMH complex at pH 6.0.

In the plot of the mole ratio method, there was an initial increase in the absorbance intensity with increasing volume of Fe(II), the curve then flattened out (Fig. 5.32). The flattening signified that all the ligand had been used up and the addition of more Fe(II) could not produce more of the absorbing complex. The composition of the complex ([Fe(II):PIMH]) was determined as 1:3 by both the methods.
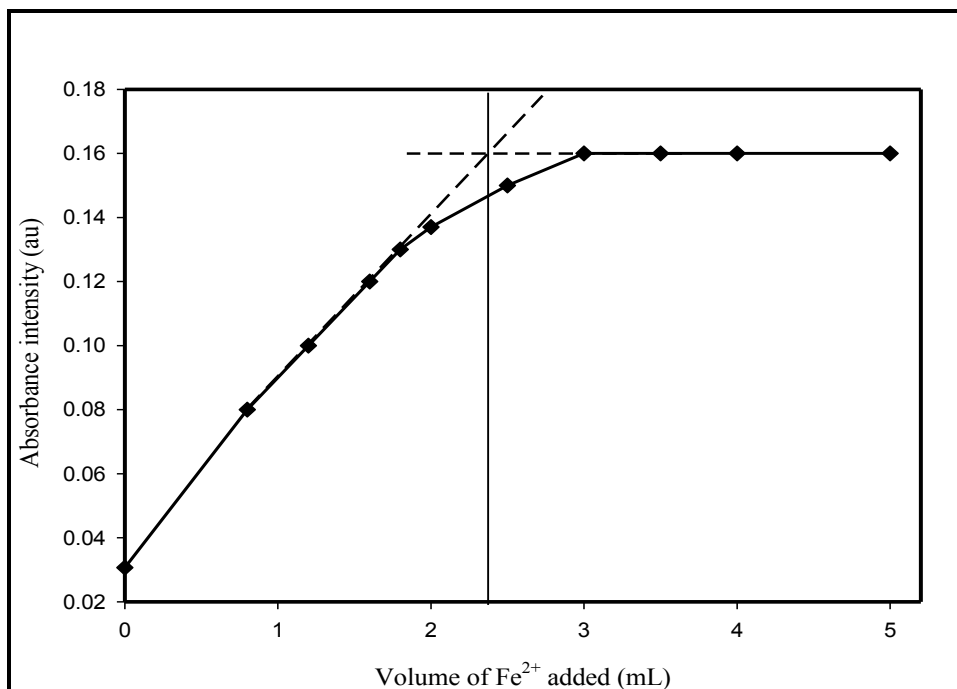
Figure 5.32: Plot of the mole ratio method for determination of M:L ratio for Fe(II)-PIMH complex, Fe(II) (1×10^{-3} M), PIMH (1 mL, 6.9×10^{-3} M) at pH 6.0.

5.3.8 Selectivity studies

When an analyte of interest exists in a complex matrix containing competing species, selectivity of the optical probe becomes an important parameter to investigate. The optical selectivity of a probe is generally linked to its relative affinity to the various structures considered (targets + competitors). Tolerance limits for the determination of 2.0 µg/mL of Fe(II) in the presence of interfering ions are given in Table 5.3. The ligand showed excellent selectivity for Fe(II) over the alkaline earth and most of the transition metal ions tested. From the results obtained, Ni(II), Cu(II) and Co(II) were found to interfere more with the determination of Fe(II) at higher concentrations.

121

Table 5.3: Spectrophotometric determination of Fe(II) in the presence of other metal ions *n = 3.*

| Interfering ions with 2.0 µg/mL Fe(II) | Quantity of the metal added (µg/mL) | Proposed method | |
		Fe(II) found method (µg/mL)	%RSD
Ni(II)	2.0	1.78	0.00
	5.0	1.28	0.10
	10.0	0.86	0.15
	20.0	0.70	0.15
	25.0	0.70	0.12
Cu(II)	2.0	1.93	0.05
	5.0	2.01	0.00
	10.0	2.00	0.11
	20.0	1.29	0.15
	25.0	1.13	0.17
Zn(II)	2.0	2.05	0.00
	5.0	2.03	0.00
	10.0	1.99	0.14
	20.0	1.95	0.70
	25.0	1.85	0.14
Mn(II)	2.0	2.01	0.00
	5.0	2.00	0.07
	10.0	1.97	0.91
	20.0	1.92	1.76
	25.0	1.80	0.77
Mg(II)	2.0	2.00	0.12
	5.0	2.00	0.00
	10.0	1.99	0.07
	20.0	1.98	0.93
	25.0	1.99	0.00
Co(II)	2.0	2.01	0.14
	5.0	2.00	0.09
	10.0	1.97	0.00
	20.0	1.92	0.07
	25.0	1.70	1.76

Ferrous ion has an affinity for amine ligands and it has been reported to interact with 1,10-phenanthroline and 2,2-bipyridine resulting in the formation of $[Fe(bipy)_3]^{2+}$ and $[Fe(phen)_3]^{2+}$ colored complexes [301]. The ferric ion does not have the same affinity for the amine ligands as the ferrous ion. Color change was not observed with PIMH even with metal ions that are considered borderline like Fe(II) at tenfold excess. However, Ni(II)

showed a faint purple color in solution. Based on the high selectivity of the PIMH, it seemed that its structural features and its coordination sites fitted the coordination tendencies of Fe(II) better than any of the other cations tested, which explained its high selectivity towards Fe(II).

5.3.9 Analytical application

To investigate the potential use of the new optical probe in complex matrices, an attempt was made to determine Fe(II) ions in certified reference material (Iron, Ferrous 1072), fish farm waste water, dam water and tap water samples. The samples were collected, acidified, stored in polyethylene bottles and analyzed within 12 h of collection. The waste water and dam water were filtered with Whatman filter papers before analysis. Each sample was analyzed in triplicate using PIMH by standard addition method. The concentration of Fe(II) in spiked samples and the reference material were determined with reference to the calibration curve.

Table 5.4: Determination of Fe(II) in various water samples $n = 3$.

Sample	Fe(II) added (μg/mL)	Proposed method		
		Fe(II) found (μg/mL)	Recovery (%)	%RSD
Waste water[a]	2	1.94	97.40	0.30
Dam water[b]	2	1.96	98.20	1.05
Tap water[c]	2	2.08	104.00	0.46

a) Collected from Swartkops river (a site near fishwater flats) in Port Elizabeth (SA)

b) Collected from Howiesons Poort Dam near Grahamstown (SA)

c) Collected from Rhodes University (SA)

The method was successfully applied for the determination of the environmental samples. The percentage recovery values for Fe(II) in the real samples were found to be above 97% (Table 5.4). The high recoveries with low % RSD values indicated that the method had good accuracy. Table 5.5 gives the quality control parameters regarding the determination of Fe(II) in aqueous certified reference material. The precision of the measurements expressed as relative standard deviation for three repeated measurements was lower than 2% confirming that the method was accurate.

Table 5.5: Analytical quality control (n = 3).

Absorbance (au)	Certified concentration (mg/L)	Concentration found (mg/L)	% RSD
0.229	2.44 ± 0.12	2.39	1.15

After quantitative analysis of Fe(II) using PIMH in solution, the ligand was used to post-functionalize electrospun poly(vinylbenzyl chloride) (PVBC) nanofibers to obtain a solid state colorimetric probe.

5.3.10 Choice and synthesis of poly(vinylbenzyl chloride) (PVBC)

Poly(vinylbenzyl chloride) was chosen as it contains reactive chloride groups which could readily undergo substitution reactions in the presence of a nucleophile. Thus, any ligand which had a suitable nucleophilic group (e.g. N-H, O-H, S-H, COOH etc.) could form a covalent bond with PVBC hence attaching itself to the polymer backbone[302].

The most popular method of producing polymeric materials is via radical initiated polymerization. This is most likely due to the wide variety of available monomers that can undergo this type of reaction. Certain vinyl monomers may undergo polymerization on heating even in the absence of an initiator; however most of the monomers require an

initiator to polymerize. Radical initiators may be divided into four major groups; peroxides and hydroperoxides, azo compounds, redox initiators and photoinitiators. The most popular initiators in the groups are; benzoyl peroxide, *tert*-butyl hydroperoxide, 2,2-azobisisobutyronitrile, potassium persulfate and benzophenone respectively.

The initiators provide the initial radical which then reacts with the vinylic monomer. The radical containing monomer then reacts with another monomer to form a dimer radical species. This process is known as chain propagation and continues until terminated by radical coupling, combination or disproportionation. Poly(vinylbenzyl chloride) was produced by free-radical polymerization of 4-vinylbenzyl chloride in toluene using azobisisobutyronitrile as the initiator (Scheme 5.7).
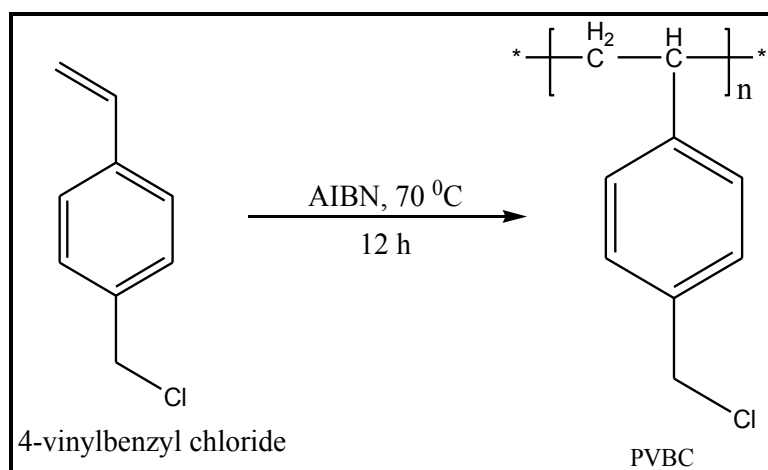
Scheme 5.7: Synthesis scheme of Poly(vinylbenzyl chloride) (PVBC).

5.3.11 Characterization of poly(vinylbenzyl chloride)

Infrared spectrum of PVBC is shown in Fig. 5.33. Benzyl ring of PVBC shows absorption at 1264.67 and 1610.67 cm^{-1} and the aliphatic C-H stretching were observed at 1364-1486cm^{-1} and 2800-3000 cm^{-1} regions. The C-Cl band of the polymer was clearly observed at 673.36 cm^{-1}.
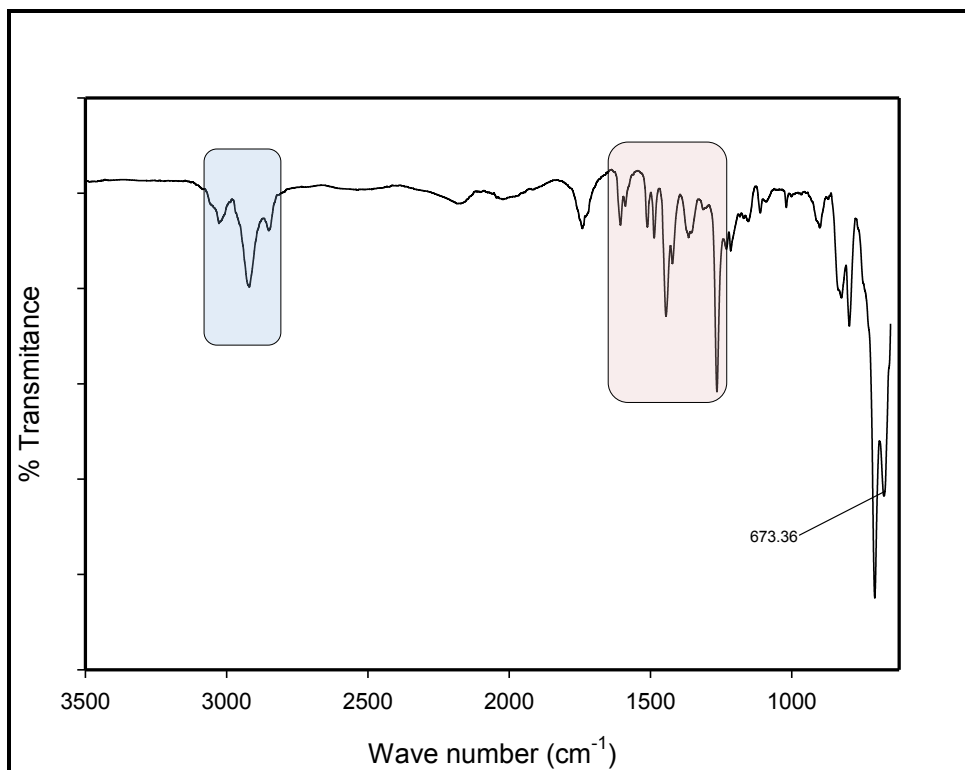
Figure 5.33: Infrared spectrum of PVBC Poly(vinylbenzyl chloride)
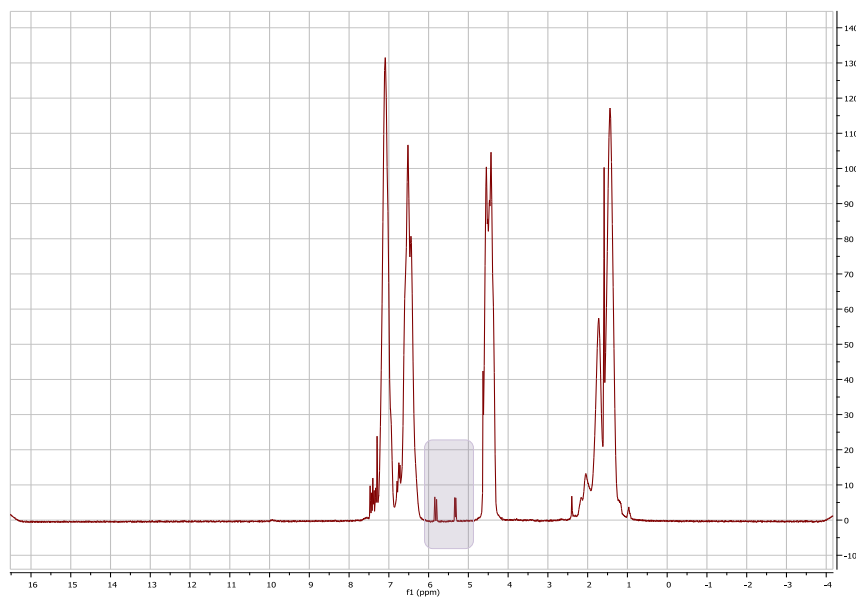
Figure 5.34: ^{1}H NMR of PVBC Poly(vinylbenzyl chloride) in CDCl$_3$.

^{1}H NMR of PVBC in (CDCl$_3$) is shown in Fig. 5.34. The peaks appearing between 1.4-1.7 ppm were assigned to chemical shifts arising from; –CH$_2$ and –CH of the main chain, between 4.4-4.6; Ph-CH$_2$-Cl, and finally between 6.4-7.1 were assigned to chemical shifts from –CH of the benzyl ring. The peaks appearing between 5-6 ppm indicated the presence of the monomer impurities in the final product. It is important to note that the monomer did not polymerize quantitatively and it was not possible to completely wash it off the product. After the polymer was obtained, it was electrospun in order to obtain nanofibers.

5.3.12 Electrospinning poly(vinylbenzyl chloride)

Homogeneous and clear Poly(vinylbenzyl chloride) solutions were prepared by dissolving PVBC in a solvent system of DMF and THF in the ratio of 1:1 at room temperature after stirring for 3 h. The polymer concentration was varied from 20% (w/v) up to 50% (w/v). By means of the electrospinning technique, micro- and nanofibers could be obtained from polymer solutions under high electrical field. A special challenge that was encountered was the fabrication of bead-free, uniform fibers. This was because, any slight change in the electrospinning parameters such as small variations in the polymer solutions and/or electrospinning experimental parameters resulted in significant variations in the final nanofiber morphology. Furthermore, it was often not the case at all times to obtain reproducible uniform electrospun nanofibers for the optimized electrospinning conditions.
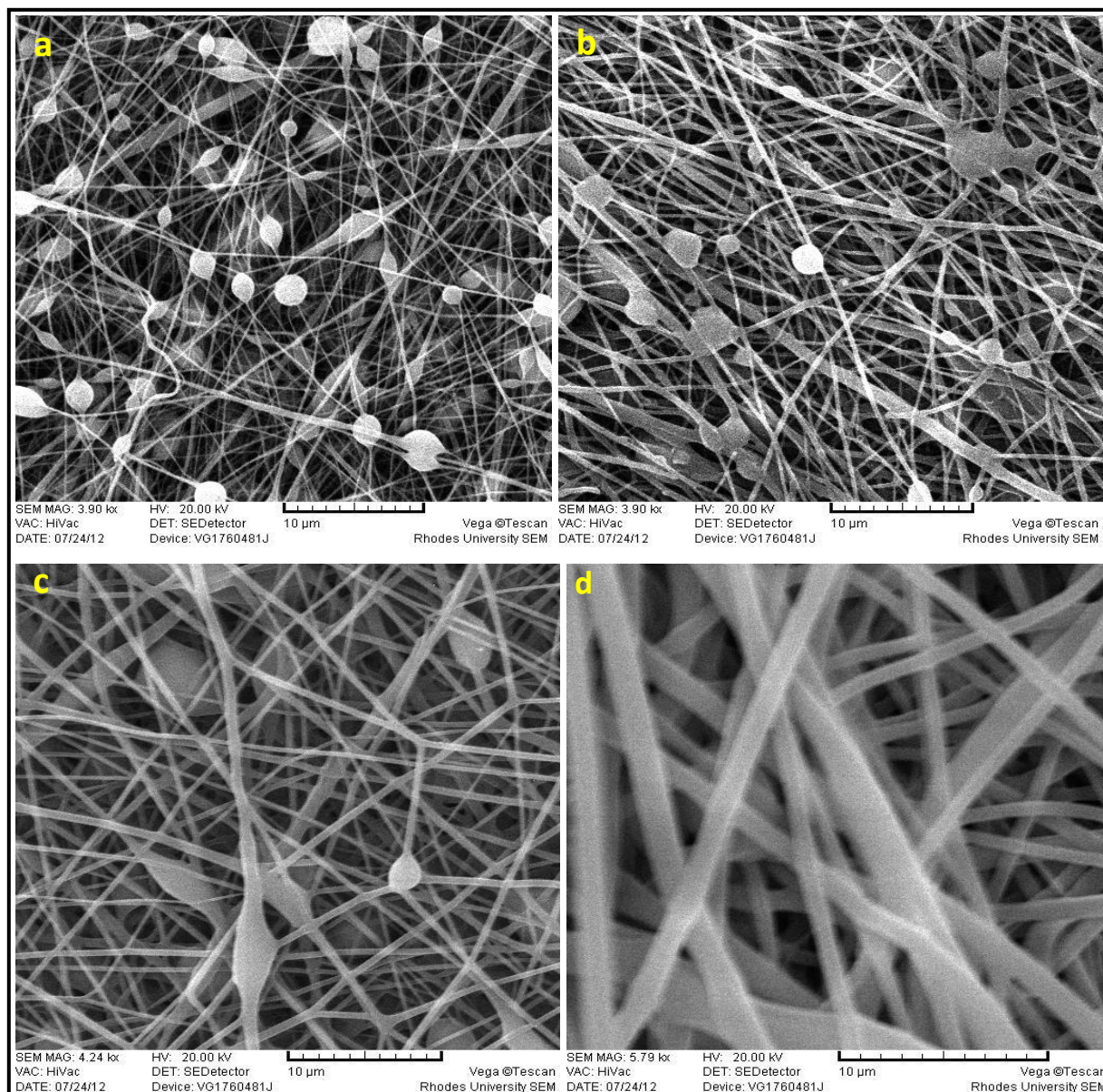
Figure 5.35: Scanning Electron Micrograph of electrospun PVBC nanofibers obtained from different concentrations of PVBC solution (a) 25% PVBC, (b) 35% PVBC, (c) 40% PVBC and (d) 50% PVBC.

For example, beaded fibers often resulted from otherwise optimized electrospinning conditions due to small changes in the polymer solutions and/or the electrospinning setup. Figure 5.35 shows the SEM images of PVBC nanofibers obtained with different polymer concentrations when the electrospinning parameters were kept constant (15 kV, 12 cm, 1.2

mL/h). It was clear from these results that varying the polymer concentration had an influence on the fiber morphology. From detailed studies on the electrospinning of PVBC, reproducibility problems were experienced and that meant that the electrospinning conditions had to be optimized every time in order to produce bead-free nanofibers.
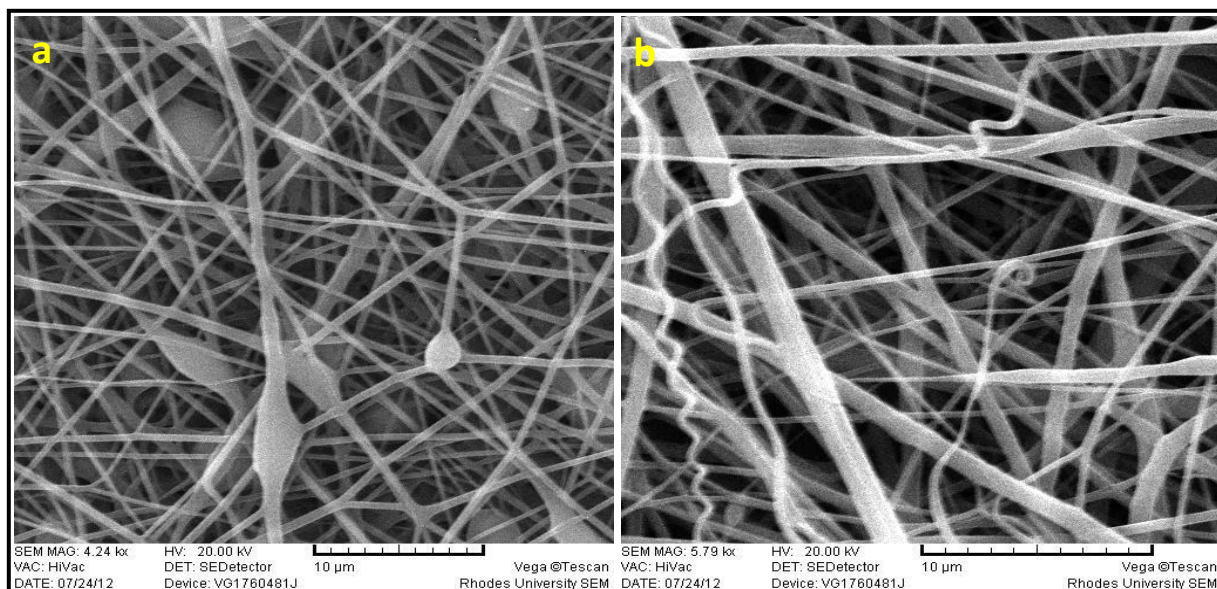
Figure 5.36: Scanning Electron Micrograph of electrospun PVBC fibers obtained from 40% (w/v) solutions, (a) 15 kV, 12 cm, 1.2 mL/h, (b) 15 kV, 12 cm, 0.8 mL/h.

However, even when the electrospinning conditions were optimized i.e. polymer concentration of 40% (w/v), applied voltage of 15 kV and tip to collector distance of 12 cm, the flow rate had an effect. The flow rate of 0.8 mL/h produced bead-free nanofibers while 1.2 mL/h gave beaded fibers (Fig. 5.36). Hence optimized flow rate was achieved by a slight reduction of the flow rate from 1.2 mL/h to 0.8 mL/h.

5.3.13 Fabrication of the colorimetric probe by post-functionalization of the nanofibers

The incorporation of 2-(2′-Pyridyl)-imidazole functional groups was achieved by the post-electrospinning reaction with PVBC nanofibers. Post-electrospinning modifications have paved the way for future developments of advanced composite systems. Surface functionalization of electrospun nanofibers are meant to allow modification of chemical properties of nanofibers without changing their morphology. Moreover, an attempt to prepare a pre-electrospinning functionalized PVB-PIM was not possible owing to the fact that the product was insoluble in several solvents. Hence, post-electrospinning functionalization was the only way out of the dilemma. Reacting the PVBC nanofibers with PIMH with the use of KOH as a base at a mild temperature of 40 ^{0}C for a period of five days provided a successful route of binding the ligand to the polymer backbone.

5.3.13.1 Characterization of the post-functionalized PVBC nanofibers

The scanning electron microscope (SEM) image of electrospun membrane of PVBC is shown in Fig. 5.37. The nanofiber mat had a 1-dimentional structure with a random fiber orientation that was evenly distributed. The obtained fibers had diameters ranging between 340 nm to 1.08 μm. After post-functionalization of the nanofibers, the SEM image (Fig. 5.37b) indicated that the fibrous structure of the mat was not lost but, the diameters of the fibers increased to between 860 nm to 1.9 μm. The increase in fiber diameters could be attributed to swelling which resulted from attachment of the bulky ligand (PIMH) on to the fiber surface. The image also revealed breakage of the nanofibers upon post-functionalization and this could have resulted from the stirring and heating during the reaction.
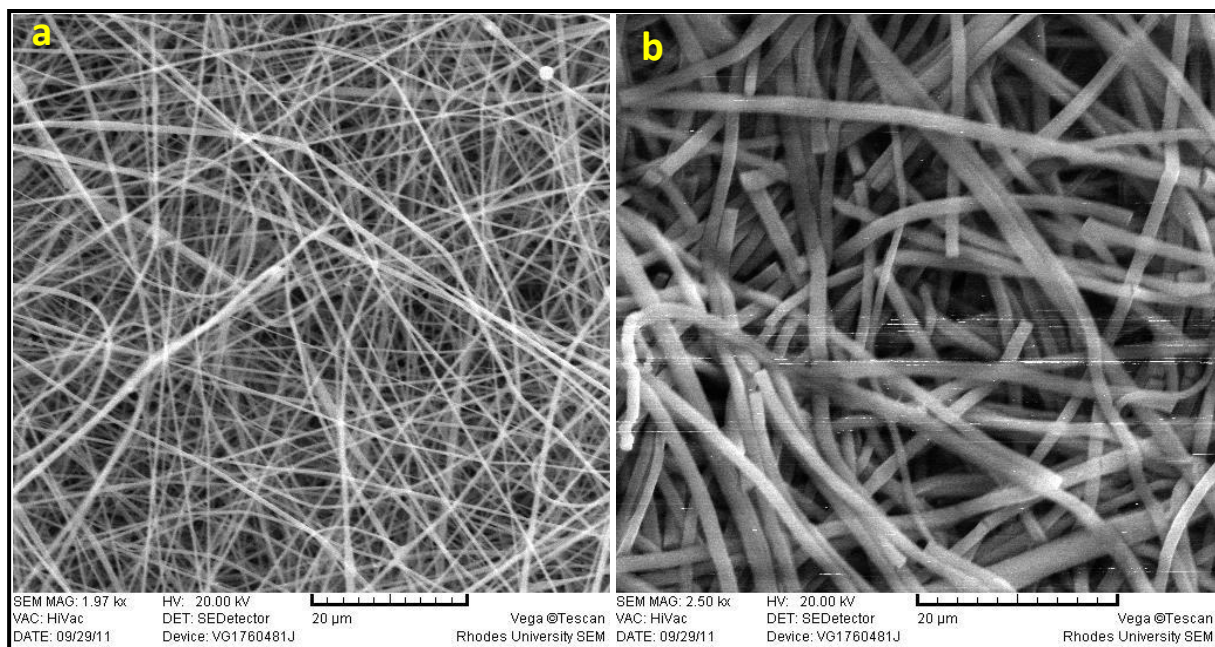
Figure 5.37: Scanning electron micrograph of; (a) Poly(vinylbenzyl chloride) nanofibers, (b) Surface-modified PVBC electrospun nanofiber mats.

The composition of the nanofibers after functionalization was verified by elemental analysis. The appearance of nitrogen in the results of the functionalized fibers was a pointer that PIMH had been successfully attached to the polymer back bone (Table 5.6). The successful attachment of the ligand to the polymer was further confirmed from the FTIR spectra.

Infrared spectra of PVBC, PVB-PIM and PIMH are presented in Fig. 5.38. The PIM unit of PVB-PIM showed several medium or strong peaks in the 1454-1512 cm^{-1} range due to C=N and C-N ring vibrations. Benzene ring of PVBC showed absorptions at 1267 and 1658 cm^{-1} and the aliphatic C-H stretching were observed at 1267-1454 cm^{-1} and 2800-3000 cm^{-1} region. Furthermore the disappearance of C-Cl band of the PVBC at 672 cm^{-1} and N-H band around 3100 of PIMH was a clear confirmation of the successful functionalization of the electrospun nanofibers.

Table 5.6: Elemental analysis results of PVBC and PIMH functionalized PVBC nanofibers.

	Results (%)		
	C	H	N
PVBC	70.20	6.296	-
PVB-PIM	75.65	6.988	10.92
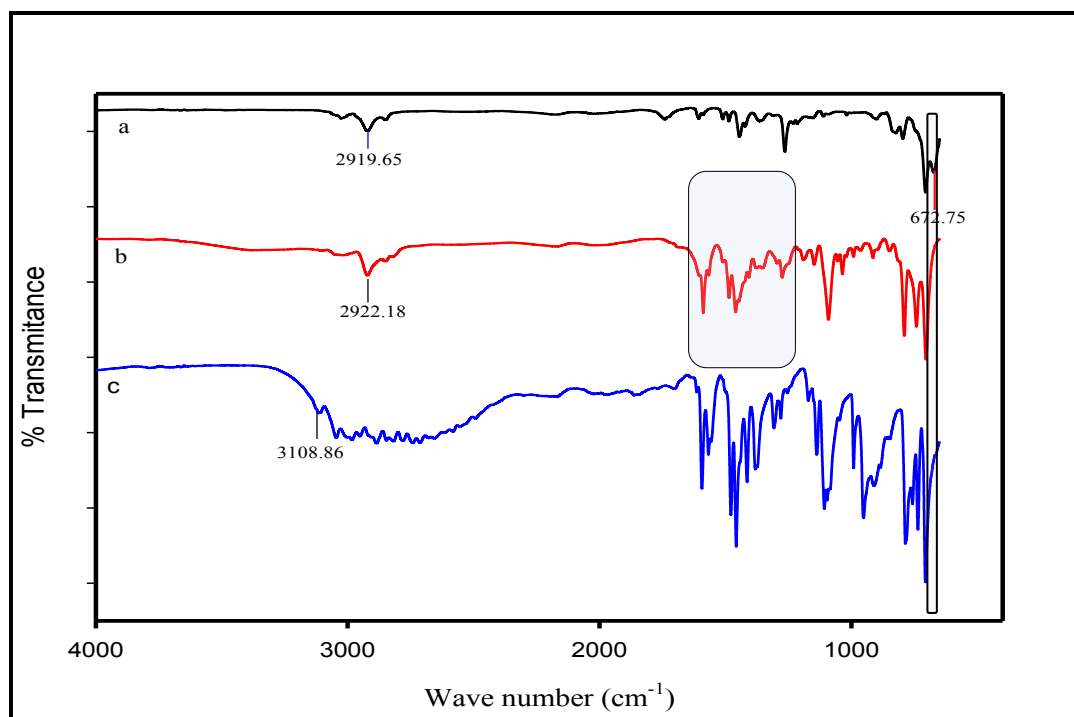
Figure 5.38: Infrared spectra of (a) Poly(vinylbenzyl chloride) nanofibers (b) PVB-PIM nanofibers (c) PIMH.

The elemental composition on the surface of modified fibers was further examined by Energy Dispersive X-ray Spectroscopy (EDX). The appearance of nitrogen in the histogram of the functionalized nanofibers was an indicator that PIMH had been attached to the polymer back bone and mapping results indicated uniform distribution of nitrogen on the fiber surface (Figs. 5.39a & b).The peaks corresponding to K and Al were ascribed to the

use of KOH as a base in the reaction and aluminum as the collector respectively. The peak corresponding to O was attributed to oxygen contamination during the reaction.
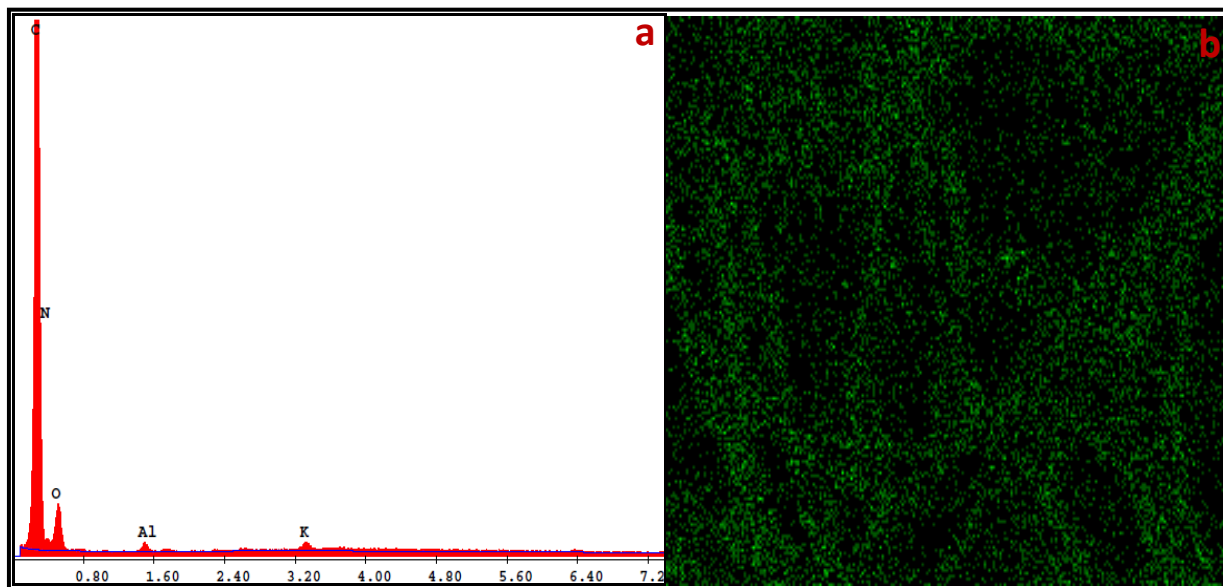
Figure 5.39: (a) Energy dispersive x-ray histogram of PIMH modified nanofibers; (b) Mapping results of nitrogen on the surface of the functionalized nanofibers.

After successful functionalization of the PVBC nanofibers, the mats were cut into circular shapes having diameters of 0.9 cm and 1.4 cm and without any treatment were dipped into the test solutions. While the color change of the nanofibers from yellow to red-orange associated with the reaction of PIMH with Fe(II) was readily detectable visually, no significant color changes were promoted by other metal ions (Fig. 5.40a).
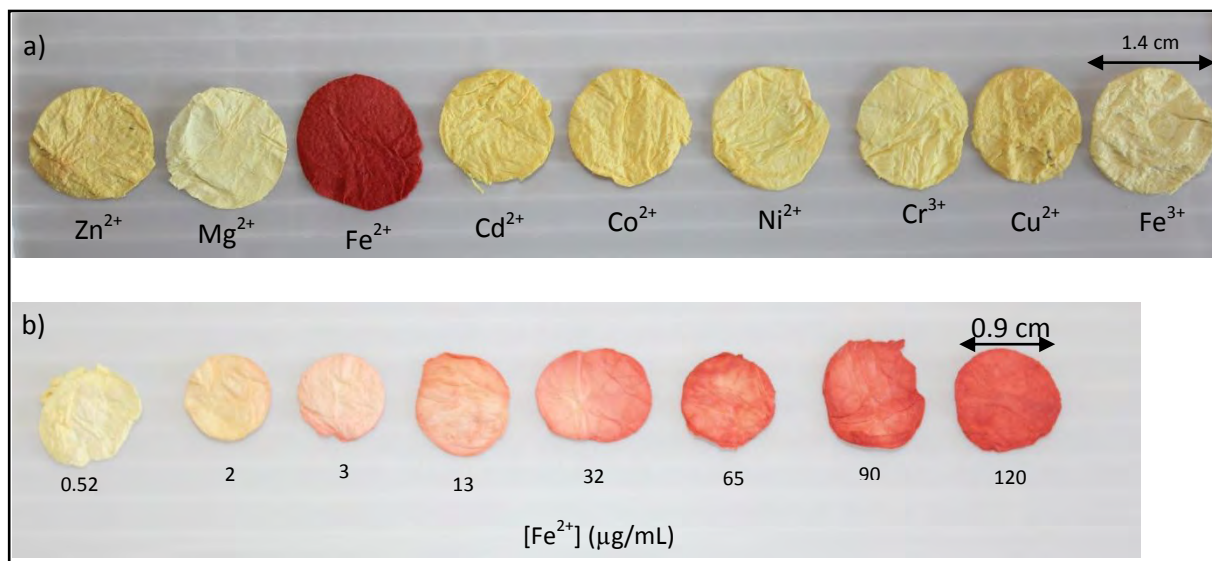
Figure 5.40: (a) Photographs of PIMH functionalized PVBC nanofibers upon treatment with different metal ions (0.01 M) and (b) different concentrations of Fe(II).

The diagnostic probe showed a marked red-orange color in the presence of Fe(II) that was detectable down to 3.0 μg/mL (Fig. 5.40b). Therefore 3.0 μg/mL was taken as the cut-off for the "eye-ball" detection of Fe(II) using the solid state probe.

Covalent immobilization of polymer chains onto another polymer surface by coupling reactions (grafting techniques) have also been reported as a simple way of introducing desired functionalities to the fiber surface. Consequently, the possibility of employing grafting technique to attach 2-(2′-Pyridyl)-imidazole onto polymeric electrospun nanofiber substrate was also investigated.

5.3.14 Functionalization of nylon 6 nanofibers by graft polymerization

Grafting provides a method of adding certain desirable properties to a substrate without greatly disrupting its mechanical properties and strength. Grafting is normally accomplished by generating radical sites on the first polymer backbone onto which the

monomer of the second polymer is to be co-polymerized. So the polymer substrate must contain protons that can be abstracted during the grafting process to create radical sites. For this reason, we chose to use nylon 6 (Fig. 5.41) nanofibers as the substrate. Polyamides (i.e. nylon 6) contain functional groups which are capable of forming a complex with the initiator on the fibers. Further decomposition of the obtained complex leads to the formation of free radicals on the fibers, thus paving the way for direct grafting almost without the formation of homopolymer.
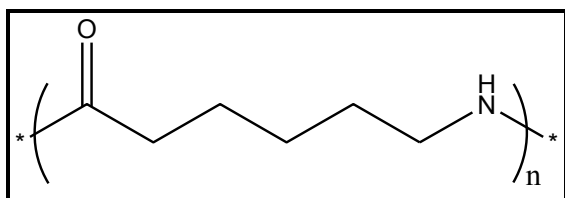
Figure 5.41: Chemical structure of nylon 6.

For graft copolymerization to take place, radicals or groups which can produce radicals like peroxide groups must be introduced onto the polymer surface first. For most of the chemically inert polymers, this can be achieved via inducing methods such as photo-induced grafting (UV-induced grafting) and thermal-induced grafting among others. We chose to use the UV-induced surface graft polymerization because of its low cost, easy operation and mild reaction conditions.

The main goal of this part of the work as already mentioned was to graft PIMH onto electrospun nylon 6 nanofibers and evaluate the characteristics of the resulting material. 2-(2'-Pyridyl)-imidazole did not contain any polymerizable group hence; the first step was to introduce a group that could undergo polymerization. Consequently; 2-(2'-Pyridyl)-imidazole was modified with 4-vinylbenzyl chloride (4-VBC) (Scheme 5.8).
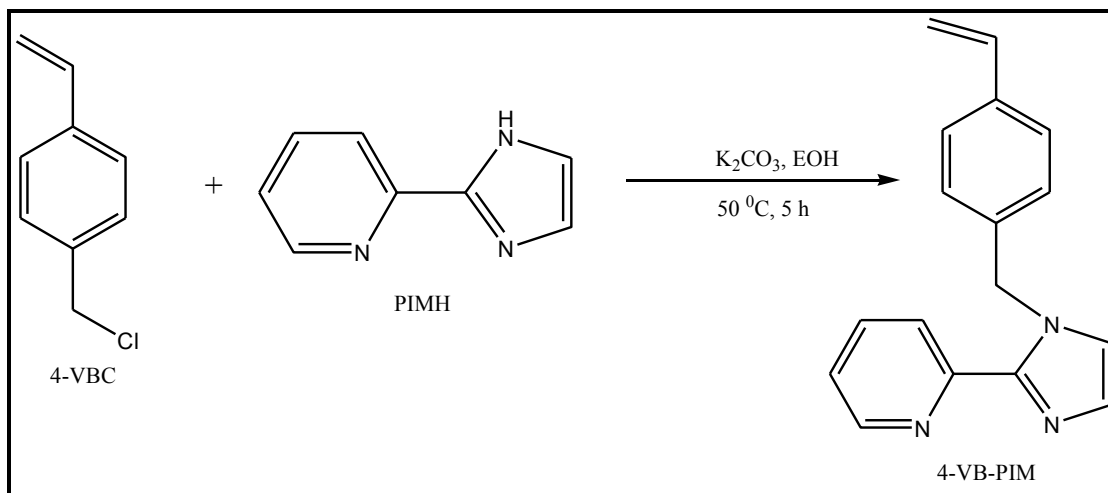
Scheme 5.8: Synthesis scheme of 4-vinylbenzyl-2-(2′-Pyridyl)-imidazole (4-VB-PIM).

4-vinylbenzyl chloride (4-VBC) was chosen because it was commercially available and could react with nucleophiles by substitution reaction, thereby connecting the ligand to the styryl group. Typically nucleophilic substitution reactions are carried out in polar aprotic solvents such as acetonitrile or DMF in the presence of a base like triethylamine, potassium carbonate or potassium hydroxide [303]. Once the ligand was functionalized with a styryl group, it was then incorporated into nylon 6 backbone by graft polymerization.

5.3.14.1 Characterization of 4-vinylbenzyl-2-(2′-Pyridyl)-imidazole

FT-IR spectra of 4-vinylbenzyl-2-(2′-Pyridyl)-imidazole is represented in Fig. 5.42. It was evident that the two peaks appearing at 675.28 and 1261.79 cm^{-1} in the spectrum of 4-vinylbenzyl chloride corresponding to v(C-Cl) and v(CH$_{2)}$ completely disappeared in the spectrum of 4-vinylbenzyl-2-(2′-Pyridyl)-imidazole. This was a clear indication that PIMH reacted with 4-vinylbenzyl chloride via the reactive chloride group which could readily undergo substitution reactions in the presence of a nucleophile. After the reaction, a shift from 1592.97 cm^{-1} to 1585.39 cm^{-1} peaks corresponding to C=N of the imidazole ring was also observed confirming the anchoring of the functional group.
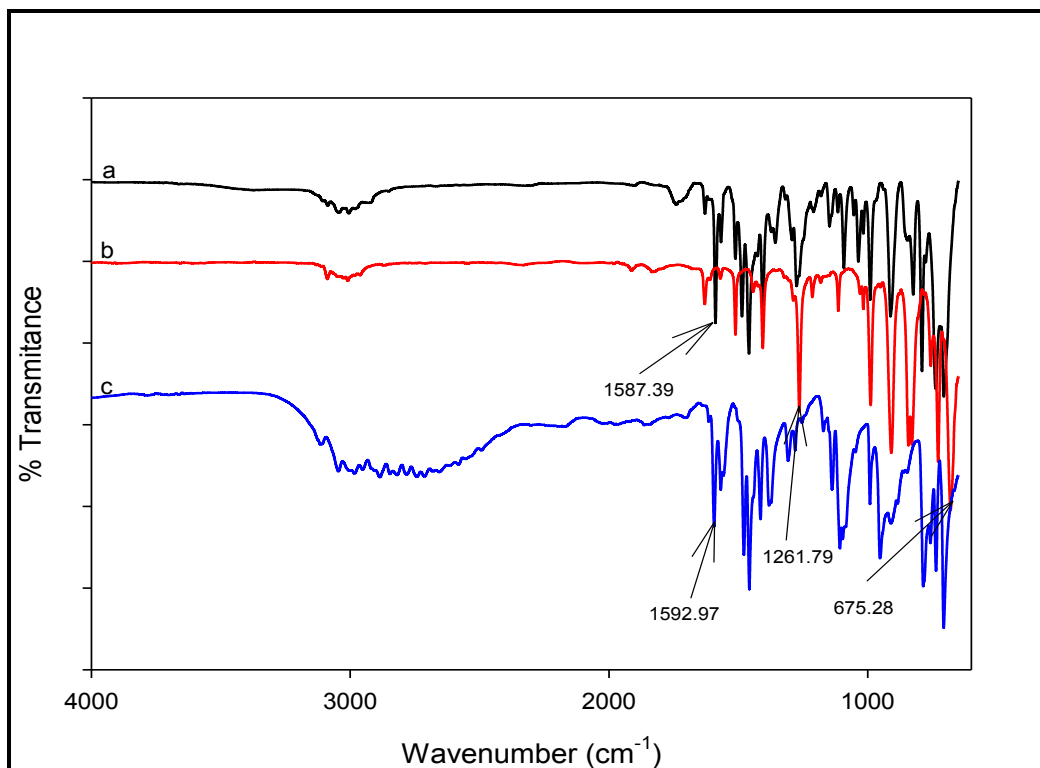
Figure 5.42: Infrared spectra of (a) 4-vinylbenzyl-2-(2′-Pyridyl)-imidazole; (b) 4-vinylbenzyl chloride; (c) 2-(2′-Pyridyl)-imidazole.

Attachment of the styryl group on the imidazole ring of 2-(2′-Pyridyl)-imidazole was further confirmed by ^{1}H NMR spectroscopy. The disappearance of the peak at 12.05 ppm depicting the imidazole nitrogen proton in the spectrum of this compound (Fig. 5.43) signified that the reaction had taken place. The disappearance of the peak corresponding to the imidazole nitrogen proton also confirmed that the styryl group was connected to the ligand via the imidazole nitrogen. The functionalization of PIMH was further confirmed by appearance of more peaks in the aromatic region, between 7-8 ppm of the spectrum (Fig 5.43b).
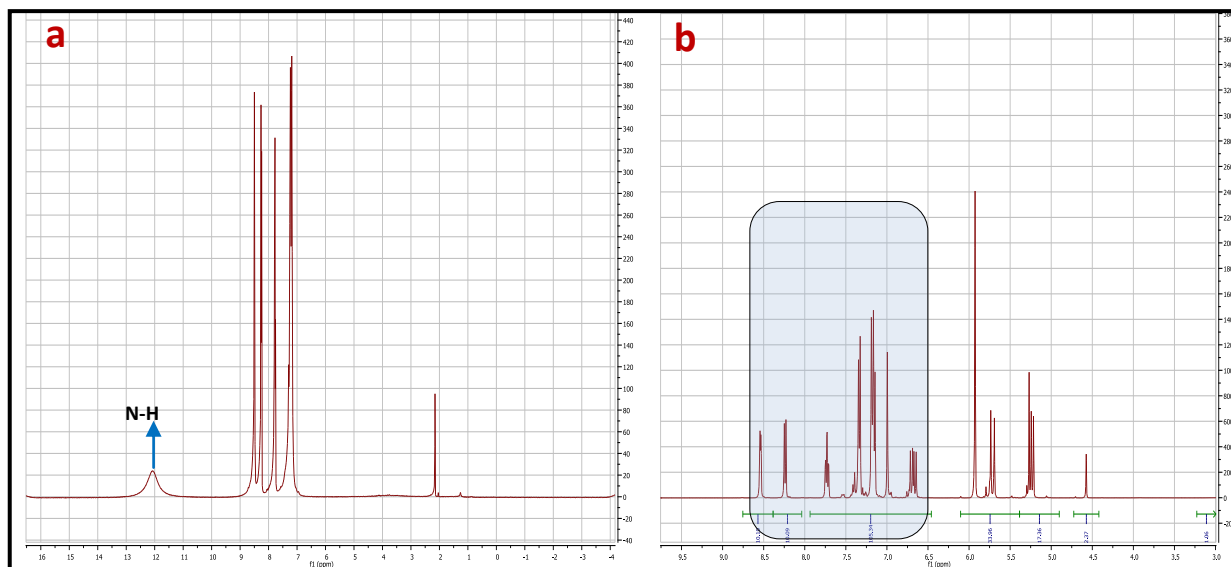
Figure 5.43: ^{1}H NMR of (a) 2-(2′-Pyridyl)-imidazole; (b) 4-vinylbenzyl-2-(2′-Pyridyl)-imidazole.

The ^{13}C NMR spectrum of 4-VB-PIM is shown in Fig. 5.44. The peak at 51.73 was attributed to the C atom that attaches imidazole ring to the benzyl group. The benzyl group appeared around 128-132 ppm. The peak at 151.17 was assigned to the C of the imidazole ring attached to N atoms.
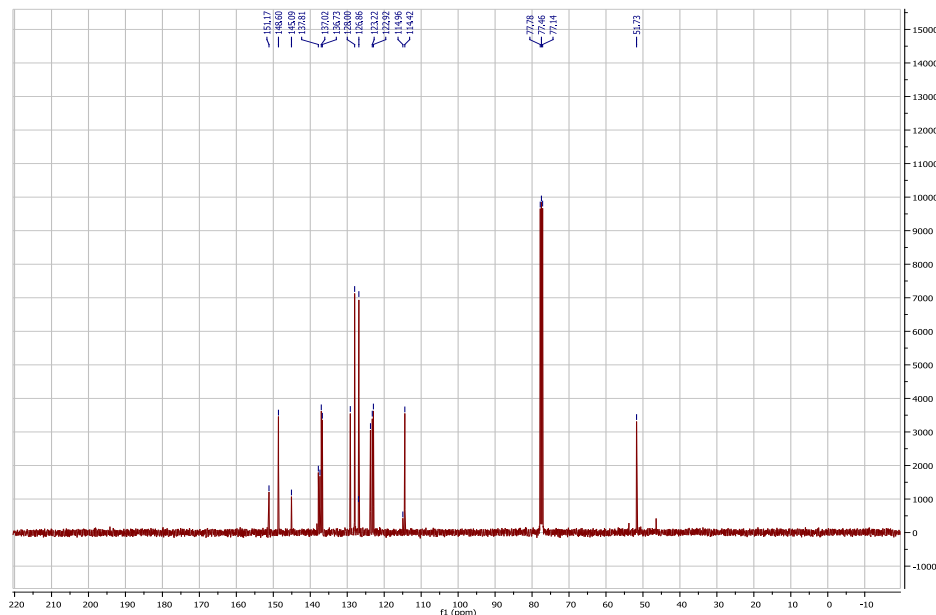
Figure 5.44: ^{13}C NMR spectrum of 4-vinylbenzyl-2-(2′-Pyridyl)-imidazole.

5.3.14.2 Grafting 4-vinylbenzyl-2-(2′-Pyridyl)-imidazole onto nylon 6 nanofibers

After synthesis of the monomer, heterogeneous modification of nylon 6 nanofibers with 4-VB-PIMH was accomplished in a two step process (Scheme 5.9). The two-step approach involved:

(1) Placing the substrate into a methanol solution of benzophenone (BP). In this step, the initiator (BP) was expected to abstract hydrogen from the polymer surface in order to create free radicals under UV irradiation.

(2) Introducing the monomer solution in methanol and placing the contents under UV irradiation. In this step, the monomer solution was added onto the active substrate, and the radicals on the surface of the substrate were expected to initiate the graft polymerization under UV irradiation.

The two step procedure reduced the formation of the non-grafted polymer in solution unlike in the single step procedure where the monomer and the initiator in solution were introduced at the same time. The sequential approach also provided additional control over grafting. This is because, the process of hydrogen abstraction and graft polymerization were split into two separate steps.

Step 1: Creating surface radicals;

Step 2: Graft polymerization;

▊; Electrospun Nylon 6,   ∿∿∿; Poly(vinylbenzyl)-PIM
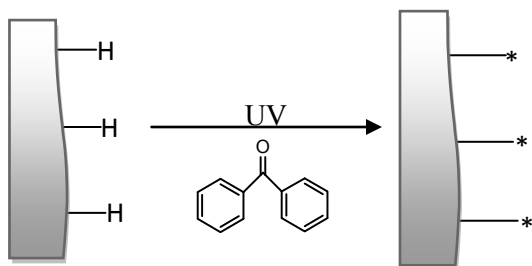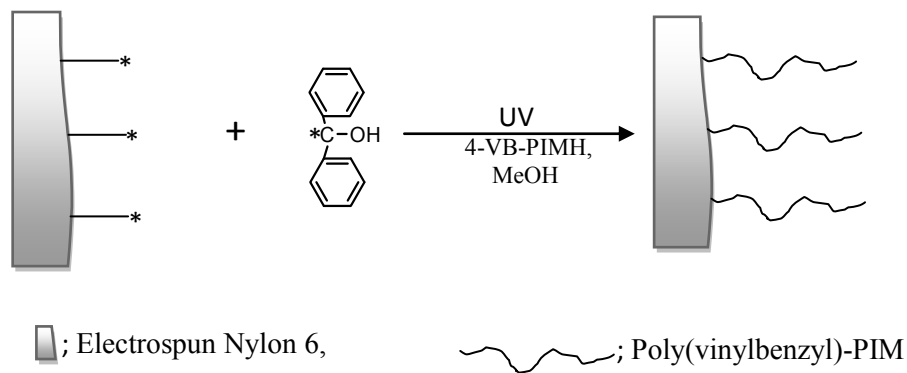
Scheme 5.9: The two step photografting procedure.

5.3.14.1.1 Characterization of surface modified nanofibers

After the electrospun nanofibers were subjected to surface modification, the surface chemical features of the nanofibers were examined by FTIR (Fig. 5.45). The infrared spectrum of regular nylon 6 nanofiber showed absorptions at 1641–1540, 3083, and 2925–

2852 cm^{-1}, which are typical to those of C=O and CONH, NH$_2$, NH stretching and CH stretching respectively. However, in the FTIR spectrum of the poly(vinylbenzyl)-PIM-modified nanofibers, there were new peaks which appeared between 1464 to 699 cm^{-1} corresponding to the absorption of aromatic groups from the monomer. The peaks got stronger as the grafting density of poly(vinylbenzyl)-PIM increased. The increasing peak intensities suggested that; not only was poly(vinylbenzyl)-PIM successfully grafted onto the nanofibers, but that nanofiber surfaces with different grafting percentages of poly(vinylbenzyl)-PIM chains were obtained.
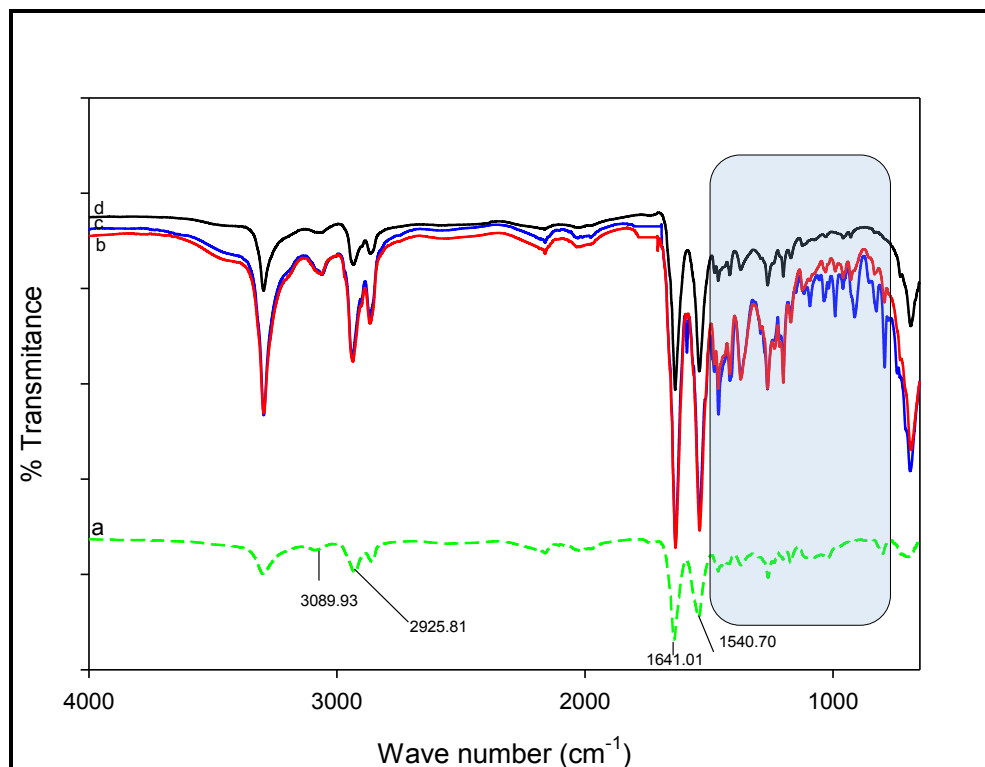
Figure 5.45: Infrared spectra of; (a) Unmodified nylon 6 nanofibers, (b) Poly(vinylbenzyl)-PIM Modified nanofibers with grafting percentage of 226 (b), 94.7 (c), 30.6 (d).

The elemental compositions on the surfaces of the unmodified and modified nanofibers were further examined by Energy Dispersive X-ray Spectroscopy (EDX). From the EDX

histograms obtained, it was not obvious that grafting had taken place since the elemental compositions of the substrate and the monomer were similar. But from the EDX data, the atomic compositions and atomic ratio (N/C) on the surfaces were calculated and summarized in Table 5.7. The atomic ratio value of N/C increased from 0.0978 to 0.3228 with different grafting percentages. The grafting percentages were calculated using eqn 5.6 [304].

$$\% \, Grafting = \frac{W_1 - W_0}{W_0} \times 100 \qquad (5.6)$$

Where, W_1 and W_0 are the weight of grafted and unmodified nylon 6 fibers, respectively.

Table 5.7: Atomic compositions and atomic ratios (N/C) from EDX.

Grafting percentage	Atomic compositions (at. %)			Atomic ratio
	C	N	O	(N/C)
0	83.10	8.13	8.78	0.0978
30.6	82.22	11.04	5.65	0.1342
94.7	72.26	23.33	3.89	0.3228

Surface morphology of a grafted substrate could provide valuable information on the effect of grafting reactions on the surface. Figure 5.46 presents the SEM images corresponding to unmodified and poly(vinylbenzyl)-PIM modified nylon 6 nanofibers. It could be seen from the SEM images that unmodified nylon 6 nanofibers surface had a smooth and a relatively homogeneous appearance (Fig. 5.46a). After grafting poly(vinylbenzyl)-PIM onto the nylon 6 fibers, the surface gained some roughness. The heterogeneous appearance after grafting could be attributed to the formation of a layer of poly(vinylbenzyl)-PIM on the surface of

the nanofibers. However, the substrate still maintained its fibrous structure (Fig. 5.46b). The heterogeneous appearance of the surface was another proof of the successful grafting of poly(vinylbenzyl)-PIM.
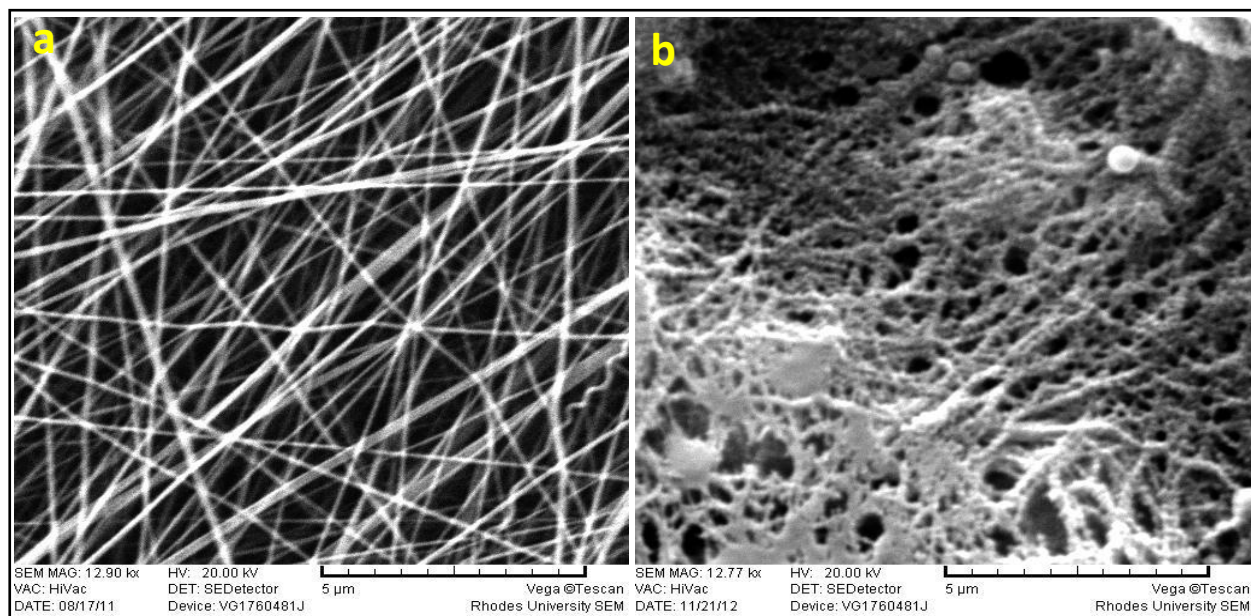
Figure 5.46: Scanning electron micrographs of; (a) nylon 6 nanofibers and, (b) poly(vinylbenzyl)-PIM grafted nylon 6 nanofibers.

5.3.14.1.2 Effect of monomer concentration on grafting percentage

There are a number of grafting parameters that have been reported to influence the percentage grafting. Grafting parameters, e.g., initiator concentration, UV irradiation time and monomer concentration could influence the degree of grafting in the procedure of photo-initiated surface graft polymerization. The effect of monomer concentration on the degree of grafting was investigated.

The degree of grafting on nylon 6 was affected by the concentration of 4-vinylbenzyl-PIM as shown in Fig. 5.47. It was evident that increasing the monomer concentration up to

about 2.48 w/v caused an outstanding enhancement in the degree of grafting and further increase in the monomer concentration beyond 2.48 w/v led to a decrease. Upon introducing the monomer into the reaction system, they were expected to immediately react with the activated surface of nylon 6 fibers. When the monomer concentration was low, the main reaction sites that would initiate the grafting process would be the radicals on the backbone leading to formation of graft copolymer other than homopolymer. Therefore, the degree of grafting was seen to increase as the monomer concentration was increased. But as the monomer concentration was increased beyond 2.48 w/v, grafting was inhibited.

The decrease in grafting percentage could be probably due to the formation of homopolymer as a result of a high concentration of the monomer in solution. The presence of homopolymer in the grafting solution could also bring about an increase in the viscosity of the reaction system, and hence hinder further formation of graft copolymer, which could have led to a low degree of grafting at higher monomer concentrations.
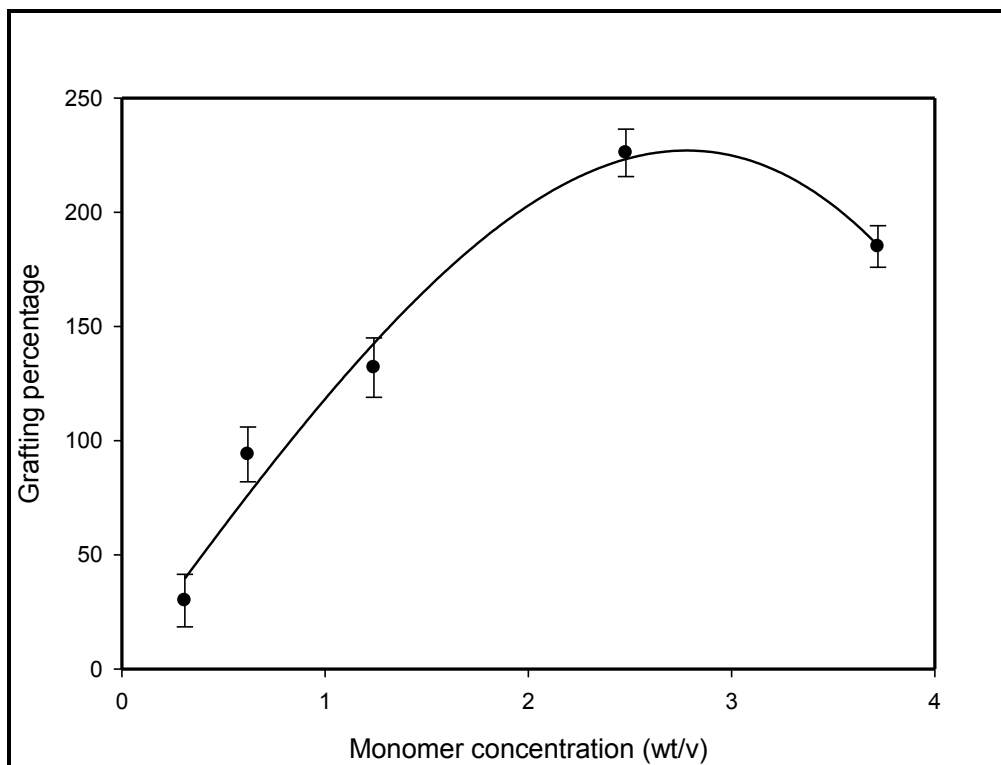
Figure 5.47: Influence of the concentration of 4-vinylbenzyl-2-(2′-Pyridyl)-imidazole on the degree of grafting (Temperature, 40 ^{0}C, BP concentration 0.8%, UV irradiation time 4 h, The error bars: standard deviations, n = 3.)

Chapter 6 Conclusions and Recommendations

The thesis presents an evaluation of the use of polymeric electrospun nanofibers as solid supports for optical probes. In the light of the urgent need for development of new, more efficient, accessible, economically viable, and environmentally friendly techniques for detection of toxic metal ions in water, current research developments in the field of nanotechnology and the efficient immobilization of signaling reagents onto nanofibers offer promising solutions. Nanomaterials, such as electrospun nanofibers offer an alternative method of incorporating active chemical groups in order to fabricate cheap and efficient probes.

The results obtained demonstrated that polymeric nanofibers are attractive as solid supports for signaling reagents based on the enormous possibilities that exist to tailor their chemical and physical characteristics. The high surface area and porosity, the ease of fabrication and the highly modifiable characteristics allow for the development of polymeric nanofibers with a wide range of chemical characteristics. Suitable chemical functionalization could also efficiently orient their properties towards certain classes of chemicals to achieve high selectivity. This thesis has shown that diagnostic probes could easily be fabricated by functionalizing nanofibers through simple processes that yield selective and sensitive nanofibers.

The methods presented in this thesis demonstrated the possibility of having alternative ways to complement the conventional methods for detection and quantification of metal ions in water which often include; the use of large sample volumes, extensive sample preparation steps and the use of expensive instrumentation.

It should be noted that despite the excellent results that were obtained on application of metal nanoparticles to detect metal ions, there is a growing evidence that metal nanoparticles could exhibit cytotoxic effects on higher organisms [305]. This raises the need for further investigation into their impact on the environment and human health especially when used in water bodies.

Our future research would be geared towards the fabrication of diagnostic probes that could be able to detect more than one metal ion with totally differing responses. Such a product will be highly applicable for multi-element detections hence reducing the cost of analytical procedures.

References

1. U. Foerstner, G.T.W. Wittmann, *Metal Pollution in the Aquatic Environment. 2nd Ed*. 1981: Springer-Verlag. 486.

2. E. Merian, *Metals and Their Compounds in the Environment: Occurrence, Analysis, and Biological Relevance*. 1991: VCH. 1438.

3. T. Westermark, S. Forberg, *Nor. Vet.-Tidsskr*.**84,** 1972, 281-294.

4. L. Sigg, H. Xue, *Euro Courses: Chem. Environ. Sci.,* **5,** 1994, 153-81.

5. J. Szpunar, R. Lobinski, *Fresenius' J. Anal. Chem.,* **363,** 1999, 550-557.

6. D. Radisky, J. Kaplan, *J. Biol. Chem.,* **274,** 1999, 4481-4484.

7. D. Beyersmann, *The significance of interactions in metal essentiality and toxicity*. 1991, VCH.

8. Y. Wang, G. Qian, Z. Xiao, H. Wang, L. Long, H. Wang, Z. Li, X. Liu, *Inorg. Chim. Acta,* **363,** 2010, 2325-2332.

9. L. Jaerup, *Br. Med. Bull.,* **68,** 2003, 167-182.

10. J.O. Duruibe, M.O.C. Ogwuegbu, J.N. Egwurugwu**,** *J. Phy. Sci.,* **2**(5), 2007, 112-118.

11. J.R. Garbarino, H.C. Hayes, D.A. Roth, R.C. Antweiler, T.I. Brinton, H.E. Taylor, *Heavy Metals in the Mississippi River.*, R.H. Meade, Editor. 1995, U.S. Geological Survey Circular 1133: Reston, Virginia.

12. A. Shokrollahi, M. Ghaedi, M. Montazerozohori, A.H. Kianfar, H. Ghaedi, N. Khanjari, S. Noshadi, S. Joybar, *E-J. Chem.,* **8,** 2011, 495-506.

13. P.J. Aggett, J.E. Whitley, *Spec. Publ. - R. Soc. Chem.,* **154,** 1994, 326-34.

14. S.B. Mulrooney, R.P. Hausinger, *FEMS Microbiol. Rev.,* **27,** 2003, 239-261.

15. WHO, Guidelines for drinking-water quality, fourth edition, 2011,ISBN 978 92 4 154815 1.

16. R.P. Beliles, ed. *The metals*. Pt. C ed. Patty's Industrial Hygiene and Toxicology (4th Edition) ed. G.D.C. Clayton, Florence E. Vol. 2(Pt. C) 1994, Wiley. 1879-2352.

17. A.R. Young, *Toxicity Profiles. Toxicity summary for nickel and nickel compounds*. 1995 [cited 2011 03.03.]; Available from: http://risk.lsd.ornl.gov/tox/profiles/nickel

18. T.P. Coogan, D.M. Latta, E.T. Snow, M. Costa, *Crit. Rev. Toxicol.,* **19,** 1989, 341-384.

19. L. Friberg, C.G. Elinder, *Scand. J. Work, Environ. Health,* **19,** 1993, 7-13.

20. P. Grandjean, *IARC Sci Publ,* 1984, 469-85.

21. B.K. De, J. Buekers, C. Cornelis, C.E. Schlekat, A.R. Oller, *Sci. Total Environ.,* **419,** 2012, 25-36.

22.   M.C. Talio, M.O. Luconi, L.P. Fernandez, *Microchem. J.,* **99,** 2011, 486-491.

23.   B.R. Von, *J Appl Toxicol,* **17,** 1997, 425-31.

24.   L. Reclaru, R.E. Unger, C.J. Kirkpatrick, C. Susz, P.-Y. Eschler, M.-H. Zuercher, I. Antoniac, H. Lüthy, *Mater. Sci. Eng., C* **32**, 2012, 1452-1460.

25.   V. Bencko, *J. Hyg., Epidemiol., Microbiol., Immunol.,* **27,** 1983, 237-47.

26.   R.F. Hertel, T. Maass V.R. Muller, *Nickel. (Environmental Health Criteria 108). 383 Seiten, 36 Tab. World Health Organization, Geneva 1991.* Food / Nahrung, **36**(1), 1992, 102-102.

27.   K. Prystupa, E. Rudzki, *Contact Dermatitis,* **39,** 1998, 326.

28.   I. Al-Saleh, I. Al-Doush, *Sci. Total. Environ.,* **216,** 1998, 181-192.

29.   D. Baralkiewicz, J. Siepak, *Pol. J. Environ. Stud.,* **8,** 1999, 201-208.

30.   J.O. Nriagu, J.M. Pacyna, *Nature*, **333,** 1988, 134-139.

31.   T.R. Dickson, *Introduction to Chemistry*. 6th ed. ed. 1991, New York: John Wiley.

32.   K.M. Mackay, R.A. Mackay, W. Henderson, *Introduction to modern inorganic Chemistry*. 6th ed. 2002, London: Nelson Thrones.

33.   A. Stoyanova, *Trakia J. Sc,* **3,** 2005, 10-15.

34.   J. McMurry, Fay, R.C., *Chemistry*. 3rd ed. 2001, New Jersey: Prentice- Hall.

35.   S. Tautkus, L. Steponeniene, R. Kazlauskas, *J. Serb. Chem. Soc.,* **69,** 2004, 393-402.

36.   E.P. Achterberg, T.W. Holland, A.R. Bowie, R. F. C. Mantoura, P. J. Worsfold, *Anal. Chim. Acta,* **442,** 2001, 1-14.

37.   A. Townshend, *Encyclopedia of Analytical sciences*. Vol. 4. 1995, London: Academic press.

38.   V. Cannizzaro, A.R. Bowie, A., Sax, E.P. Achtrberg, P.J. Worsfold, *Analyst,* **125,** 2000, 51-57.

39.   H. Obata, M.G. Constant, V.D. Berg, *Anal. Chem.,* **73,** 2001, 2522-2528.

40.   P.N. Sedwick, P.R. Edwards, D.J. Mackey, F.B. Griffiths, J.S. Parslow, *Deepsea Res.,* **44,** 1997, 1239-1253.

41.   D.B. Botkin, E.A. Keller, *Environmental science: Earth as a planet of living*. 5th ed. 2005, U.S.A: John Wiley.

42.   F.A. Cotton, G. Wilkinson, *Advanced Inorganic Chemistry*. 3rd ed. 1988, NewYork: Wiley Interscience.

43.   M.I. Pascual-Reguera, I. Ortega-Carmona, A. Molina-Diaz, *Talanta,* **44,** 1997, 1793-1801.

44.   C.C. Winterbourn, *Toxicol. Lett.,* **82/83,** 1995, 969-974.

45.   J.D. Herron, D.A. Kukla, M.A. Dispezio, C.L. Schrader, J.L. Erickson, D. Morrison, D. Scodellaro, *Health Chemistry*. Canadian edition ed. 1987, Toronto: D.C Canada Ltd.

46.   S.S. Zumdahl, *Chemical principles*. 1992, Toronto: D.C Heath and Company.

47.   K. Sozgen, E. Tutem, *Anal. Sci.,* **17,** 2001, 1861-1864.

48.   D.T. Richens, *The chemistry of aqua ions*. 1997, Chichester: Jhon Wiley.

49.   Z. Zeng, R.A. Jewsbury, *Analyst*, **125.** 2000, 1661-1665.

50.   J.F. Van Stadan, E.B. *S. Afr. J. Chem.,* **53,** 2000, 191-205.

51.   J.T. Ellis, I. Schulman, C.H. Smith, *Am. J. Pathol,* **30,** 1954, 287-309.

52.   J.V. Corbett, *MCN Am J Matern Child Nurs,* **20,** 1995, 234.

53.   D.S.S. Herman, M. Geraldine, C.C.,Scott, T. Venkatesh, *Toxicol. Ind. Health,* **22,** 2006, 249-54.

54.   A. Prange, A. Kngchel, *Anal. Chim. Acta,* **172,** 1985, 79-100.

55.   H. Berg, *Bioelectrochem. Bioenerg.,* **46,** 1998, 155-156.

56.   O.S. Wolfbeis, *Fiber Optic Chemical Sensors and Biosensors,* **2**, 1991: CRC. 358.

57.   Merck, *Reflectoquant Datasheets.* Merck, Darmstadt, 1996.

58.   I. Oehme, O.S. Wolfbeis, *Mikrochim. Acta,* **126,** 1997, 177-192.

59.   K.J. Albert, N.S. Lewis, C.L. Schauer, G.A. Sotzing, S.E. Stitzel, T.P. Vaid, D.R. Walt, *Chem. Rev.,* **100,** 2000, 2595-2626.

60.   J.M.,Lehn, *Supramolecular Chemistry: Concepts and Perspectives*. 1995: VCH. 262.

61.   P. Buehlmann, E. Pretsch, E. Bakker, *Chem. Rev.* **98,** 1998, 1593-1687.

62.   F.P. Schmidtchen, M. Berger, *Chem. Rev.,* **97,** 1997, 1609-1646.

63.   A. Spaeth, B. Koenig, *Beilstein J. Org. Chem.,* **6,** 2010, 32.

64.   R.G. Pearson, *J. Am. Chem. Soc.,* **85,** 1963, 3533-3539.

65.   K. Rurack, *Spectrochim. Acta, Part A,* **57A,** 2001, 2161-2195.

66.   M. Lerchi, E. Reitter, W. Simon, E. Pretsch, D.A. Chowdhury, S. Kamata, *Anal. Chem.,* **66,** 1994, 1713-1717.

67.   E. Wanninen, *Int. Ser. Monogr. Anal. Chem.,* **51,** 1972, 231-435.

68.   O.S. Wolfbeis, *J. Am. Chem. Soc.,* **117,** 1995, 8492-8493.

69.   R.P. Haugland, *Handbook of Fluorescent Probes and Research Products.* Molecular Probes, 2001.

70.   F. Pavlikova, M. Stradal, *CHEMagazin,* **10,** 2000, 39.

71.   H. Kautsky, *Trans. Faraday Soc.,* **35,** 1939, 216-219.

72.   D.B. Papkovsky, G.V. Ponomarev, W. Trettnak, P. O'Leary, *Anal. Chem.,* **67,** 1995, 4112-4117.

73.   J. Biwersi, B. Tulk, A.S. Verkman, *Anal. Biochem.,* **219,** 1994, 139-143.

74.   C. Huber, I. Klimant, C. Krause, O.S. Wolfbeis, *Anal. Chem.,* **73,** 2001, 2097-2103.

75.   K.D. Legg, D.M. Hercules, *J. Phys. Chem.,* **74,** 1970, 2114-2118.

76.   C. Huber, I. Klimant, C. Krause, T. Werner, T. Mayr, O.S. Wolfbeis, *Fresenius' J. Anal. Chem.,* **368,** 2000, 196-202.

77.   W.H. Chan, R.H. Yang, K.M. Wang, *Anal. Chim. Acta,* **444,** 2001, 261-269.

78.   C. Sanchez-Pedreno, J.A. Ortuno, M.I. Albero, M. S. Garcia, M.V. Valero, *Anal. Chim. Acta,* **414,** 2000, 195-203.

79.   N. Mahendra, P. Gangaiya, S. Sotheeswaran, R. Narayanswamy, *Sens. Actuators, B,* **B81,** 2002, 196-201.

80.   N. Malcik, O. Oktar, M.E. Ozser, P. Caglar, L. Bushby, A. Vaughan, B. Kuswandi, R. Narayanaswamy, *Sens. Actuators, B,* **B53,** 1998, 211-221.

81.   A.A. Vaughan, R. Narayanaswamy, *Sens. Actuators*, B, **B51,** 1998, 368-376.

82.   E. Antico, M. Lerchi, B. Rusterholz, N. Achermann, M. Badertscher, M. Valiente, E. Pretsch, *Anal. Chim. Acta,* **388,** 1999, 327-338.

83.   F. Szurdoki, D. Ren, and D.R. Walt, *Anal. Chem.,* **72,** 2000, 5250-5257.

84.   A.V. Legin, Y.G. Vlasov, A.M. Rudnitskaya, E.A. Bychkov, *Sens. Actuators, B,* **B34,** 1996, 456-461.

85.   W. Retig, B. Strehmel, S. Schrader, H. Seifert, *Applied Fluorescence in Chemistry, Biology and Medicine*. 1999: Springer. 562.

86.   A. Chaumont, M. Nickmilder, X. Dumont, T. Lundh, S. Skerfving, A. Bernard, *Toxicol. Lett.,* **210,** 2012, 345-352.

87.   H. Zhao, B. Xia, C. Fan, P. Zhao, S. Shen, *Sci. Total Environ.,* **417-418,** 2012, 45-54.

88.   C. Lopez-Garcia, E. Varea, J.J. Palop, J. Nacher, C. Ramirez, X. Ponsoda, A. Molowny, *Microsc. Res. Tech.,* **56,** 2002, 318-331.

89.   Available from: http://www.epa.gov/safewater/methods/inch_tbl.html. 2012.

90.   A.W. Czarnik, *Fluorescent Chemosensors for Ion and Molecule Recognition. (Developed from a Symposium Sponsored by the Division of Organic Chemistry at the 204th National Meeting of the American Chemical Society, Washington, DC, August 23-28, 1992.) [In: ACS Symp. Ser., 1993; 538]*. 1993: ACS. 235.

91. A.P. de Silva, H.Q.N. Gunaratne, T. Gunnlaugsson, A.J.M. Huxley, C.P. McCoy, J.T. Rademacher, T.E. Rice, *Chem. Rev.* **97,** 1997, 1515-1566.

92. J.P. Desvergne, A.W. Czarnik, *Chemosensors of Ion and Molecule Recognition. (Proceedings of the NATO Advanced Research Workshop, held 31 August-4 September 1996, in Bonas, France.) [In: NATO ASI Ser., Ser. C, 1997; 492]*. 1997: Kluwer. 245.

93. N.I. Georgiev, A.R. Sakr, V.B. Bojinov, *Dyes Pigm.,* **91**(3), 2011, 332-339.

94. C. Curutchet, B. Mennucci, G.D. Scholes, D. Beljonne, *J. Phys. Chem. B,* **112,** 2008, 3759-3766.

95. S.G. De, L. Fabbrizzi, M. Licchelli, C. Mangano,D. Sacchi, N. Sardone, *Inorg. Chim. Acta,* **257,** 1997, 69-76.

96. G.E. Collins, L.-S. Choi, *Chem. Commun.* 1997, 1135-1136.

97. M. Schuster, M. Sandor, *Fresenius' J. Anal. Chem.,* **356,** 1996, 326-330.

98. G. Hennrich, H. Sonnenschein, U. Resch-Genger, *J. Am. Chem. Soc.,* **121,** 1999, 5073-5074.

99. S. Pellet-Rostaing, J.-B. Regnouf-de-Vains, R. Lamartine, P. Meallier, S. Guittonneau, B. Fenet, *Helv. Chim. Acta,* **80,** 1997, 1229-1243.

100. Q.-E. Cao, K. Wang, Z. Hu, Q. Xu, *Talanta,* **47,** 1998, 921-927.

101. M.R. Eftink, *Top. Fluoresc. Spectrosc.,* **2,** 1991, 53-126.

102. J.R. Lakowicz, *Principles of Fluorescence Spectroscopy*. 2nd Edition ed. 1999, New York Kluwer Academic/Plenum Publishers.

103. J. Zimmermann, A. Zeug, B. Roeder, *Phys. Chem. Chem. Phys.,* **5,** 2003, 2964-2969.

104. B. Valeur, *Molecular Fluorescence - An Introduction: Principles and Applications, 1st Edition 2000*. 2000: Wiley-VCH. 250.

105. J.-M. Liu, Q.-Y. Zheng, J.-L. Yang, C.-F. Chen, Z.-T. Huang, *Tetrahedron Lett.,* **43,** 2002, 9209-9212.

106. M.H. Mashhadizadeh, I.S. Shoaei, N. Monadi, *Talanta,* **64,** 2004, 1048-1052.

107. V. Amendola, L. Fabbrizzi, M. Licchelli, C. Mangano, P. Pallavicini, L. Parodi, A. Poggi, *Coord. Chem. Rev.,* **190-192,** 1999, 649-669.

108. P. Pulido-Tofiño, J.M.B.M. Moreno, M.C. Pérez-Conde, Talanta, **51**(3), 2000, 537-545.

109. S. Mizukami, T. Nagano, Y. Urano, A. Odani, K. Kikuchi, *J. Am. Chem. Soc.,* **124,** 2002, 3920-3925.

110. G. Farruggia, S. Iotti, L. Prodi, M. Montalti, N. Zaccheroni, P.B. Savage, V. Trapani, P. Sale, F.I. Wolf, *J. Am. Chem. Soc.,* **128,** 2006, 344-350.

111. X. Peng, J. Du, J. Fan, J. Wang, Y. Wu, J. Zhao, S. Sun, T. Xu, *J. Am. Chem. Soc.,* **129,** 2007, 1500-1501.

112. X. Qi, E.J. Jun, L. Xu, S.-J. Kim, J.S.J. Hong, Y.J. Yoon, J. Yoon, *J. Org. Chem.,* **71,** 2006, 2881-2884.

113. D. Curiel, A. Cowley, P.D. Beer, *Chem. Commun.* 2005, 236-238.

114. L.-J. Fan, W.E. Jones, Jr., *J. Am. Chem. Soc.,* **128,** 2006, 6784-6785.

115. S.-I. Kondo, Y. Hiraoka, N. Kurumatani, Y. Yano, *Chem. Commun.* 2005, 1720-1722.

116. G. Klein, D. Kaufmann, S. Schurch, J.-L. Reymond, *Chem. Commun.* 2001, 561-562.

117. D.S. McClure, *J. Chem. Phys.,* **20,** 1952, 682-686.

118. A.W. Varnes, R.B. Dodson, E.L. Wehry, *J. Amer. Chem. Soc.,* **94,** 1972, 946-50.

119. C.-T. Chen, W.-P. Huang, *J. Am. Chem. Soc.,* **124,** 2002, 6246-6247.

120. X. Guo, X. Qian, L. Jia, *J. Am. Chem. Soc.,* **126,** 2004, 2272-2273.

121. B. Bodenant, F. Fages, M.-H. Delville, *J. Am. Chem. Soc.,* **120,** 1998, 7511-7519.

122. A.C. Bhasikuttan, M. Suzuki, S. Nakashima, T. Okada, *J. Am. Chem. Soc.,* **124,** 2002, 8398-8405.

123. J.A. Kemlo, T.M. Shepherd, *Chem. Phys. Lett.,* **47,** 1977, 158-62.

124. L. Fabbrizzi, M. Licchelli, P. Pallavicini, A. Perotti, A. Taglietti, D. Sacchi, *Chem.--Eur. J.,* **2,** 1996, 75-82.

125. W.-S. Xia, R.S. Schmehl, C.-J. Li, J.T. Mague, C.-P. Luo, D.M. Guldi, *J. Phys. Chem. B,* **106,** 2002, 833-843.

126. X. Peng, D.R. Draney, W.M. Volcheck, *Proc. SPIE-Int. Soc. Opt. Eng.,* **6097,** 2006, 60970F/1-60970F/12.

127. T.D. Gauthier, E.C. Shane, W.F. Guerin, W.R. Seitz, C.L. Grant, *Environ. Sci. Technol.,* **20,** 1986, 1162-1166.

128. D.A. Backhus, C. Golini, E. Castellanos, *Environ. Sci. Technol.,* **37,** 2003, 4717-4723.

129. C.D. Geddes, *Meas. Sci. Technol.,* **12,** 2001, R53-R88.

130. M.K. Nazeeruddin, D. Di Censo, R. Humphry-Baker, M. Gratzel, *Adv. Funct. Mater.,* **16,** 2006, 189-194.

131. D. Prabhakaran, H. Nanjo, H. Matsunaga, *Anal. Chim. Acta,* **601,** 2007, 108-117.

132. C. Bargossi, M.C. Fiorini, M. Montalti, L. Prodi, N. Zaccheroni, *Coord. Chem. Rev.,* **208,** 2000, 17-32.

133. P.D. Beer, *Acc. Chem. Res.,* **31,** 1998, 71-80.

134. A.B. Ellis, D.R. Walt, *Chem. Rev.*, **100,** 2000, 2477-2478.

135. R. Sheng, P. Wang, Y. Gao, Y. Wu, W. Liu, J. Ma, H. Li, S. Wu, *Org. Lett.,* **10,** 2008, 5015-5018.

136. T. Gunnlaugsson, J.P. Leonard, N.S. Murray, *Org. Lett.,* **6,** 2004, 1557-1560.

137. R. Martinez, A. Espinosa, A. Tarraga, P. Molina, *Org. Lett.,* **7,** 2005, 5869-5872.

138. M.E. Stewart, C.R. Anderton, L.B. Thompson, J. Maria, S.K. Gray, J.A. Rogers, R.G. Nuzzo, *Chem. Rev.* **108,** 2008, 494-521.

139. Z. Wang, L. Ma, *Coord. Chem. Rev.,* **253,** 2009, 1607-1618.

140. M. Li, D.-W. Li, Y.-T. Li, D.-K. Xu, Y.-T. Long, *Ana. Chim. Acta,* **701,** 2011, 157-163.

141. N. Kaur, S. Kumar, *Tetrahedron,* **67,** 2011, 9233-9264.

142. K.S. Suslick, N.A. Rakow, A. Sen, *Tetrahedron,* **60,** 2004, 11133-11138.

143. K. Hunger, *Industrial Dyes Chemistry, Properties, Applications*, ed. K. Hunger. 2003, WILEY-VCH Verlag GmbH & Co. KGaA, Weinheim.

144. P. Gregory, *The Chemistry and Application of Dyes*, ed. G.H. (Eds.: D. R.Waring. 1990, New York: Plenum.

145. A.L. Smith, *Transactions of the British Mycological Society,* **11**(1–2), 1926, 45-50.

146. N. Anderson, J. Weiland, J. Pharis, W. Gagné, E. Janiga, M.J. Rosenow, *Scientia Horticulturae,* **122**(2), 2009, 221-226.

147. T. Shoji, Y. Goda, M. Toyoda, A. Yanagida, T. Kanda, *Phytochem.,* **59**(2), 2002, 183-189.

148. E. Ross, R. Naumann, W. Fischer, U. Jäschke, W.-D. Mayer, G. Wieland, E. J. Newman, C. M. Wilson,, *"Indicator Reagents", Ullmann's Encyclopedia of Industrial Chemistry*. 5th ed., ed. Vol. Vol. A14. 1989: VCH, Weinheim.

149. E. Ross, R. Naumann, W. Fischer, W.-D. Mayer, G. Wieland, E. J. Newman, C. M. Wilson,, *"Indicator Reagents"*, in *Ullmann's Encyclopedia of In dustrial Chemistry , Electronic Release*. 2002, Wiley-VCH, Weinheim.

150. D. Vilela, M.C. González, A. Escarpa, *Anal. Chim. Acta,* **751**(0), 2012, 24-43.

151. F.P. Zamborini, L. Bao, R. Dasari, *Anal. Chem.* **84,** 2012, 541-576.

152. L.M. Liz-Marzan, *Mater. Today,* **7,** 2004, 26-31.

153. M. Reibold, P. Paufler, A. A. Levin, W. Kochmann, N. Paetzke, D. C. Meyer, *Nature,* **444,** 2006, 286.

154. J. Perttula, *Scand. J. Metall.,* **30,** 2001, 65-68.

155. W. Kochmann, M. Reibold, R. Goldberg, W. Hauffe, A.A. Levin, D.C. Meyer, T. Stephan, H. Muller, A. Belger, P. Paufler, *J. Alloys Compd.,* **372,** 2004, L15-L19.

156. O.D. Sherby, J. Wadsworth, *J. Mater. Process. Technol,* **117,** 2001, 347-353.

157. J. Perttula, *Scand. J. Metall.,* **33,** 2004, 92-97.

158. G.P. Wiederrecht, *Eur. Phys. J.: Appl. Phys.,* **28,** 2004, 3-18.

159. http://www.nature.com/nphoton/journal/v1/n4/full/nphoton.2007.38.html. [cited 2012 28-10].

160. K. Aslan, J.R. Lakowicz, C.D. Geddes, *Anal. Biochem.,* **330,** 2004, 145-155.

161. J. Liu, Y. Lu, *Chem. Commun.* 2007, 4872-4874.

162. A.J. Reynolds, A.H. Haines, D.A. Russell, *Langmuir,* **22,** 2006, 1156-1163.

163. C.A. Mirkin, R.L. Letsinger, R.C. Mucic, J.J. Storhoff, *Nature,* **382,** 1996, 607-609.

164. H.-K. Kim, I. Rasnik, J. Liu, T. Ha, Y. Lu, *Nat. Chem. Biol.,* **3,** 2007, 763-768.

165. D. Li, A. Wieckowska, I. Willner, *Angew. Chem., Int. Ed.,* **47,** 2008, 3927-3931.

166. Y. Lu, J. Liu, *Acc. Chem. Res.,* **40,** 2007, 315-323.

167. D.D. Jr. Evanoff, G. Chumanov, *Chem.Phys.Chem,* **6,** 2005, 1221-1231.

168. J.A. Eastman, S.U. Cho, W. Yu, L.J. Thompson, *Appl. Phys. Lett.,* **78**(6), 2001, 718-720.

169. N. Cioffi, N. Ditaranto, L. Torsi, R. A. Picca, E.D. Giglio, P.G. Zambonin, *Anal.Bioanal. Chem.,* **382,** 2005, 1912–1918.

170. R.K. Guduru, K. L. Murty, K.M. Youssef, R.O. Scattergood, C.C. Koch, Mat. Sci. Eng. A, **463**(1-2), 2007, 14-21.

171. Q. Xu, Y. Zhao, J.Z. Xu, J.J. Zhu, *Sens. Actuators B,* **114,** 2006, 379-386.

172. S. Vukojevic, O. Trapp, J.D. Grunwaldt, C. Kiener, F. Schuth, *Angewandte Chemie Int. Ed.,* **44,** 2005, 7978-7981.

173. H.C. Zeng, *Curr. Nanosci.,* **3,** 2007, 177-181.

174. I. Pastoriza-Santos, L.M. Liz-Marzan, *Langmuir,* **15,** 1999, 948-951.

175. P. Raveendran, J. Fu, S.L. Wallen, *J. Am. Chem. Soc.,* **125,** 2003, 13940-13941.

176. B.V. Deryagin, *Theory of Stability of Colloids and Thin Films*. 1986: Nauka. 206.

177. S. Moessmer, J.P. Spatz, M. Moeller, T. Aberle, J. Schmidt, W. Burchard, *Macromol.,* **33,** 2000, 4791-4798.

178. O.A. Platonova, L.M. Bronstein, S.P. Solodovnikov, I.M. Yanovskaya, E.S. Obolonkova, P.M. Valetsky, E. Wenz, M. Antonietti, *Colloid Polym. Sci.,* **275,** 1997, 426-431.

179. M.S. Fleming, D.R. Walt, *Langmuir,* **17,** 2001, 4836-4843.

180. S. Kacmaz, K. Ertekin, A. Suslu, M. Ozdemir, Y. Ergun, E. Celik, U. Cocen, *Sens. Actuators B: Chemical,* **153**(1), 2011, 205-213.

181. I. Oehme, S. Prattes, O.S. Wolfbeis, G.J. Mohr, *Talanta*, **47,** 1998, 595-604.

182. G.J. Mohr, O.S. Wolfbeis, *Anal. Chim. Acta,* **292,** 1994, 41-8.

183. B.D. Gupta, N.K. Sharma, *Sens. Actuators, B,* **B82,** 2002, 89-93.

184. Y. Kostov, S. Tzonkov, L. Yotova, M. Krysteva, *Anal. Chim. Acta,* **280,** 1993, 15-19.

185. A. Safavi, M. Bagheri, *Sens. Actuators, B,* **B90,** 2003, 143-150.

186. E. Wang, K.-F. Chow, V. Kwan, T. Chin, C. Wong, A. Bocarsly, *Anal. Chim. Acta,* **495,** 2003, 45-50.

187. T. Werner, C. Huber, S. Heinl, M. Kollmannsberger, J. Daub, O.S. Wolfbeis, *Fresenius' J. Anal. Chem.,* **359,** 1997, 150-154.

188. T.E. Brook, R. Narayanaswamy, *Sens. Actuators, B,* **B51,** 1998, 77-83.

189. M.P. Xavier, D. Garcia-Fresnadillo, M.C. Moreno-Bondi, G. Orellana, *Anal. Chem.,* **70,** 1998, 5184-5189.

190. G. Li, L. Zhang, Z. Li, W. Zhang, *J. Hazard. Mater.,* **177,** 2010, 983–989.

191. P. Hashemi, R.A. Zarjani, *Sens. Actuators, B,* **B135,** 2008, 112-115.

192. Y. Li, M. Ashizawa, S. Uchida, T. Michinobu, *Macromol. Rapid Commun.,* **32,** 2011, 1804-1808.

193. X. Wang, C. Drew, S.-H. Lee, K.J. Senecal, J. Kumar, L.A. Samuelson, *Nano Lett.,* **2,** 2002, 1273-1275.

194. M.Z. Ongun, K. Ertekin, M. Gocmenturk, Y. Ergun, A. Suslu, *Spectrochim. Acta Part A: Molec. and Biomolec. Spectros.* 2012, **90**(0), 2012, 177-185.

195. S. Kacmaz, K. Ertekin, A. Suslu, Y. Ergun, E. Celik, U. Cocen, *Mater. Chem. Phys.* **133**(1), 2012, 547-552.

196. O.S. Wolfbeis, *Adv. Mater.* **20,** 2008, 3759-3763.

197. L.S. Caroline, C. Mu-San, R .P. Ronald, E.S. Paul S.L. Francess, *Environ. Sci. Technol.,* **38,** 2004, 4409-4413.

198. O.S. Wolfbeis, *Anal. Chem.,* **76,** 2004, 3269-3284.

199. R.A. Potyrailo, S.E. Hobbs, G.M. Hieftje, *Fresenius' J. Anal. Chem.,* **362,** 1998, 349-373.

200. M. Zourob, S. Mohr, P.R. Fielden, N.J. Goddard, *Lab Chip,* **5,** 2005, 772-777.

201. K.C. Persaud, *Mater. Today*, **8,** 2005, 38-44.

202. B. Adhikari, S. Majumdar, *Prog. Polym. Sci.,* **29,** 2004, 699-766.

203. K.J. Albert, D.R. Walt, *Anal. Chem.,* **72,** 2000, 1947-1955.

204. R. Meallet-Renault, R. Pansu, S. Amigoni-Gerbier, C. Larpent, *Chem. Commun.* 2004, 2344-2345.

205. J.T. Suri, D.B. Cordes, F.E. Cappuccio, R.A. Wessling, B. Singaram, *Angew. Chem., Int. Ed.,* **42,** 2003, 5857-5859.

206. S.-H. Lee, J. Kumar, S.K. Tripathy, *Langmuir*, **16,** 2000, 10482-10489.

207. K.J. Albert, D.S. Gill, T.C. Pearce, D.R. Walt, *Anal. Bioanal. Chem.,* **373,** 2002, 792-802.

208. Y. Amao, *Microchim. Acta,* **143,** 2003, 1-12.

209. T.A. Dickinson, D.R. Walt, J. White,J.S. Kauer, *Anal. Chem.,* **69,** 1997, 3413-3418.

210. P. Bosch, F. Catalina, T. Corrales, C. Peinado, *Chem.--Eur. J.,* **11,** 2005, 4314-4325.

211. Y. Amao, K. Asai, I. Okura, H. Shinohara, H. Nishide, *Analyst,* **125,** 2000, 1911-1914.

212. Y. Zhang, R.H. Yang, F. Liu, K.'A. Li, *Anal. Chem.,* **76,** 2004, 7336-7345.

213. E.L. Doyle, C.A. Hunter, H.C. Phillips, S.J. Webb, N.H. Williams, *J. Am. Chem. Soc.,* **125,** 2003, 4593-4599.

214. Y. Liu, R.C. Mills, J.M. Boncella, K.S. Schanze, *Langmuir,* **17,** 2001, 7452-7455.

215. W. Qin, P. Parzuchowski, W. Zhang, M.E. Meyerhoff, *Anal. Chem.,* **75,** 2003, 332-340.

216. T.M. Ambrose, M.E. Meyerhoff, *Anal. Chim. Acta*, **378,** 1999, 119-126.

217. T. Mayr, G. Liebsch, I. Klimant, O.S. Wolfbeis, *Analyst*, **127,** 2002, 201-203.

218. M.R. Shortreed, S. Dourado, R. Kopelman, *Sens. Actuators, B,* **B38,** 1997, 8-12.

219. J. Lin, *TrAC, Trends Anal. Chem.,* **19,** 2000, 541-552.

220. B.M. Weidgans, K. Christian, I. Klimant, O.S. Wolfbeis, *Analyst*, **129,** 2004, 645-650.

221. H. Offenbacher, O.S. Wolfbeis, E. Fuerlinger, *Sens. Actuators,* **9,** 1986, 73-84.

222. L.A. Saari, W.R. Seitz, *Anal. Chem.,* **54,** 1982, 821-823.

223. R. Yang, J. He, L. Xu, J. Yu, *Polymer*, **50,** 2009, 5846–5850.

224. S. Ramakrishna, K. Fujihara, W.-E. Teo, T.-C. Lim, Z. Ma, *An Introduction to Electrospinning and Nanofibers*. 2005, Singapore: World Scientific Publishing Co. Pte. Ltd.

225. Y., Dzenis, *Science*, **304,** 2004, 1917-1918.

226. H. Fong, D.H. Reneker. *Electrospinning and the formation of nanofibers*. 2001: Carl Hanser Verlag.

227. D. Li, Y. Xia, *Adv. Mater.* **16,** 2004, 1151-1170.

228. A. Ziabicki, *Physical Fundamentals of Fiber Formation*. 1976: Wiley. 504.

229. L. Tong, R.R. Gattass, J.B. Ashcom, S. He, J. Lou, M. Shen, I. Maxwell, E. Mazur, *Nature*, **426,** 2003, 816-819.

230. C.J. Ellison, A. Phatak, D.W. Giles, C.W. Macosko, F.S. Bates, *Polymer,* **48,** 2007, 3306-3316.

231. E. Zhmayev, D. Cho, Y.L. Joo, *Polymer,* **51**(18), 2010, 4140-4144.

232. T. Balaji, S.A. El-Safty, H. Matsunaga, T. Hanaoka, F. Mizukami, *Angew. Chem., Int. Ed.,* **45,** 2006, 7202-7208.

233. L. Gao, J.Q. Wang, L. Huang, X.X. Fan, J.H. Zhu, Y. Wang, Z.G. Zou, *Inorg. Chem.* **46,** 2007, 10287-10293.

234. C. He, W. Zhu, Y. Xu, T. Chen, X. Qian, *Anal. Chim. Acta,* **651,** 2009, 227-233.

235. D.H. Reneker, I. Chun, *Nanotechnol.,* **7,** 1996, 216-223.

236. S. Shin, J. Jang, *Chem. Commun.* 2007, 4230-4232.

237. L. Gao, Y. Wang, J. Wang, L. Huang, L. Shi, X. Fan, Z. Zou, T. Yu, M. Zhu, Z. Li, I*norg. Chem.,* **45,** 2006, 6844-6850.

238. K. Kledzik, M. Orlowska, D. Patralska, M. Gwiazda, J. Jezierska, S. Pikus, R. Ostaszewski, A.M. Klonkowski, *Appl. Surf. Sci.,* **254,** 2007, 441-451.

239. S.J. Lee, D.R. Bae, W.S Han, S.S. Lee, J.H. Jung, *J. Inorg. Chem.,* **10,** 2008, 1559-1564.

240. M.J. Ruedas-Rama, E.A.H. Hall, *Anal. Chem.* **80,** 2008, 8260-8268.

241. K. Sarkar, K. Dhara, M. Nandi, P. Roy, A. Bhaumik, P. Banerjee, *Adv. Funct. Mater.,* **19,** 2009, 223-234.

242. A. Frenot, I.S. Chronakis, *Curr. Opin. Colloid Interface Sci.,* **8,** 2003, 64-75.

243. W.E Teo, S. Ramakrishna, *Nanotechnol.,* **17,** 2006, R89-R106.

244. J. Zeleny, *Phys Rev,* **3,** 1914, 69–91.

245. D.H. Reneker I. Chun, *Nanotechnol.,* **7,** 1996, 216-223.

246. L. Larrondo, R.J.St., Manley, *J Polym Sci Polym Phys Ed,* **19,** 1981, 909 –920.

247. S, L.W. Koombhongse, D.H. Reneker, *J. Polym. Sci, Polym. Phys. Ed,* **39,** 2001, 2598 –606.

248. A. Buer, S.C. Ugbolue, S.B. Warner, *Textile Res J,* **71,** 2001, 323 –328.

249. M. Bognitzki, H. Hou, M. Ishaque, T. Frese, M. Hellwig, C. Schwarte, A. Schaper, J.H. Wendorff, A. Greiner, *Adv Mater,* **12,** 2000, 637– 40.

250. M. Bognitzki, T. Frese, M. Steinhart, A. Greiner, J.H. Wendorff, A. Schaper, M. Hellwig, *Polym Eng Sci,* **41,** 2001, 982 –989.

251. J.-S. Kim, D.H. Reneker, *Polym Eng Sci,* **39,** 1999, 849 –854.

252.   A. Theron, E. Zussman, AL. Yarin, *Nanotechnol.,* **12,** 2001, 384 –390.

253.   A.L. Yarin, E. Zussman, *Polymer,* **45,** 2004, 2977-2980.

254.   I. Chun, D.H. Reneker, H. Fong, X. Fang, J. Deitzel, N.B. Tan, K. Kearns, *J. Adv. Mater.,* **31,** 1999, 36-41.

255.   A. Pedicini, R.J. Farris, *Polymer,* **44,** 2003, 6857-6862.

256.   G.L.Wilkes, *electrospinning.* 2001, Available from: http:yywww.che.vt.eduyWilkesy/electrospinningyelectrspinning.html.

257.   J. M. Deitzel, J. Kleinmeyer, D. Harris, N.C.B. Tan, *Polymer,* **42,** 2001, 261 –72.

258.   A. Frenot, I.S. Chronakis, *Curr. Opin. Colloid Interface Sci.,* **8,** 2003, 64–75.

259.   H. Dong, T. Bell, *Surf. Coat. Technol,* **111**(1), 1999, 29-40.

260.   Y. Uyama, K. Kato, Y. Dcada, *Adv. Polym. Sci.,* **137,** 1998, 1-39.

261.   K. Kato, E. Uchida, E.T. Kang, Y. Uyama, Y. Ikada, *Prog. Polym. Sci.,* **28**(2), 2003, 209-259.

262.   C.-S. Zhao, S.-Q. Nie, M. Tang, S.-S. Sun, *Prog. Polym. Sci.,* **36**(11), 2011, 1499-1520.

263.   D. He, M. Ulbricht, *J. Mater. Chem.,* **16,** 2006, 1860–1868.

264.   Y.B. Zhu, C.Y. Gao, X.Y. Liu, J.C. Shen, *Biomacromolec.,* **3, 6,** 2002, 1312-1319.

265.   J. Li, J. Wang, X. Liu, *Chromatographia,* **56,** 2002, 401-406.

266.   D. D. Perrin, B. Demsey, *Buffers for pH and Metal Ion Control*. 1974, London: Chapman and Hall Laboratory Manuals.

267.   T.I.A. Gerber, E. Hosten, P. Mayer, Z.R. Tshentu, *J. Coord. Chem.,* **59,** 2006, 243-253.

268.   A. Fasil C.S.E. Abebe, G. Ramakrishna, E. Sinn, Tetrahedron Lett, **52**(43), 2011, 5554–5558.

269.   N.A. Gavrilenko, N.V. Saranchina, *Anal. Chem.,* **64**(3), 2009, 226-230.

270.   M. Balazy, A.S. Nies, *Biomed. Environm. Mass Spectrom.,* **18,** 1989, 328-336.

271.   W. W. Christie, E. Y. Brechany, Jie, M. S. F. Lie Ken; O. Bakare, *Biol. Mass Spectrom,* **20,** 1991, 629-635.

272.   J.R. Lakowicz, *Principles of Fluorescence Spectroscopy*. 1983: Plenum Press. 496.

273.   B.F. Rocks, *Fluorescence Spectroscopy. New Methods and Applications Edited by Otto S. Wolfbeis.* Analyst, **119,** 1994, 142N.

274.   L. Li, Y.-L. Hsieh, *Polymer,* **46,** 2005, 5133-5139.

275.   Y. Liu, Y. Chen, L. Li, H.-Y. Zhang, S.-X. Liu, X.-D. Guan, *J. Org. Chem.,* **66,** 2001, 8518-8527.

276.   S.J. Formosinho, *Mol. Photochem.,* **7,** 1976, 13-39.

277. H. M. N. H. Irving, H. Freiser, T. S. West, *IUPAC Compendium of Analytical Nomenclature, Definitive Rules*. 1981, Pergamon Press: : Oxford.

278. L.L.E. Salins, E.S. Goldsmith, S. Elizabeth C.M. Ensor, S. Daunert, *Anal. Bioanal. Chem.,* **372,** 2002, 174-180.

279. S.W. Mike Fay, H. Abadin, L. Ingerman, S.G. Swarts, *Agency for Toxic Substances and Disease Registry (ATSDR)*, P.H.S.D.o.P.H.a.H. Services, Editor. 2005: Atlanta, GA.

280. C. Kokkinos, A. Economou, I. Raptis, T. Speliotis, *Anal. Chim. Acta,* **622,** 2008, 111-118.

281. X. He, H. Liu, Y. Li, S. Wang, Y. Li, N. Wang, J. Xiao, X. Xu, D. Zhu, *Adv. Mater.* **17,** 2005, 2811-2815.

282. U. Kreibig, and M. Vollmer, *Optical Properties of Metal Clusters. (Springer Series in Materials Science 25)*. 1995: Springer. 532.

283. A. Dutta, S.S. Mahapatra, J. Datta, *Int. J. Hydrogen Energy,* **36,** 2011, 14898-14906.

284. I.I.S. Lim, D. Mott, W. Ip, P.N. Njoki, Y. Pan, S. Zhou, C.-J. Zhong, et al., *Langmuir,* **24,** 2008, 8857-8863.

285. P. Heikkila¨, T. Aimo, L. Matti H. Ali, *Polym. Eng. Sci.,* **48**, 2008, 1168-1176.

286. K.S. Virender, A.Y. Ria, L. Yekaterina, *Adv. Colloid Interface Sc.,* **145,** 2009, 83–96.

287. A.S. Korchev, M.J. Bozack, B.L. Staten, G.J. Mills, *J Am Chem Soc,* **126**(1)**,** 2004, 10-11.

288. A.B.R. Mayer, J.E Mark, *Polymer,* **41**(4), 1999, 1627-1631.

289. T.M. Tolaymat, A.M. El Badawy, A. Genaidy, K.G. Scheckel, T.P. Luxton, M. Suidan, *Sci. Total Env.,* **408**(5), 2010, 999-1006.

290. P. Mulvaney, *Langmuir,* **12,** 1996, 788-800.

291. G.C. Papavassiliou, *J. Phys. F,* **6,** 1976, L103-L105.

292. K. Torigoe, Y. Nakajima, K. Esumi, *J. Phys. Chem.*, **97,** 1993, 8304-8309.

293. R.J. Chimentao, I. Cota, A. Dafinov, F. Medina, J.E. Sueiras, J.L.G. de, la Fuente, J.L.G. Fierro, Y. Cesteros, P. Salagre, *J. Mater. Res.,* **21,** 2006, 105-111.

294. J.-S. Seo, D.-M. Son, H. Lee, J. Kim, Y. Kim, *Bull. Korean Chem. Soc.,* **30,** 2009, 2651-2654.

295. M. Bieri, T. Buergi, *J. Phys. Chem.* B, **109,** 2005, 22476-22485.

296. M.M. Jones, W.K. Vaughn, *J. Inorg. Nucl. Chem.,* **40,** 1978, 2081-2088.

297. Y.H. Lee, Y. Komatsu, Y. Yamamoto, K. Kato, T. Shimizu, A. Ohta, T. Matsui, S. Hayami, *Inorg. Chem. Commun.,* **14,** 2011, 1498-1500.

298. K. Busaranon, W. Suntornsuk, L. Suntornsuk, *J. Pharm. Biomed. Anal.,* **41,** 2006, 158-164.

299. W.C. Vosburgh, G.R. Cooper, *J. Am. Chem. Soc.,* **63,** 1941, 437-42.

300. J.H. Yoe, A.L. Jones, *Ind. Eng. Chem., Anal. Ed.,* **16,** 1944, 111-15.

301. N. Rajendraprasad, K. Basavaiah, *J. Anal. Chem.,* **65,** 2010, 482-488.

302. J. Deng, L. Wang, L. Liu, W. Yang, *Prog. Polym. Sci.,* **34**(2), 2009, 156-193.

303. B.P. Branchaud, *J. Am. Chem. Soc.,* **127,** 2005, 14117-14118.

304. S.M. Kolhe, A. Kumar, *Radiat. Phys. Chem.*, **76**(5), 2007, 901-906.

305. A.V. Glushkova, A.S. Radilov, S.A. Dulov, *Gig. Sanit.,* 2011, 81-86.